Photothermal beam deflection for non-destructive evaluation of semiconductor thin films

Thesis submitted to

Cochin University of Science and Technology

In partial fulfilment of the requirements for the award of the degree of

Doctor of Philosophy

Under the Faculty of Science

Anita R Warrier

Applied Optics Division
Department of Physics
Cochin University of Science and Technology
Cochin 682 022, Kerala, India

August 2010

Photothermal beam deflection for non-destructive evaluation of semiconductor thin films

PhD thesis in the field of Material Science

Author

Anita R Warrier
Applied Optics Division
Department of Physics
Cochin University of Science and Technology
Cochin 682 022, Kerala, India

Supervising Guide

Prof K P Vijayakumar
Thin film Photovoltaic & Applied Optics Division
Department of Physics
Cochin University of Science and Technology
Cochin 682 022, Kerala, India
kpv@cusat.ac.in

Cochin University of Science and Technology, Cochin 682 022, Kerala, India
August 2008

Dedicated to my beloved grandma,
Who chose the abode of God.
But continues to inspire me,
And whose loving memories are forever
A reason to smile...

Dr K P Vijayakumar
Professor
Department of Physics
Cochin University of Science and Technology
Cochin 682 022, Kerala, India

Certificate

Certified that the work presented in this thesis entitled ***"Photothermal beam deflection for non-destructive evaluation of semiconductor thin films"*** is based on the authentic record of research done by ***Ms Anita R Warrier*** under my guidance in the Department of Physics, Cochin University of Science and Technology, Cochin 682 022 and has not been included in any other thesis submitted for the award of any degree.

Cochin 22 **Dr K P Vijayakumar**
Date: **(Supervising guide)**

Phone: +91 484 2577404 extn 33 **Fax**: 91 484 2577595 **Email**: kpv@cusat.ac.in

Declaration

I hereby declare that the work presented in this thesis entitled *"**Photothermal beam deflection for non-destructive evaluation of semiconductor thin films**"* is based on the original research work done by me under the supervision and guidance of ***Prof K P Vijayakumar***, Department of Physics, Cochin University of Science and Technology, Cochin 682 022 and has not been included in any other thesis submitted previously for the award of any degree.

Cochin 22

Date: **Anita R Warrier**

Acknowledgements

It is the human mind's quest to ponder the mystery of creation, sustenance and destruction. This quest is in itself a journey covering the dark and beautiful phases of life and in the finale what remains is a realisation that, every war we fought and every obstacle we crossed was worth the life we lived.

I express my deepest gratitude to my guide Prof K P Vijayakumar for steering me through the journey and holding the torch for me to envisage the beautiful path it covers. His ideas and visions always helped me understand the problem better and find the solution. I am indebted to Prof C Sudha Kartha for the moral support I got. I have always admired her ability to view any predicament in true light and give right focus to work. Her suggestions and criticism helped me improve in many ways.

I am forever grateful to the Head of the Department, Prof M R Anantharaman and all my teachers in Physics Department for the interesting and delightful classes during my post graduation days and the help I received throughout my research period. I am also grateful to all the staff in this department for assisting me earnestly whenever I approached them.

I am very much grateful to Dr R Jayakrishnan for the support I received during the initial stage of my work. His insights and the long discussions we had, helped me view the problem in a new perceptive. I always cherish the wonderful relation with Pramitha, who is always a source of strength and happiness and I will forever rejoice the memories of my days shared with her in this department. I would also like to mention my gratitude to Vimal for being the patient and trusty friend who listens and lighten the hurdles in the path.

I would like to thank my seniors Dr Teny Theresa John, Dr M Paul Raj, Dr S Ramkumar, Dr Ratheesh Kumar P M, K C Wilson, Dr Beena Mary John, Dr R Sreekumar, Dr V C Kishore, Dr Deepa K G, Dr Tina Sebastian, Dr Meril Mathew for their love and support. I would always remember with love and affection my juniors Sajeesh, Angel, Rajesh Menon, Rajesh C S, Sreeroop, Subramanian, Nimmi, Sona, Poornima, Rajeshmon, Aneesh, Minu, Anaswalih, Santhosh and Deepu for the fun filled days in this department.

I am glad expressing my gratitude to MSc project students Anuradha, Chandhrasekhar, Anand, Leshma, Abdul Rasheed and Linda. The discussions we had were thought provoking and improved my understanding of the subject.

And the entire work was possible only because of my mother and father, who in every turn of life holded my hands gave me strength and supported me whole heartedly to move forward. I would like to thank my brother and sister for the constant encouragement and inspirations. The love and support I received from my in laws for this pursuit were

magnificent. I am very much grateful to my husband for the freedom I had in pursuing my work, despite numerous problems we faced he never let me stray away from the path. Finally I would like to express my admiration to my son Aditya, who is the beautiful butterfly that flutters around my life teaching me every day, in every way the true essence of life and keeps the child in my alive.

I remember with gratefulness all my friends and well wishers for their blessings and prayer.

Anita R Warrier

The scientist does not study nature because it is useful;
He studies it because he delights in it,
And he delights in it because it is beautiful

If nature were not beautiful, it would not be worth knowing,
And if nature were not worth knowing,
Life would not be worth living

Henri Poincare
(French Mathematician 1854-1912)

Preface

Non-destructive testing (NDT) is the use of non-invasive techniques to determine the integrity of a material, component, or structure. Engineers and scientists use NDT in a variety of applications, including medical imaging, materials analysis, and process control.

Photothermal beam deflection technique is one of the most promising NDT technologies. Tremendous R&D effort has been made for improving the efficiency and simplicity of this technique. It is a popular technique because it can probe surfaces irrespective of the size of the sample and its surroundings. This technique has been used to characterize several semiconductor materials, because of its non-destructive and non-contact evaluation strategy. Its application further extends to analysis of wide variety of materials. *Chapter one* of the thesis covers the principle, application and review of R&D works concerning photothermal techniques and application.

Instrumentation of a NDT technique is very crucial for any material analysis. *Chapter two* explores the various excitation sources, source modulation techniques, detection and signal processing schemes currently practised. The features of the experimental arrangement including the steps for alignment, automation, data acquisition and data analysis are explained giving due importance to details.

Theoretical studies form the backbone of photothermal techniques. The outcome of a theoretical work is the foundation of an application. *Chapter three* brings forth the importance of theoretical studies carried out in this area and explains the steps of theoretical model developed for analysis of semiconductor thin films. The reliability of the theoretical model developed and used is proven from the studies done on crystalline silicon.

The technique is applied for analysis of transport properties such as thermal diffusivity, mobility, surface recombination velocity and minority carrier life time of the material and thermal imaging of solar cell absorber layer materials like $CuInS_2$, $CuInSe_2$ and SnS thin films. *Chapter four* briefs the results of the photothermal analysis of these materials and its application for optimisation of thin film fabrication process.

Chapter five deals with analysis of In_2S_3 thin films, which are used as buffer layer material in solar cells. The various influences of film composition, chlorine and silver incorporation in this material is brought out from the measurement of transport properties and analysis of sub band gap levels.

The application of photothermal deflection technique for characterization of solar cells is a relatively new area that requires considerable attention. *Chapter six* thus elucidates the theoretical aspects of application of photothermal techniques for solar cell analysis. The experimental design and method for determination of solar cell efficiency, optimum load resistance and series resistance with results from the analysis of $CuInS_2/In_2S_3$ based solar cell forms the skeleton of this chapter.

The C*hapter seven* attempts to depict the state of art, achievements and future prospects of the studies done.

Publications

Journal publications

1. Transverse photothermal beam deflection technique for determining the transport properties of semiconductor thin films. **Anita R Warrier**, Tina Sebastian, C Sudha Kartha, K P Vijayakumar 2010 *Journal of Applied Physics* **107** 073701.

2. Non-destructive evaluation of carrier transport properties in $CuInS_2$ and $CuInSe_2$ thin films using photothermal beam deflection technique. **Anita R Warrier**, K G Deepa, Tina Sebastian, C Sudha Kartha, K P Vijayakumar 2010 *Thin Solid Films* **518** 1767.

3. Structural and optical properties of Indium sulphide thin films by SILAR technique. **Anita R Warrier**, Teny Theresa John, K P Vijayakumar, C Sudha Kartha 2009 *The Open Condensed Matter Physics Journal* **2** 9.

4. Optimization of parameters of chemical spray pyrolysis to get n and p layers of SnS. T H Sajeesh, **Anita R Warrier**, C Sudha Kartha, K P Vijayakumar 2010 *Thin Solid Films* **518** 4370.

5. Measurement of surface recombination velocity, minority carrier lifetime and mobility of tin sulfide thinfilms using photothermal beam deflection technique. **Anita R Warrier**, T H Sajeesh, C Sudha Kartha, K P Vijayakumar (*communicated*).

Conference publications

International

1. Non-destructive evaluation of thermal and electronic transport properties of semiconductor thin films. **Anita R Warrier**, R Sreekumar, C Sudha Kartha, K P Vijayakumar, *International symposium for research scholars on metallurgy, material science and engineering -ISRS 2008*, IIT Madras, India. December 10-12, 2008.

2. Non-Destructive evaluation of carrier transport properties in $CuInS_2$ and $CuInSe_2$ thin films using photothermal deflection technique. **Anita R Warrier**, Deepa K G, Tina

Sebastian, C Sudha Kartha, K P Vijayakumar, *XVII International Materials Research Congress –IMRC 2008*, Cancun, México. August 17-21, 2008.

3. Measurement of thermal and electronic transport properties of semiconductor thin films using Photothermal deflection technique. **Anita R Warrier**, Tina Sebastian, K P Vijayakumar, C Sudha Kartha, *9th International symposium on measurement and quality control*, *ISMQC-2007*, Chennai, India. November 21-24, 2007.

4. Use of SHI irradiation in gamma In_2Se_3 thin films for PV devices in outer space applications. R Sreekumar, **Anita R Warrier**, C Sudha Kartha, K P Vijayakumar, S K Khan, D K Avasthi, *2nd European Optical Society Tropical meet; Optical Microsystems-2007*, Capri, Italy, September 30-October 3, 2007.

National

1. Photothermal beam deflection technique for characterization of optoelectronic materials. **Anita R Warrier**, C Sudha Kartha, and K P Vijayakumar, *National conference on advances in material science - NCAMS-2008*, Chennai, December 22-23, 2008.

2. Non-radiative transitions in Indium sulphide thin films. **Anita R Warrier**, Teny Theresa John, Meril Mathew, C Sudha Kartha, and K P Vijayakumar, *Proceedings of the 53rd DAE Solid State Physics Symposium*, Mumbai, December 16-20, 2008.

3. Photothermal deflection technique for non destructive evaluation of semiconductor thin films, **Anita R Warrier**, Tina Sebastian, K P Vijayakumar, C Sudha Kartha, *National symposium on ultrasonics NSU-XVI*, STIC, Cochin, December 17-19, 2007.

4. Photothermal investigation of minority carrier mobility in $CuInS_2$ thin films prepared by chemical spray pyrolysis. **Anita R Warrier**, Tina Sebastian, K P Vijayakumar and C Sudha Kartha, *New horizons in experimental and theoretical physics NHTEP-2007*, Cochin, October 8-10, 2007.

Contents

1

Photothermal beam deflection technique

Photothermal beam deflection technique is an efficient non-destructive method for evaluating semiconductor thin films. Since birth it has evolved in different stages and developed into a technique that can do multi purpose analyses of a variety of materials like polymers, ceramics, semiconductors and various biological samples. Development of this technique for investigating the opto-electronic properties of semiconductor thin films particularly useful for photovoltaic application is the subject of our interest. This chapter, apart from giving a brief introduction to the technique, its principle and applications, looks through the resourceful contributions from various groups all over the world applying photothermal effect for analysis of semiconductors.

Non-destructive testing (NDT) is the study of a material without causing any damage or loss to the material under study. Non-destructive evaluation of a material ensures its reliability, cost effectiveness, and safety of operation. It also helps to avoid failures, maintain the product quality level and control of manufacturing process. Photothermal (PT) techniques offer a large range of methods by which the materials can be evaluated non-destructively. PT techniques for thermal NDT measurements were first developed around 1980 and have ever since been in use for a wide range of spectroscopic and imaging applications. It is an emerging technique in the NDT field and is yet to be introduced for actual field application.

Among a wide variety of NDT techniques such as ultrasonics; x-ray radiography; eddy current, dye penetrant and visual inspection, PT techniques offers the most simple, flexible and reliable solutions. Early examples of non-destructive imaging studies with PT techniques include detection of subsurface structure and imaging of surface breaking fatigue cracks. This technique has come a long way and has been adopted by several cutting edge technologies for process monitoring and control. PT techniques have several advantages over other characterization methods. This does not make physical contact with the explored sample and does not always need an enclosed cell for making measurements. It offers wide range of detection schemes and hence it is possible to select the detection technique suiting the material demands. These techniques provide localized information to an area of micrometer range and are mostly limited by the thermal diffusion length or diameter of the beam used for excitation. The ability of these techniques to detect interfaces between media of differing thermal properties makes the investigation of multilayer films possible. Again, potential for large area scanning for defects makes these desirable tools for

industrial process monitoring. Here material property being probed is the thermal behaviour, which is quite unique and different from the properties probed using other NDT methods. Another important advantage of PT techniques over other optical characterization techniques is the immunity to scattering losses, as only the absorbed radiation gives rise to the signal in this case. But in other conventional techniques intensities of incident, reflected and transmitted light are recorded as a function of wavelength and the absorption is calculated from numerical difference.

Initial sections of this chapter reveal the history along with the basic principle and applications of PT techniques. Final section presents a review of the progress made by PT techniques in the analysis of semiconductors and photovoltaic (PV) cells. PV is one of the most promising future energy technologies where lack of non-destructive evaluation and testing is the large barrier impeding the achievement of high performance and cost effective solutions. PT techniques offer simple and reliable ways for characterization of solar cells right from the first processing step; hence early detection of errors and control and/or alter the processes to achieve better results becomes possible.

1.1 History of photothermal science

Sir Alexander Graham Bell (1880) [1] and his assistant Tainter at some stage of the invention of photophone, accidentally discovered that when a periodically interrupted beam of sunlight shines on a solid in an enclosed cell, an audible sound could be heard (Photoacoustic effect), whose pitch depended on the periodicity of interruption, and could be heard clearly using a hearing tube. Bell subsequently experimented with a variety of solids, liquids and gases and this work generated a brief flurry of interest in that period [2]. Motivated by Bells discovery, Tyndall and Rontgen found that an acoustic signal could also be produced when a gas in an enclosed cell is illuminated with chopped light. This was soon developed as spectrophone, using which the absorption spectra of the samples could be obtained by dispersing light through a prism and recording the sound intensity as it varied with the wavelength of light. The spectrophone had found applications in gas detection using hot gases as sources of resonant infrared radiation [3]. Despite triggering many investigations, photoacoustic effect lingered on as a subject of scientific curiosity with no practical application. Mordern era of science, triggered by invention of lasers, revitalised the interest in photothermal science. Kreuzer and Patel in 1971 [4] demonstrated that the use of lasers as radiation source could increase the spectrophone's sensitivity by several orders of magnitude. Thus ninety years later, the photoacoustic or optoacoustic effect was re-examined and this was indeed the beginning of a new branch viz., photothermal science, with wide applications. Several theories were put forth to explain the basis of the sound produced and the information it carried. However the theoretical investigations by Rosencwaig in 1973 [5] resulted in building a solid foundation for this technique and established it as a useful technique for spectroscopic analysis of solid and semisolid materials. This led to the upsurge of several theoretical and experimental developments that had a multitude of interesting applications in all areas of science.

1.2 Photothermal effect

When a material is irradiated with electromagnetic radiation, energy is absorbed and a part of it is released as heat. This phenomenon is called PT effect. Heating of a sample through absorption of optical energy results in various photothermal effects that causes several changes in both the material aswell in the medium around it (Figure 1.1). Some of the most common heating effects are listed below.

Temperature rise

The most direct method for measuring heating due to PT effect is monitoring of rise in temperature; this is sometimes referred to as "optical calorimetry" or "laser calorimetry" since a laser is frequently used for excitation. To detect the induced temperature rise, thermocouples or thermistors have been used [6], and pyroelectric detectors with high sensitivity have also been exploited [7]. Major advantage of this method is that observed temperature change can be directly related to the material parameters like absorption coefficient, thickness, thermal diffusivity etc. But the response of the method is usually slow and sensitivity is also low compared to other PT methods.

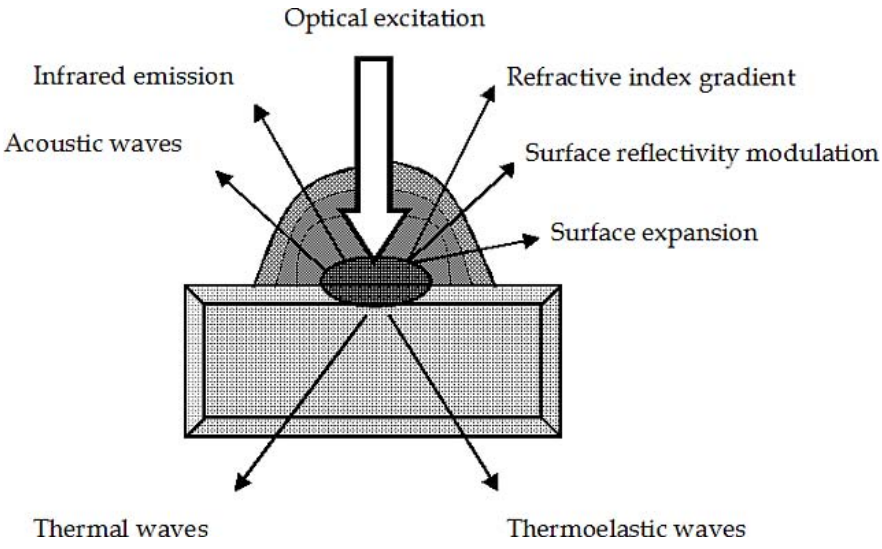

Figure 1.1 Photothermal phenomena caused by illumination of a surface by a modulated beam of light

Thermal refractive index gradient

Refractive index gradient is produced in the irradiated material and in medium surrounding by the heat gradient due to absorption of the excitation beam. Refractive index gradient produced by excitation beam affects its own propagation, resulting in well-known effect of self-defocusing or thermal blooming. Self-defocusing occurs because the derivative of the refractive index with temperature is usually negative, so that temperature gradient

results in a negative lens. On other hand, the refractive index gradient also affects propagation of another weak probe beam in the vicinity of the excitation beam. Thus the refractive index gradient can be monitored either by self-defocusing or by probe beam refraction (PBR). PBR method of detection with an additional collinear beam provides higher sensitivity than single beam self-defocusing method and this is called "thermal lensing" spectroscopy. Various methods have been used to detect the PT refractive index gradient. A probe beam that is parallel to but displaced from excitation beam was found to have higher sensitivity. This is because, in the thermal lens method, the probe is situated in the center but not at maximum refractive index gradient, which is situated approximately one beam radius from the axis of the excitation beam. This parallel configuration of probe beam with displacement of one beam radius gives maximum probe deflection. However this configuration is not possible always, since transmission measurements cannot be performed on opaque samples. Hence, for this purpose, orthogonal PBR detection is generally used. Orthogonal photothermal PBR or "mirage" probing has been used for several spectroscopic applications. This technique is very sensitive for detecting weak absorption fraction as small as 10^{-8}.

Surface deformation

PT heating of a surface causes distortions due to thermal expansion. These distortions can be very small (10^{-4} nm). Such small distortion can be detected by a new technique called 'photothermal displacement technique'. The other methods for detecting the surface deformation include the use of optical interferometry and attenuated total reflection. The main parameters limiting the sensitivity of displacement measurements are the probe laser intensity and pointing instabilities.

Acoustic wave generation

Photoacoustic (PA) effect has very significant role in the development of photothermal science and is still the most widely used detection technique. Acoustic waves are generated by heating of the gas layer adjacent to the optically heated region, thermal expansion of the sample, evaporation of a volatile material, gas evolution, etc. The harmonic heating of the thin layer of gas close to the sample surface (thermal piston model) is the primary source of acoustic signal generation. This method is particularly suited for investigation of gases and powdered solids that have large surface area to volume ratios; temperature rises as small as 10^{-6} ^{0}C are detectable. A serious limitation of PA detection is the need to enclose the sample being studied in a cell.

Infrared wave emission

Various infrared thermal radiations emitted from a sample that is excited by electromagnetic radiation of varying intensity or wavelength can be detected using photothermal radiometry (PTR) technique. This is one of the most widely exploited detection technique as it offers a simple means of monitoring sample temperature. The successful use of infrared detection in photothermal application depends on maximizing the infrared radiation collected by the detector and on minimizing the incidence of

excitation source radiation on detector. Among all the different photothermal detection mechanisms, the entire work presented here focus on the principle and applications of transverse photothermal beam deflection (PTBD) technique in skimming configuration.

1.3 Transverse photothermal beam deflection technique in skimming configuration

In optical beam deflection (OBD) or PTBD technique the spatial variation of refractive index of heated materials, or that of gas or fluid in contact with it, will deflect a laser beam (Figure 1.2). This deflection can be monitored and used as means of detecting thermal waves. This method is based on the periodic heating of a sample by a frequency modulated excitation beam. Heat diffusion in both sample and surrounding medium produces a temporally varying gradient of refractive index, which can deflect a probe beam from its initial trajectory. PTBD technique when used in its transverse configuration uses the probe beam travelling in air (medium) nearly at the top of the studied sample, while a modulated excitation beam impinges on the sample surface, perpendicular to the surface. This is an indirect method of detection because here we measure refractive index gradient produced in the medium around that sample due to thermal waves emanating from the photothermally-heated sample.

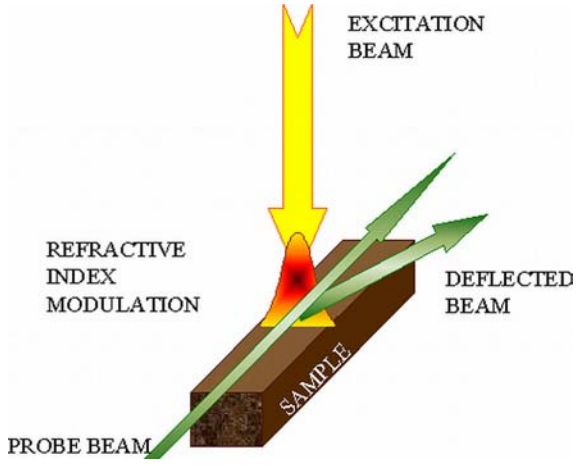

Figure 1.2 Beam deflection due to photothermal effect

The probe beam is deflected from its trajectory by an angle Φ given by,

$$\phi = \frac{1}{n}\frac{dn}{dT}\int_{path}\Delta_t T(r,t)ds \qquad 1.1$$

Where n is the refractive index of the surrounding medium, s the optical path length, and Δ_t the gradient transverse to the propagation direction.

1.4 Advantages

Transverse PTBD technique has several advantages over the other detection methods. Below given is a brief comparison of advantages (and disadvantages) of the PTBD technique over other PT techniques.

Lower background noise PTBD has several distinct advantages when one considers noise and background. The probe laser usually has relatively large intensity fluctuations. Such fluctuations give rise to significant noise in the case of thermal lensing method but are reduced in PTBD by a factor of 1000.

Versatility PTBD also has versatility as advantage over other techniques. Spectra of opaque samples or scattering samples can be measured using transverse PTBD. Again moving the beam overlap region through the sample can perform 3-D depth profiling of absorption. Hence PTBD is as sensitive as other techniques with more versatility and ease of use.

Remote sensing and insitu monitoring PTBD is more sensitive, particularly in the case of liquids and has potential for remote sensing and *in situ* monitoring.

Resistant to hostile environments PTBD works efficiently under pressure and temperature extremes or caustic substances.

Simplicity The experimental arrangement of PTBD is rather undemanding compared to PA technique, since acoustic-shielding requirements is less stringent. The complication of gas coupling physics is eliminated. Spatial probing of absorption is also possible in PTBD.

The major disadvantages of PTBD over these techniques are:

i) Alignment is more difficult
ii) Sample surface should not be exceedingly rough.

However the simplicity and robustness of PT techniques make it attractive to industrial environments.

1.5 Applications

Important applications of photothermal measurements are in the fields of semiconductor doping control, flaw detection and adhesion control in compound materials and film thickness determination.

Chemical analysis

Photothermal lens spectroscopy technique is used for sensitive chemical analysis, trace analysis and chromatographic detection**.** There are reports stating that detection limits of the order of 10^{-7} au and 10^{-3} au for stationary samples or flowing samples respectively can be achieved [8]. It has also been used for measuring excited state relaxation and chemical

reaction rates and photo physical parameters such as triplet-state quantum yields [9]. PT and PA are among the most sensitive spectroscopic techniques available yielding part per million or part per billion sensitivities for trace detection in gases and fluids. These techniques have been used for pollutant detection and spatial imaging of pollutants in liquids for environmental and agricultural investigations [10].

Measuring thermal diffusivity

Basic thermal characterization of a material can be understood from the thermal diffusivity and effusivity. Measurement of temperature and thermo-physical properties (such as emissivity, thermal diffusivity and conductivity) is the primary aim of several photothermal techniques and it is widely used to study various materials and devices. This technique is found to be fast precise; again, thermal diffusivity values ranging from 0.01 to 10 cm^2/s can be measured without any special requirements on the size of the sample [11]. Thermal diffusivity of super conducting-film-substrate composite has been measured using this technique [12]. This technique has also been applied for study of phase transition and laser ablation of solids. Phase transition temperatures of tri-glycine sulphate (TGS) and ferroelectrics gadolinium molybdate (GMO) crystals were obtained using this technique [13]. Photothermal technique was developed for ultrahigh resolution measurements of thermal diffusivity in liquid mixtures using thermal wave resonator cavity. This system is proposed to be implemented into a self-contained in-situ pollution monitor [14].

Thermal wave imaging

Origin of the development of thermal wave imaging technique and material characterization using this can be traced back to the time of first international workshop on PA and PT phenomena in 1979. Thermal wave imaging is capable of detecting and imaging previously invisible thermal features. Its application in material analysis is diverse. It allows detection and imaging of microscopic surface and sub surface features including the sub surface mechanical defects [15], interfacial flaws and micro cracks [16], metallic grains and grain boundaries [17], dislocation network and dopant regions in semiconductor crystals [18]. It also includes detection and characterization of areas of a crystalline lattice that have been modified through the introduction of foreign ions or defects. 'Photothermal imager' is for mapping purely optical or thermal defects efficiently in coatings of low damage threshold and low absorbance. A detailed mapping of minor inhomogenietes at low pump power has been achieved.

Thickness measurement

Determination of coating thickness is an important requirement for different industries. This technique is also used for monitoring the formation of thin films [19].

Depth profiling

It is a valuable tool in obtaining depth information on thermal parameters of materials and can be used to evaluate different types of inhomogenietes such as macroscopic sub surface

defects in homogeneous material, or microscopic structural modifications, which produce local thermal conductivity and diffusivity changes [20].

Dielectric measurements

This technique is useful for determining the dielectric, pyroelectric and thermal properties of polymeric materials [21].

Determination of the thermal conductance of interfaces and cracks

Phase sensitive photothermal technique was applied for determining the thermal conductance of an interface, a thin interlayer, or crack embedded within a plate [22]. This is based on periodic heating at one point and measurement of the phase lag at some other point. It is also possible to determine the thermal diffusivity of solids and thermal conductance of embedded interfaces, interlayer and cracks. Thermal wave technique is employed for simultaneous determination of ultra shallow junction depth and abruptness due ion implantation and rapid thermal annealing in a semiconductor wafer. The results obtained showed better than 99% correlations to the corresponding secondary ion mass spectroscopy data [23].

Monitoring ion implantation

Thermal probe tool is used for monitoring ion implantation dose [24] and process control in IC manufacturing with thermal waves. This helps in controlling the ion implantation process and control of mettalization process.

Others

PT techniques can be used for determination of speed of sound in solids in different materials [25], for monitoring the degradation of paint film [26], crack detection by a mobile photothermal probe [27], flying spot photothermal camera [28] for nuclear and aviation industry (CEDIP infra red systems), photothermal camera for inspection of plate welds [29] and to measure low levels (as low as 50 $\mu g/m^3$ corresponding to light absorption of 5×10^{-6} cm^{-1}) of smoke emitted from diffusion flame [30].

1.6 Review of photothermal analysis of semiconductors

Clean and non-destructive methods are required for in-line and in situ process control. Thermal wave techniques have gained increasing attention in semiconductor process control mainly due to the non-invasive nature whereby the possibility of contamination is avoided. Characterization of semiconductor materials is an important and successful application of photothermal science. Photothermal spectroscopy, a highly sensitive non-destructive technique, has become a common tool for absorption studies in both semiconductor films and bulk material. This technique has shown to be effective for monitoring a variety of wafer processing stages and for rapidly identifying the changes during the processing itself [31]. The ability to monitor each stage of wafer processing can

lead to the identification of parameters, which critically affect the wafer quality. The characterizations include monitoring of wafer quality and determination of electronic parameters. In addition to these it is possible to measure the dimension of implanted regions.

Defect analysis in semiconductors

In the year 1981, N Mikoshiba and K Tsubouchi [32] carried out PA and PL measurements at room temperature in order to get new spectroscopic information on defects in semiconductors such as GaAs, InP, Si and a-Si. From the experimental results it was proved that a dark line defect, an oxidation layer and surface states on GaAs surface and a thin a-Si layer on Si surface act as spatially localized non-radiative regions. The bending model by Jackson and Amer was applied to the analysis of results on the light modulation frequency dependence of the signal amplitude. Combined PT and PL heterodyne measurement was used for analysing subsurface damages in Si. Different defect states can be separated using this technique. Both invisible defect structures and subsurface defects introduced by transport, handling, and processing can be found out and evaluated. Residual damage caused by abrasive processes can also be found out in early stages of wafer manufacturing [33]. Deep level photothermal spectroscopy was developed for the defect level characterization of GaAs wafer. Here the thermal recovery of carriers after excitation is monitored using sub band gap laser absorption [34].

Measurement of surface and interface states

A careful analysis of the modulations found in the signal wavelength spectra (produced by optical interference of the heating light source), it is possible to discriminate between the absorption due to surface states located at the film front surface and that due to buried interface states located at substrate interface. This can be achieved in films with large difference between the film and substrate refractive index values [35]. A method was presented by U Zammit et al [36], which, (through simultaneous analysis of the photothermal deflection spectroscopy signal amplitude and phase spectra), enables to detect the surface states and buried interface even in cases where there is no difference in refractive index values of the two layers. Measurements were performed on single crystalline GaAs wafers with ion-implanted layers on the front surface or buried beneath the front surface. Their group [37] had also devised a method for analysis of PT signal amplitude and phase, which enables to find out the location of the semiconductor wafer surface where surface states are present, and to measure their absorption. This analysis also allows the determination of sample's thermal conductivity value.

Determination of transport properties

N Mikoshobi et al [38] extended the Jackson-Amer model for PA spectroscopy to include the effects of diffusion, bulk lifetime and surface recombination of excess-minority carriers. They used the model to evaluate the bulk lifetime and surface recombination velocity of Si wafers by measuring the chopping frequency dependence of PA signals.

Photothermal approach was adopted by Daniele Fournier et al [39] to measure transport processes based on principle of optical beam deflection. This measurement technique, which is an extension of photothermal deflection, has significant advantages as it is contactless and directly yields both thermal and electronic transport parameters within the bulk / at surface / interface of a semiconductor. Another important advantage of the technique is that it can be used to measure these transport properties in a spatially resolved (μ^3) manner. This model allows for the explicit measurement of important parameters such as thermal and electronic diffusivity, electronic mobility, and carrier recombination kinetics-both in bulk and surface or interface.

Later, in 1995, PA heat-transmission measurements were used to study transport in a nearly intrinsic Ge single crystal by M D Dramicanin et al [40]. A theoretical model was developed which quantitatively describes excess carrier and thermal wave space distributions, within the semiconductor under monochromatic continuous wave modulated excitation. It was shown that both the normalized phase and amplitude, as a function of the modulation frequency, could be used to determine the values of the thermal diffusivity, the excess carrier lifetime, surface recombination velocity and a method to eliminate the frequency characteristics of the measuring system which can cause errors in the determination of the measured parameters. D M Todorovic et al [41] investigated photoacoustic effect as a function of the modulation frequency in a 'transmission-detection configuration' for semiconductor samples. Dependence of photoacoustic effect on thermal diffusion, thermoelastic, and electronic-transport parameters was identified**.** Infrared PTR was found to be extremely useful in measuring thermal and several electronic properties of semiconductors. PTR allows measurement of optically induced black body radiation from semiconductor surface. It has been shown that the frequency-domain PTR signal is extremely sensitive to the photoexcited carrier plasma-wave in semiconductors. Hence this technique has been attractive for ion implantation and process monitoring with carrier plasma wave technology. Applications of technique to ion implanted Si wafer for qualitative analysis of the influence of thermal annealing and sensitivity of the carrier plasma wave to implantation induced damage in Si technique have been reported [42]. This technique was successfully demonstrated to be capable of characterization of ion implantation effects on the electronic properties, as well as monitoring the contamination of Si wafers [43] and Si electronic devices [44]. But all these works were done under the assumption that semiconductors were homogeneous or discontinuously homogeneous; however modern device processing requires improvement of the spatial resolution of PTR, allowing for measurements within the 'scribe lines'. Three dimensional measurement technique taking into account of the finite size of excited laser beam, the sample thickness and plasma-thermal wave contributions to the signal were adopted by Tetsuo Ikari et al [45] for analysing semiconductor wafers patterned for LSI circuits. Photothermal deflection technique was used for measuring thermal diffusivity of double epitaxial layer of n-type GaAs doped with various concentration of Si and a p-type Be doped GaAs layer grown on GaAs substrate by molecular beam epitaxial method. Thermal diffusivity is evaluated from the slope of the graph of the phase of the photothermal signal as a function of pump-probe

offset. Doping concentration was found to have a great influence on the thermal diffusivity value [46].

Studies using photopyroelectric technique have shown that the generation and propagation of thermal waves in crystalline Si depends on the thermal history and formation native a-SiO_2 in the sample. It was also used for analysis of recombination processes in semiconductors [47]. Photothermal techniques were also used for measuring the optical and thermal properties of porous silicon [48]. This technique also finds application in measuring thermal and electronic transport properties of CdTe thin films and powders of RuTe, RuS, $RuSe_2$ and CdTe [49]. E Marin et al determined non-radiative lifetime in direct band gap semiconductors, such as GaAs, GaSb and InSb [50]. A Mandelis et al showed that a new photothermal technique of 'lock-in-rate window infrared radiometery' is capable of completely separating out photoexcited free-carrier-wave and thermal wave contribution to the photothermal signal from an n-type, Cr-doped Si wafer with a superior temporal resolution in the determination of electronic lifetime and thermal transport time constant [51]. Three dimensional photothermal radiometric microscopic imaging and laser-intensity-modulation frequency scan were used for the non contact measurements of electronic transport properties of integrated circuits in patterned Si wafers [52]. Laser induced infrared photocarrier radiometry is a powerful tool for carrier density diagnosis through non-contact characterization in semiconductors. It was employed to determine the temperature dependence of carrier mobility in Si wafers [53].

Optical studies

Optical properties of GaAsNSe/GaAs superlattice were investigated using piezoelectric photothermal deflection and piezoelectric spectroscopy [54]. Optical absorption spectra of glow discharged undoped a-Si: H films were determined using photothermal deflection spectroscopy. PT experiments in low frequency regions were performed as a function of thickness; to confirm the existence of surface and interface absorption in device quality undoped a-Si-H samples [55].

Thickness measurement

Photothermal methods based on analysis of photothermal phase variation with wavelength in the vicinity of the substrate energy gap were used for measuring the thickness (~1000 nm) of very thin layer of GaInAs of InP/GaInAs/InP heterostructure [56].

Depth profiling

Photothermal deflection technique was used for depth profiling of a semiconductor thin films [57]. The amplitude of interference fringes in optical absorption spectra of thin films have been analysed in the range of low absorption coefficients and were related to a depth profile of absorbers, e.g. defects. This method was applied to the sub-bandgap optical absorption spectra measured using photothermal deflection spectroscopy, for a-Si: H thin films. It was shown that the analysis of interference fringes provides unique information about surface and interface defects in this material [58].

Internal quantum and energy efficiencies of photoelectrodes

The first quantitative photothermal investigations of semiconductor electrodes were performed using 'photothermal thermistor spectroscopy'. Energy efficiency and stabilization of a polycrystalline ZnO photoanode in an electrolyte solution containing redox agents was investigated using photothermal technique by measuring the temperature change of the electrode surface [59, 60].

Photovoltaic studies

David Cahen et al (1978) used PA measurements to characterize photovoltaic devices. Such measurements are useful for the optimisation of multicomponent, photovoltaic systems such as semiconductor/liquid junction devices [61]. Later in 1984, yet another work by same group showed PA phase angle dependence on series resistance and how phase shift can be used for interpretation of thermal losses in PV cells [62]. The photothermal pyroelectric technique is applied for the characterization of photovoltaic cells and they have compared results with the photoacoustic detection using a simple model for junction type solar cell [63]. S I Yun used PA technique for measuring energy conversion efficiency and quantum efficiency of photovoltaic process in Si solar cell [64]. Reitte et al have reported on the additional thermal losses in PV signal of Si solar cells due to current dissipation in the internal resistance of the cell [65, 66]. P Grunow et al [66] used photothermal deflection to investigate electronic transport in silicon solar cells. They simulated the dependence of deflection signal on external bias voltage in the closed circuit condition and additional bias illumination on open circuit condition. Diode parameters describing the dark currents, due to recombination at interface or in the space charge region, are used, as free parameters to fit experimental data and the values were identical with conventional electrical measurements. This technique can be used for contactless quality control of silicon solar cells in different stages of their preparation process. Photoacoustics was used as calorimetric method in conjunction with electrical measurements to determine the mechanisms involved in conversion of most of the absorbed radiation to thermal energy in solar cells. Harvey Flaisher et al formulated a model for heat generation in solar cells that allowed quantitative separation of loss mechanisms. These results were proven for Si solar cells and $CuInSe_2$/CdS thin film solar cell [67]. Karem Boubaker developed an enhanced photothermal technical protocol for diagnosing spatial distribution of dislocation inside photovoltaic polycrystalline silicon solar cells [68].

References

[1] A G Bell 1880 *Am J Sci* **20** 305
[2] A G Bell 1881 *Philos Mag* **11** 510
[3] J Tyndall 1881 *Proc R Soc* **31** 307
[4] L B Kreuzer, C K N Patel 1971 *Science* **173** 45
[5] A Rosencwaig 1973 *Science* **181** 657
[6] G H Brilmyer, A Fujishima, K S V Santhanam, A G Bard 1977 *Anal Chem* **49** 2057
[7] T Baumann T, F Dacol, R L Melcher 1983 *J Appl Phys* **43** 71

[8] S E Bialkowski **1996** *Photothermal Spectroscopy Methods for Chemical Analysis Vol **134*** Wiley, New York
[9] M Terazima, T Azumi, N Hirota 1992 *J of Photochem & Photobio A: Chemistry* **65** 21
[10] S Schilt, L Thévenaz, M Niklès, L Emmenegger, C Hüglin 2004 *Spectrochim Acta Part A* **60** 3259
[11] D Fournier, W Coatesworth, J P Roger 2001 *Anal Sci* **17** S490.
[12] P K Wong, P C W Fung, H L Tam 1998 *J of Appl Phys* **84** 12
[13] S I Yun, H J Seo 1992 *Chinese J of Phys* **30** 153
[14] A Matvienko, A Mandelis 2005 *Phys IV France* **125** 269
[15] Y H Wong, R L Thomas, G F Hawkins 1978 *Appl Phys Lett* **32** 538
[16] H G Walther, W Karpen 1994 *Anal Chim Acta* **297** 87
[17] L J Inglehart, A Broniatowski, D Fournier, A C Boccara, F Lepoutre 1990 *Appl Phys Lett* **56** 1749
[18] A Rosencwaig, J Opsal 1986 IEEE *Trans on Ultrason Ferroelec & Freq control* **33** 516
[19] P M Torres, J J Alvarado- Gil 2007 *Int J Thermophys* **28** 996
[20] R Li Voti, G L Liakhou, S Paoloni, C Sibilia, M Bertolotti 2001 *Anal Sci* **17** S414
[21] C Y Iguchi, W N dos Santos, D Gregorio Jr 2007 *Polym Test* **26** 788
[22] K R Mc Donald, J R Dryden, A Majumdar, F W Zok 2000 *J Heat Transfer* **122** 10
[23] M Bakshi, L Nicolaides, S Cherekdjian, R Tichy, *AIP Conf Proc* **683** 656
[24] W L Smith, A Rosencwaig, D L Willenborg, J Opsal, M W Taylor 1987 *Nucl Instr & Meth in Phys Res B* **21** 537
[25] E Marın, J M Antuna, P D Arencibia 2002 *Eur J Phys* **23** 523
[26] R E Imhoft, D J S Bircht, F R Thornley, J R Gilchristt and A S Trivens 1985 *J Phys D: AppI Phys* **18** L103
[27] J L Bodnar, M Egée, C Menu, R Besnard, A Le Blanc, M Pigeon, J Y Sellier 1994 *J Phys IV France* **04** C7-591
[28] S H Lara, P Y Joubert, D Placko 2003 *Eur Phys J Appl Phys* **24** 223
[29] L Legrandjacques, M Piriou, J Gros, D Gente 2000 *2nd International Conference on NDE in Relation to Structural Integrity for Nuclear and Pressurized Components*, New Orleans, USA.
[30] R W Pitz 1990 *Appl Opt* **29** 2418
[31] A Rosencwaig 1990 *Review of progress in quantitative non-destructive evaluation*, Plenum press, New York.
[32] N Mikoshiba, H Nakamura, K Tsubouchi 1982 *Proc IEEE Ultrason Symp* 580.
[33] H D Geiler, H Karge, M Wagner, A Ehlert, M Kerstan, D Helmreich 1997 *J Appl Phys* **81** 7548
[34] A Asano, M Stutzmann 1991 *J of Non-Cryst Solids* **137/138** 623.
[35] W B Jackson, D K Biegelsen, R J Nemanich, J C Knights 1983 *Appl Phys Lett* **42** 105
[36] U Zammit, M Marinelli, R Pizzoferrato 1991 *J Appl Physics* **69** 3286
[37] U Zammit, F Gasparrini, M Marinelli, R Pizzoferrato, F Scudieri, S Martellucci 1991 *J Appl Phys*, **69** 2577.
[38] R C Frye, J J Kumler, C C Wong 1983 *Appl Phys Lett* **50** 101
[39] D Fournier, C Boccara, A Skumanich, N M Amer 1986 *J Appl Phys* **59** 787
[40] M D Dramicanin, Z D Ristowski, P M Nikolic, D G Vasiljevic, D M Todorovic 1995 *Phys Rev B* **51** 20
[41] D M Todorovic, P M Nikolic, A I Bojieie, K T Radulovic 1997 *Phys Rev B* **15** 631
[42] A Salinick, A Mandelis, F Funak, C Jean 1997 *Appl Phys Lett* **71** 1531
[43] A Salinick, C Jean, A Mandelis 1997 *Solid-State electron* **41** 591
[44] A Mandelis, A Othonos, C Christofides, J Bousy-Said 1996 *J Appl Phys* **80** 5332
[45] T Ikari, A Salinick, A Mandelis 1999 *J of Appl Phys* **85** 7392.
[46] S D George, P Radhakrishnan, V P N Namboodiri, C P G Vallabhan 2003 *Phys Rev B* **68** 165319
[47] S Kumar 1996 *Appl Phys Lett* **69** 23

[48] A F da Silva, T S da Silva, O Nakamura, M M F d`Aguiar Neto, I Pepe, L S Roman, E Veje 2001 *Materials Research* **4** 23
[49] J B Alvarado, M V Luna 2001 *Anal Sci* **17** S309.
[50] E Marin, I Reich, P Diaz, J J Alvarado-Gil, R Baquero, H Vargas, A Cruz-Orea, M Vargas 1998 *J Appl Phys* **83** 2604
[51] K Sakai, S Fukushima, A Fukuyama, K Usegi, I Suemune, T Ikari 2004 *IEEE Proc-Optoelectron* **151** 328.
[52] M E Rodriguez, A Mandelis, G Pan, J A Garcia, Y Riopel 2001 *Anal Sci* **17** S262.
[53] J Batista, A Mandelis, D Shaughnessy 2003 *Appl Phys Lett* **82** 4077
[54] A Mandelis, R Bleiss, F Shimura 1993 *J Appl Phys* **74** 3431
[55] L Chaed and M L Theye, D Fournier, J P Roger, A C Boccara, Y M Li, A Turner, W Paul 1991 P*hys Rev B* **43** 18
[56] N Yacoubi, C Alibert 1991 *J Appl Phys* **69** 8310.
[57] M Paulraj, S Ramkumar, K P Vijayakumar, C S Kartha, P Magudapathy, K G M Nair, B Viswanathan 2004 *Nucl Instr & Meth in Phys Res B* **222** 123
[58] A Asano, M Stutzmann 1991 *J of Non-Cryst Solids* **137/138** 623
[59] Y Maeda, A Fujishma, K Honda 1982 *Bull Chem Soc Jpn* **55** 3373
[60] A Mandelis 1990 *Anal Sci* **6** 491
[61] D Cahen 1978 *Appl Phys Lett* **33** 810.
[62] D Cahen, S D Hale 1985 *Appl Phys Lett* **46** 446
[63] I F Faria, Jr C C Ghizoni, L C Miranda, H Vargas 1986 *J Appl Phys* **59** 3294.
[64] S I Yun, B K Yun, B K Moon, H G Seo, H L Park 1985 *J Korean Phys Soc* **18** 224
[65] H L Riette, L C M Miranda, H Vargas 1987 *Appl Phys A* **44** 219
[66] S M N Mello, C C Ghizoni, L C M Miranda, H Vargas 1987 *J Appl Phys* **61** 5176
[67] H Flaisher, M Wolf, D Cahen 1989 *J Appl Phys* **66** 1832
[68] K Boubaker 2007 *Sol Energy Mater Sol Cells* **91** 1319

2

Instrumentation

Instrumentation is the most significant part of any material analysis technique. This chapter describes the instrumentation and automation of transverse photothermal beam deflection technique (PTBD) in its skimming configuration for material characterization. The PTBD unit, that measures deflection signal with appreciable sensitivity and precision, was indigenously fabricated in our laboratory. The most important components of PTBD technique include the excitation source, excitation intensity modulator, detector, signal processing unit and data acquisition system. As a part of this work, a program was developed using LabVIEW 7 for real time data acquisition and analysis, which promises greater accuracy and reliability of the experimental data. Automation of the set up has also reduced the labour involved in performing the investigations.

2.1 Introduction

Photothermal technique is a sensitive optical tool for material analysis. Transverse PTBD technique in skimming configuration has the advantages that it can be operated at room temperature and requires no predetermined experimental conditions. But the preliminary instrumentation part has to be done with extreme care and accuracy for getting reliable and reproducible data [1]. The major components of a photothermal system are:

1. Excitation source
2. Modulator
3. Detection system
4. Signal processing and analysing unit

2.1.1 Sources

Nature of application determines the type of source to a large extent. In general all photothermal systems employ modulated source of electromagnetic radiation, usually a light source, to generate modulated heating in a sample medium.

Photothermal sources fall into two main classes:

1. Broad spectral range sources
2. Lasers

Lasers are widely used because they provide well defined localized region of heating required for thermal wave probing techniques; then they have high power or pulse energy over very narrow bandwidth. Also the spatial coherence properties of laser sources enable

the light to be focussed to small area. Due to all these reasons the most commonly used broad sources and lasers (continuous wave (CW) and pulsed) and their principal characteristics are shown in table 2.1. (a) and (b) [2].

Table 2.1(a) Incoherent optical sources used in photothermal studies

Optical source	*Spectral range (μm)*	*Power*	*Comment*
Xenon lamp	*2-2.0*	*0.2 W/mm² Sr*	*High pressure arc lamp*
Globar	*2-30*	*-*	*Electric heated filament*
Nernst	*2-30*	*-*	*Electric heated*

Table 2.1(b) Coherent optical sources used in photothermal studies

Type	*Wavelength*	*Power/Energy*	*Comment*
Helium-Neon (gas)	*632.8 nm*	*0.1-50 mW*	*CW*
Ruby (solid)	*694.2 nm*	*0.03-100 J/pulse*	*Pulsed*
Carbon dioxide (gas)	*1.6 μm*	*3-100 W*	*CW*
Nd-YAG (solid)	*1.064 μm*	*0.04-600 W*	*CW*
Nd glass (solid)	*1.06 μm*	*0.15-100 J*	*Pulsed*
Argon ion	*488, 514 nm*	*5 mW-20 mW*	*CW*
Dye (liquid)	*400-900 nm*	*2-800 mW*	*CW/pulsed*
Argon fluoride (eximer)	*193 nm*	*Up to 10 W*	*Pulsed*
Hydrogen fluoride (chemical)	*2.6-3.0 μm*	*0.01-150 W or 2-600 mJ/pulse*	*CW /pulsed*
Gallium arsenide (semiconductor diode)	*780-900 nm*	*1-40 mW*	*CW*
Semiconductor diode array	*780-900 nm*	*250 mW-10 W*	*CW*
He-Cd	*325, 442 nm*	*80 mW*	*CW*

2.1.2 Modulators

Modulation of the excitation beam is essential for obtaining the PT response. There are numerous ways to modulate the intensity of a light beam. A mechanical chopper may provide the simplest method for intensity modulation in the order of 100 Hz to 1000 Hz. For high frequencies of the order of MHz to GHz, different types of electro-optic and acousto-optic modulators are usually used. Several techniques have been employed to impose a temporal variation on the optical energy applied to a sample. The modulation can be of the following types,

1. Periodic (sinusoidal or square wave)
2. Transient (short, long or finite pulse)
3. Frequency multiplexed
4. Spatially modulated

For serving the purpose various choppers are used such as mechanical choppers, direct electrical modulation, acoustic-optic modulator, electro-optic modulation. Table 2.2

presents the various modulation techniques available with their advantages and limitations.

Table 2.2 Different modulation techniques

Modulator	*Type of modulation*	*Advantage*	*Limitation*
Mechanical chopper	*Square wave modulation by rotating a sectored blade wheel*	*100% modulation depth in frequency range 1 Hz to 20 KHz*	*Frequency range limitation due to maximum motor speed in high frequency region and high phase jitter that develops at low frequency region due to poor motor performance in providing uniform rotation at very low speeds*
Direct electrical modulation	*The optical out put from sources such as CO_2 gas lasers and semiconductor lasers can be modulated directly by varying the electrical current drive*	*There is no need for separate modulator and hence the noise and low frequency jitter problems can be avoided. Pure sinusoidal or any other desired wave form can be produced*	*Modulation at high frequency cannot be achieved in gas lasers and the depth of modulation is not in all cases the 100% as achieved in mechanical choppers.*
Acoustic-optic modulator	*By spatial modulation of a laser beam by an acoustically formed diffraction grating.*	*High quality sinusoidal intensity modulation is achieved*	
Electro-optic modulator	*Modulation is achieved by changing the plane of polarization of an incoming polarised laser beam in a non linear crystal by application of a modulated electric field*	*High performance in the visible and near infrared spectral region. The depth of modulation achieved a 100% in frequency region 0-20 MHz.*	
Photo elastic modulator	*Photo elastic effect is used to vary the birefringence of optical element and modulation is achieved by polarizing the light source*	*Accurate measurement over the wide spectral range from 190 to 2100 nm.*	

2.1.3 Detection techniques

A wide choice of detection schemes to monitor the photothermal phenomena is available. After development in photothermal research several detection techniques were developed. The three general scheme of detection of thermal wave generation are: acoustic, optical and thermal. Table 2.3 shows various detection techniques available.

Table 2.3 Various detection techniques

Detection schemes	*Generation*
Photoacoustic detection [3]	*Acoustic waves generated by heating a gas layer adjacent to optically heated region is detected using microphone*
Piezoelectric detection [4]	*A piezoelectric transducer in contact with the sample senses Photoinduced thermal expansion.*
Optical beam deflection [5]	*The surface temperature gradient causes a thermal refractive index lens to be generated in the fluid adjacent to the sample surface. An optical probe beam is directed through the thermal lens and is deflected by changes in the refractive index of the thermal lens.*
Modulated optical reflectance [6]	*It probes the samples modulation of the samples optical reflectance. The probe beam reflection is measured using a photodiode*
Photothermal displacement [7]	*Thermoelastic expansion/deformation of the sample upon absorption of electromagnetic radiation is detected from the variation of reflection angle of a probe beam.*
Photothermal radiometry [8]	*The direct lattice heating of sample due to optical absorption is measured using infrared detector*
Photopyroelectric detection [9]	*The optical heating on one side of the sample is detected using a pyroelectric detector*
Photothermal interferometry [10]	*Measurement of fringe shift due to optical heating of samples*
Photothermal lens spectroscopy [11]	*Photothermal signal is derived from the lens like element produced in the sample on optical irradiation. It is detected using a probe laser.*
Photorefractive interferometry [12]	*The phase shift of a signal beam is demodulated using an active two-wave mixing photorefractive interferometer.*
Photothermal microscopy [13]	*Both lasers are focussed through a microscope and thus heating and temperature measurements are done at the micron scale.*

2.1.4 Signal Processing

Type of modulation used in generating the signal determines the method of signal recovery used in photothermal system. This forms the signal processing part of the instrumentation. For periodic modulation, Lock in amplifier is used for extracting signals contaminated with noise.

2.2 Experimental set up

Source: The different sources used for excitation of samples for the present work are shown in table 2.4. Pump beam is focused using a convex lens and directed to the centre of the sample using mirrors.

Table 2.4 Excitation sources used in the experiment

Source	*Wavelength (nm)*	*Diameter (mm)*	*Power (mW)*
He Ne [MELLES GRIOT-0430AG]	*632.8*	*0.5*	*10/15*
Solid state diode pump [COMPASS ™ 215M]	*532*	*0.32*	*20*
He-Cd [KIMMON –IK 5651R-G]	*441.5*	*1.2*	*80*

The sample cell is a cylindrical crucible fixed on XYZ translation stage and is provided with three windows for passing the pump, probe and deflected beam. The sample is mounted vertically on the sample holder and immersed into the crucible containing CCl_4. By placing the sample in the holder noise due to vibrations in room can be reduced. CCl_4 was chosen as coupling medium since it absorbs only wavelength less than 250 nm and has high temperature coefficient of refractive index ($5x10^{-4}$ K^{-1}) nearly 10^2 times higher than air ($1x10^{-6}$ K^{-1})[14]. Backing material (the substrate) and fluid are not light absorbing; hence do not contribute to heat generation. Only a relatively thin region of fluid surrounding the sample adjacent to the surface responds thermally to the periodic heat flow from the film to the surrounding fluid

The probe beam In transverse PTBD, in skimming configuration the probe beam is allowed to run parallel to sample surface at some fixed height and its deflection has two components, a normal and lateral component. A well focussed laser beam of wavelength 546.5 nm (1 mW), is allowed to graze parallel to the sample surface at a distance of ~100 μm and perpendicular to the pump beam axis.

Modulator The incident beam is square wave modulated using optical chopper (SR540). The chopper unit can chop light beam at the rate of 4 Hz to 4 KHz. A 30-slot wheel is used

for 400 Hz to 4 KHz and the 6-slot wheel for 4 Hz to 400 Hz. A BNC output is connected to the Lock in amplifier's reference input.

Detection The deflection in the path of probe beam is detected using bi-cell position sensitive detector (PSD) (EG&G, UV-140, BQ-2). A solid-state position sensitive detector can be used for monitoring the location of optical spot that is incident upon the active surface of the device. When a narrow beam of light illuminates the photosensitive strip of the PSD, two photocurrents, each inversely proportional to the distance of the spot from the far ends of the strip, are produced. The difference in photocurrents is amplified and converted to a voltage by a simple circuit.

For measuring displacements in one dimension, two types of monolithic photo detectors are commercially available. The lateral effect detector incorporates an electrically resistive layer over the active surface area of a single photodiode, with electrical contacts at either end of the layer. This type of detector is useful for measuring the centroid of an optical spot that may move across the entire photosensitive area. The other type, called the bi-cell, is sensitive to displacements that are small compared to the size of the optical spot, and is commonly used to monitor perturbations of a probe beam caused by mechanical vibration or optical misalignment. Bi-cell is suitable for sensitive detection of photothermal signals. Position sensitive detectors are used widely in photothermal deflection spectroscopy [15].

Theory The bi-cell consists of two photodiode segments manufactured from a single piece of doped semiconductor material**.** Bi-cell uses three electrical leads. One lead is common to both sides of the detector, and the other two provide separate paths for the photocurrent allowing for discrimination based on position. Both designs require electronic amplification; here there are two op-amps with feed back resistors for converting the currents produced by the photodiode segments into measurable voltages. The difference between op amp output voltages (V_2-V_1) is taken as a measure of the deflection signal. It is also possible to use the sum of the two op-amp output voltages, (V_1+V_2), as a measure of optical power, for normalization purposes. Under optimal design conditions, the dominant source of electrical output noise V_n (V), for each op-amp in the circuit is the thermal (Johnson) noise, which originates from feedback resistors.

$$V_n = \sqrt{4kTBR} \qquad 2.1$$

Where k is the Boltzmann constant ($1.38x10^{-23}$ J/K), T is the temperature (K), B is the noise bandwidth (Hz), and R is the feedback resistance (Ω).

In this type of current-to-voltage amplifier, value of the feedback resistor R is equal to the gain of the circuit in units of V/A. Therefore, the effective current measurement noise, in (A), is inversely proportional to the square root of the gain:

$$I_n = \sqrt{4kTB/R} \qquad 2.2$$

Equation 2.2 implies that maximizing the value of feedback resistors reduces electrical noise in a measurement of photocurrents. However there is practical limitation on increasing the value of R as the output of each op-amp become saturated. If a conventional PSD is used to monitor a 2 mW He-Ne laser (λ=633 nm), and the sensitivity of the detector at this wavelength is 0.33 A/W (typical for silicon photodiodes), then the photocurrent input to each op-amp is equal to 0.33 mA. An op-amp might specify a maximum output voltage of 10 V, which would limit the gain of each op-amp circuit to no more than $3x10^4$ V/A. The difference between the op-amp voltages, (V_2-V_1), is taken as a measure of the deflection signal

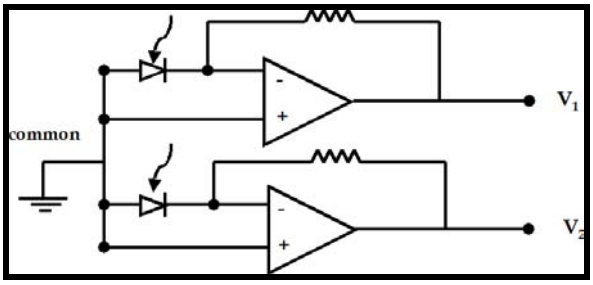

Figure 2.1 Schematic diagram for electronic amplification of a conventional bi-cell detector.

The entire set up is placed on an optical breadboard placed on a vibration isolation table and thus the noise could be reduced to a certain extend. Mechanical pointing instabilities of a probe beam contribute to noise in measurements. Using corrective detector designs can control the magnitude of this noise. Because internal electrical noise may limit the ultimate performance of these systems, it might be of value to design a laser beam-pointing stabilizer that incorporates discrete photodiode devices rather than conventional PSDs. Also a low noise detector enables the deflection measurements from an incoherent probe beam. The detector response is directly proportional to the deflection and therefore to the heat which produced this deflection. The distance between the sample and the detector was 10 cm. Deflection of 0.3 cm of the probe beam on the detector yielded amplitude of 1 volt, when observed using a cathode ray oscilloscope (CRO).

Signal processing The signal is then amplified and recorded using Dual phase Lock-in-amplifier (SR830) for making sensitive and accurate measurements. The signal is embedded with large amount of background noise and is extracted from the noise by using filtering techniques. In this work we use synchronous (Lock-in) detection, as this method is much efficient in reducing noise [1]. In synchronous detection, noise at same frequency as the signal can be rejected as the noise has random phase and Lock–in looks for signals with the same frequency and phase as the reference signal. Hence for the present studies, Lock-in-amplifier was used for measurements of amplitude and phase. The Lock-in-amplifier is interfaced with the computer using LabVIEW 7.1 via RS232 serial port for data acquisition and system control.

The schematic sketch of the entire experimental set up is shown in figure 2. 2. and figure 2.3 shows the photograph of the experimental arrangement used for this work.

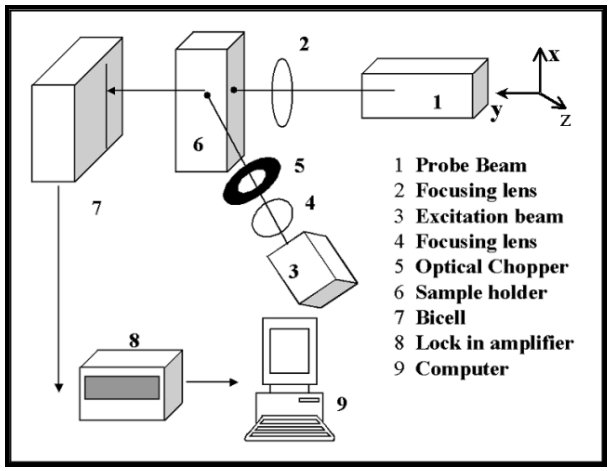

Figure 2.2: Schematic sketch of photothermal beam deflection set up

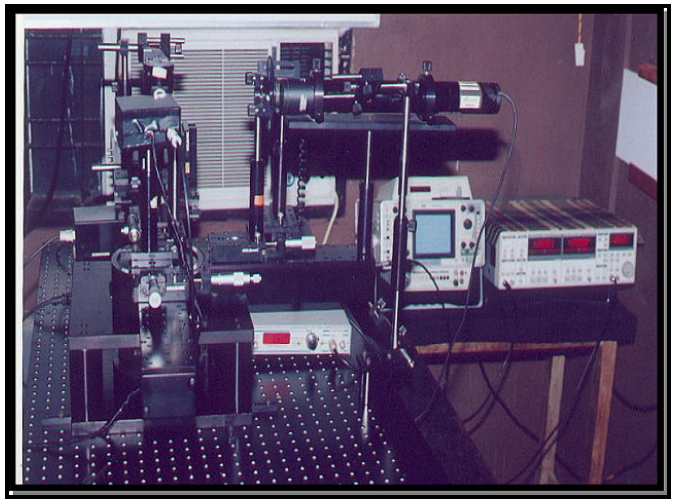

Figure 2.3: Photothermal beam deflection set up

2.3 Photothermal imaging

In 2-D photothermal imaging, the beam spot is scanned over the sample surface by moving the sample holder mounted on XYZ translation stage over an area of 100x100 mm^2. Here resolution of the image is restricted by the spot size (0.5 mm) of the illuminating beam. The photothermal signal amplitude data versus the distance scanned thus obtained is plotted. The colour contrast in the image gives information on thermal inhomogenietes in the sample. Figure 2.4 shows the photothermal image information from a semiconductor thin film. Where the regions coloured in red shade show the region high non-radiative loss and blue indicate regions of lower loss.

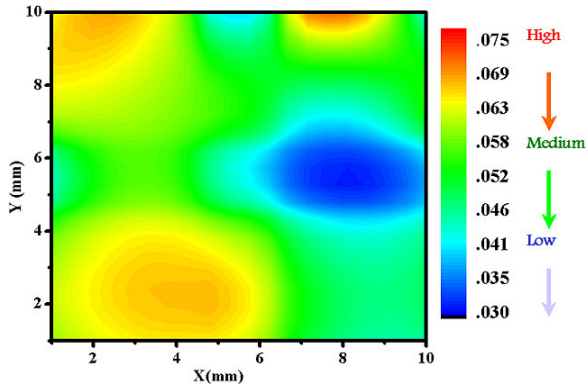

Figure 2.4 Photothermal image

2.4 Communicating with RS232

The SR830 DSP Lock-in-amplifier can be remotely programmed via either the RS232 or GPIB (IEEE- 488) interfaces. Any computer, supporting one of these interfaces, may be used to program the SR830. SR830 sends responses to only one interface. It is required to specify the output interface with the (Set Up) key or use the OUTX command at the beginning of every program to direct the responses to correct interface. Here the communication was carried out using RS232 interface. The RS232 interface, baud rate and parity must be set. These are also set with the (Set up) key. The RS232 word length is always 8 bits. Communications with the SR830 use ASCII characters. Commands may be in either upper or lower cases and may contain any number of embedded space characters. A command to the SR830 consists of a four-character command terminator. A command functions identically on GPIB and RS232. SR830 has a 250 character input buffer and processes commands in the order received. Similarly it has an output buffer to store outer outputs until the host computer is ready to receive. If either buffer over flows, both buffers are cleared and an error is reported.

2.5 Automation using LabVIEW 7

LabVIEW (Laboratory Virtual Instrument Engineering Workbench) is a powerful high-level graphical programming language from National Instruments, which integrates data acquisition, analysis and presentation in one system. It can support interfaces such as GPIB, USB, IEEE 1394, MODBUS, SERIAL, PARALLEL, IRDA, TCP, UDP, Blue tooth, NET ActiveX, SMTP, etc. LabVIEW is usually used for data acquisition, instrument control, and industrial automation on all kinds of platforms including Microsoft Windows, UNIX, Linux and Mac OS. The latest version of LabVIEW released is version 9. For this work, we have used LabVIEW version 7. The instrument control and data acquisition is carried out using RS232 and VISA (Virtual instrument software architecture). Automation of these experiments can reduce significantly the time spent by a student performing routine data collection; it also provides digitized formats that lend themselves to easy display, analysis,

and comparison of data. The acquired data in both cases can be saved to a text-delimited file, permitting detailed data analysis and display using software packages such as ORIGIN and MATHEMATICA. However LabVIEW programs can be written to analyze the acquired data and calculate various results. This enables us to get the measurement analysis and report soon after completing the data acquisition thus obtains fast results. Our LabVIEW program was developed for simultaneous measurement of signal amplitude, phase and modulation frequency. The step resolution can be varied in accordance with experimental requirements; the lower limit (1 Hz) is set by the optical chopper. Time given for collection of single data is 0.5 s and hence large number of data can be collected in a short span of time. This allows us to repeat the experiment any number of times without much loss of time and averages the results for accurate data analysis. Front panel (Figure 2.5) has control for on, off and pause. Moreover it shows the step count, chopping frequency, signal amplitude and phase. The panel also depicts three graphs (Figure 2.5) 1) signal amplitude versus chopping frequency, 2) signal phase versus chopping frequency and 3) Log_e (signal amplitude) versus (chopping frequency) $^{1/2}$. Figure 2.6 show the block diagram panel, which represents the graphical programming done for developing the driver for SR830.

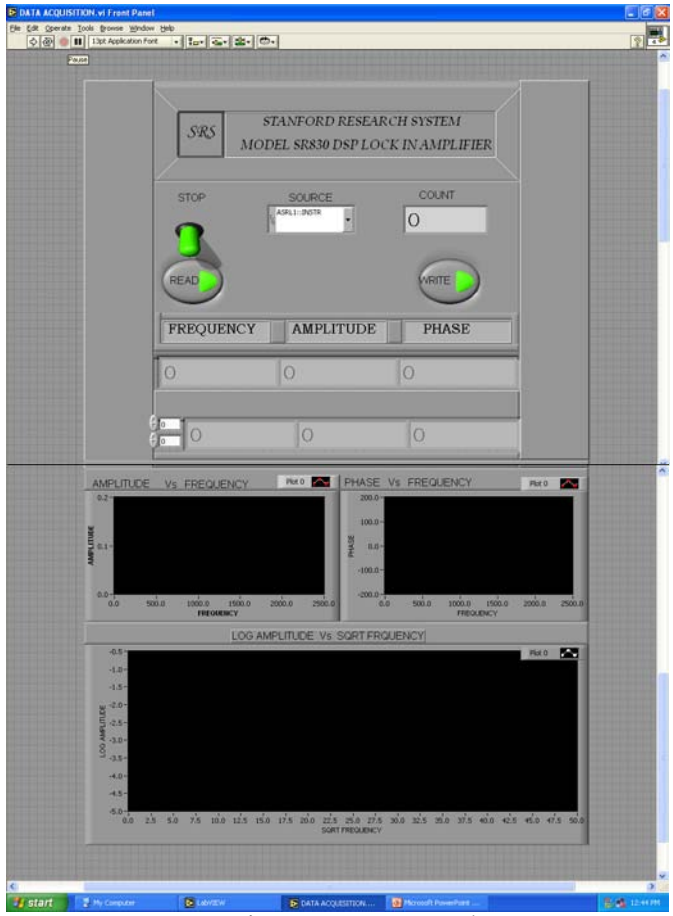

Figure 2.5 Front panel

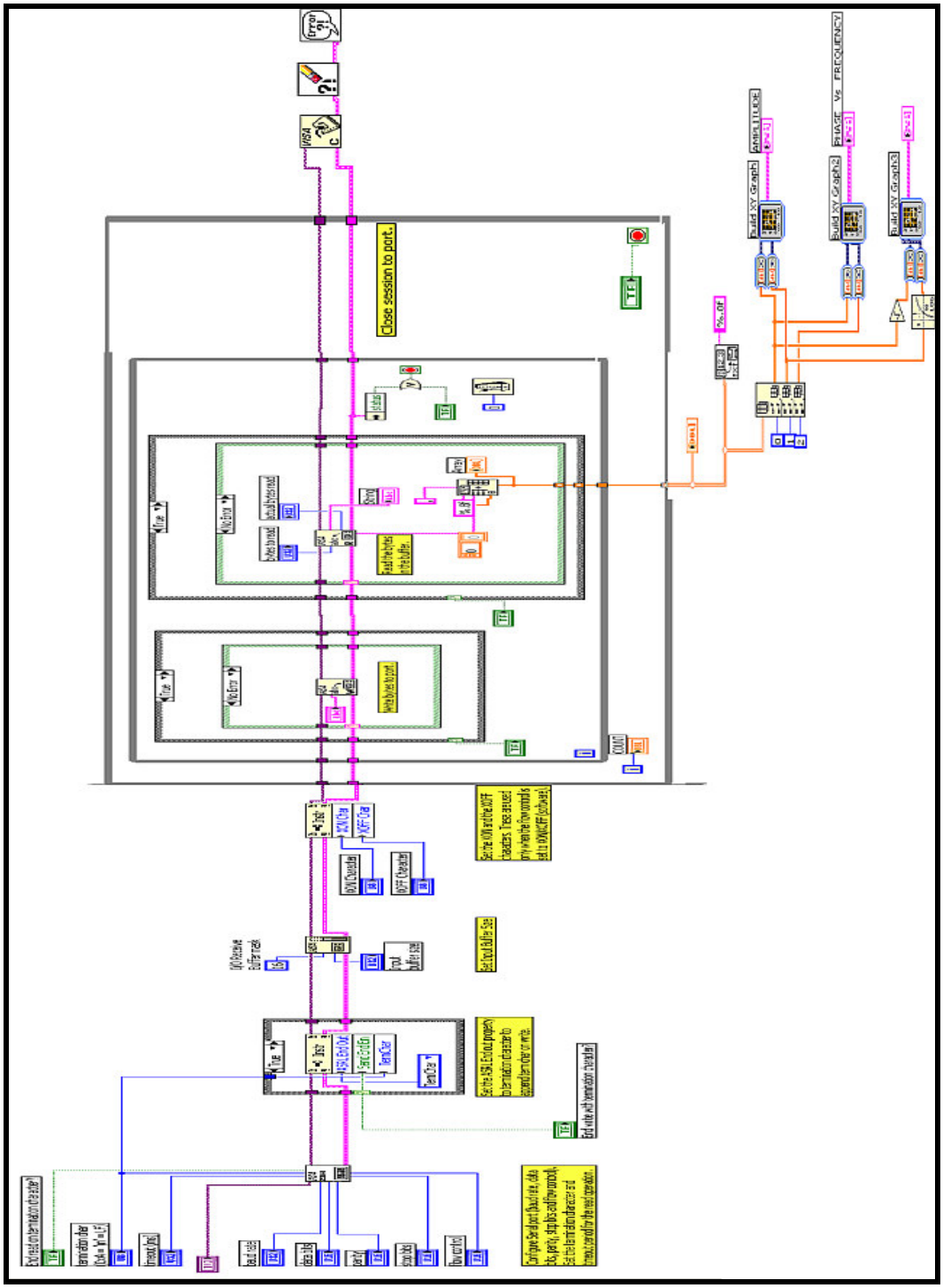

Figure 2.5 Block diagram panel (graphical programming language)

2.6 Conclusion

This chapter describes layout and technical details of the PTBD technique used for material analysis. PTBD technique was successfully automated using LabVIEW and used for data acquisition and analysis.

Reference

[1] S Ramkumar 2006 *PhD Thesis* Cochin University of Science and Technology, India
[2] D P Almond, P M Patel 1996 *Photothermal Sciences*, Chapman & Hall publications, London
[3] A G Bell 1880 *Am J Sci* **20** 305
[4] M M Farrow, R K Burnham, M Auzanneau, S L Olsen, N Purdie, E M Eyring 1978 *Appl Opt* **17** 1093
[5] G Meyer, N M Amer 1988 *Appl Phys Lett* **53** 2400
[6] J Opsal, M W Taylor, W L Smith, A Rosencwaig 1987 *J Appl Phys* **61** 240
[7] M A Olmstead, N M Amer, S Kohn, D Fournier, A C Boccara 1983 *Appl Phys A* **32** 3
[8] P E Nordal, S O Kanstad 1979 *Phys Scripta* **20** 659
[9] A Mandelis, M Zver 1985 *J Appl Phys* **57** 4421
[10] Z Sodnik, H J Tiziani 1986 *Opt Commun* **58** 295
[11] A Chartier, S E Bialkowski 1997 *Opt Eng* **36** 2303
[12] H Tuovinena, S Krishnaswamy 1998 *Appl Phys Lett* **73** 2236
[13] M Harada, M Shibata, T Kitamori, T Sawada 1995 *Anal Chim Acta* **299** 343
[14] W B Jackson, N M Amer, A C Boccara, D Fournier 1981 *Appl Opt* **20** 1333
[15] J D Spear, R E Russo 1996 *Rev Sci Instrum* **67** 2481

3

Theoretical background

Theoretical modelling forms a major segment of material investigation using PTBD technique. Theory introduced by Rosencwaig and Gersho explains the origin and diffusion of thermal waves due to photothermal effect in solids and gases. Later this basic model was modified for explaining the photothermal signal generation in semiconductors due to additional non-radiative heat sources. With these two models as foundation, in the present work, a one-dimensional theoretical model was structured that explains both the origin and propagation of thermal waves in semiconductor thin films. This suits the analysis using transverse PTBD technique in skimming configuration. The reliability and accuracy of this theory was proven from the studies done on crystalline silicon.

3.1 Outcome of theoretical studies

"Mirage effect" or Photothermal beam deflection (PTBD) phenomenon deals with bending of a light beam due to the thermal gradient in the medium through which it travels. Due to lack of satisfactory theoretical explanations, this effect remained dormant for a long period without any commendable application. A strict mathematical interpretation of thermal wave propagation in solids is essential to give a good theoretical explanation of the experimental results observed using photothermal phenomenon and for the retrieval of the necessary information related to material properties. The interest in this area was revived by Rosencwaig et al [1], which resulted in the development of 'photoacoustic' technique for spectroscopic investigation of solid and semisolid materials. This theoretical model gave sufficient explanation for generation and propagation of thermal wave and this led to the boom of several photothermal detection techniques with wide spread applications.

Transverse PTBD technique, in skimming configuration, where the probe beam propagates perpendicular to the pump beam and at a fixed distance from the sample surface, has been widely studied by several groups [2-5] since past three decades. Table 3.1 gives a review of theoretical works done in photothermal deflection spectroscopy for analysis of solids, fluids and gases since 1980.

Table 3.1 A brief review of theoretical studies for material analysis using photothermal technique

Theoretical model	*Application*	*Authors*	*Year*
1. Theory developed to measure the spatial and angular dependence of the optically detected signal.	*Determine the temperature dependent thermal diffusivity of gases. Also accounts for microwave absorption in liquids*	*J C Murphy and L C Aamodt* [6]	*1980*
2. Solution for many one-dimensional problems in heat conduction by extension of flash method to step irradiation using Laplace transform method	*For determination of thermal diffusivities for temperature rise followed quite small time t.*	*Hubert M James* [7]	*1980*
3. One dimensional model for depth profiling	*Deriving expression for temperature distribution at surface and thermal response beneath surface layers.*	*Jon Opsal & Allen Rosencwaig* [8]	*1982*
4. One-dimensional theory that determines the temperature and carrier distribution throughout the entire solid and accounts for the deflection amplitude and phase	*To measure the transport properties within the bulk and surface of semiconductor*	*Fournier et al* [9]	*1985*
5. Theoretical analysis of amplitude and phase signal to locate surface states	*Measure absorption of surface states aswell as of buried interface states*	*U Zammit et al* [10]	*1990*
6. Theoretical studies of AC photothermal and AC electro thermal responses of semiconductor p-n junction devices.	*Can identify the major energy losses in p-n junction devices*	*Shu-Yi Zhang & Jian-Chun Cheng* [11]	*1991*
7. A Three dimensional theoretical model that accounts for photothermal deflection effect of semiconductor samples at high modulation frequency.	*For measuring the thickness of transparent and opaque films with high spatial resolution*	*Jian-chun Cheng et al* [12]	*1991*

8. Theoretical model of behaviour of mirage effect with probe beam propagating through a transparent solid	*For determining the effective value of dn/dT*	*Jonathan D Spear et al* [13]	*1991*
9. Three dimensional thermal conduction equation in an anisotropic medium using Fourier transform	*Thermal conductivity tensor measurement of polymer crystal*	*Xavier Quelin et al* [14]	*1993*
10. The dependence of the deflection signal on an external bias voltage in the closed circuit and on additional bias illumination in the open circuit case is simulated	*Contact characterization of electronic transport in solar cells*	*P Grunow & R Schieck* [15]	*1994*
11. Model for depth profiling using phase data	*The surface problems are over come by reconstructing the depth profile from photothermal phase data*	*T T N Lan & H G Walther* [16]	*1996*
12. Theoretical analysis to obtain the electron and phonon temperature distributions in the sample as function of both time and position.	*Deduce information on electron and phonon parameters.*	*G Gonzalez & Yu G Guevich* [17]	*1996*
13. A three-dimensional theoretical model for fundamental and harmonic response generation as a result of periodic heating of a layered structure consisting of an upper thin non linear layer in intimate contact with a semi-infinite linear substrate.		*Andreas Mandelis* [18]	*1998*
14. Numerical simulation of photothermal effects in solid with inhomogeneous thermal properties	*Calculation of surface temperature in thermally inhomogeneous solids*	*S Galovic et al* [19]	*1999*
15. Error analysis in reconstruction as a function of depth and noise by neural network approach.		*C Glorieux et al* [20]	*1999*

16. Genetic algorithms were used for photothermal depth profiling	*Determination of thermal conductivity depth profile in inhomogeneous samples*	*Roberto Li Voti* [21]	*2001*
17. Theoretical model for thermal wave back scattering is used for photothermal depth profiling in inhomogeneous materials.	*Reconstruction of thermal diffusivity depth profile for various sample treatments*	*Roberto Li Voti et al* [22]	*2001*
18. Damaged based theoretical modelling that combines quantum mechanics based calculation of the ion-induced damage depth profiles	*Determination of thermal and carrier plasma parameters and calculation of the photothermal response from a multilayer sample.*	*Alex Salnick & Jon Opsal* [23]	*2001*
19. Theoretical model for thermal wave produced by periodic heat generation in homogeneous and inhomogeneous solids	*Calculation of effective thermal conductivity and effective thermal diffusivity in two layer structures*	*Yuriy G Gurevich et al* [24]	*2002*
20. Theory on conduction of heat in solids taking into account the relaxation time needed for the onset of heat flux which leads to a second derivative in heat diffusion equation	*Proves existence of a critical modulation frequency at which heat flux changes its diffusive character to a wave propagation process with the velocity of sound. Evidence is provided for possibility of detecting second sound in solids*	*E Marin et al* [25]	*2002*
21. A diffraction theory of continuous wave photothermal deflection spectroscopy with fundamental and second harmonic responses.	*Measure thermal and optical properties of thin films and bulk and layered-structure materials.*	*Jianhua Zhao et al* [26]	*2002*
22. Theoretical model for thermal waves with analysis for boundary conditions, thermal wave attenuation in a non-dissipate medium. Evaluated the physical meaning of reflected thermal wave and reason for thermal wave attenuation	*Calculation of effective thermal conduction and effective thermal diffusivity in two layer structures*	*Y G Gurevich et al* [27]	*2003*

23. Theoretical model for a three layered to describe thermal conduction in ceramic samples taking into account the thermal resistance between grain boundaries	*Measure thermal properties of alumina ceramic materials and investigation of their thermal shock behaviour*	*Bincheng Li & Andreas Mandelis* [28]	*2004*
24. Theoretical model based on both conduction and radiation for steel sample heated by guassian pulsed beam.	*A new calculation method devised to build up isothermal generative lines in the vicinity of targeted surface*	*Karem Boubaker* [29]	*2004*
25. A three dimensional model for deriving the expression for temperature distribution function and photothermal deflection of probe beam based on greens function and integral transformation	*Determine effective thermal length and deflection signal and its variation with modulation frequency. It is also shown that focal length of photothermal lens in normal direction is much greater than that of in tangential direction*	*M Soltanokotabi and M H Naderi* [30]	*2004*
26. General boundary conditions for thermal diffusion equation to include surface thermal conductivity, surface thermal capacity and surface capacity thermal impedance.	*Measurement of surface thermal conductivity, surface thermal capacity and thermal impedance*	*G N Logvinov et al* [31]	*2005*
27. Theory and mathematical analysis for frequency modulated thermal wave imaging	*To obtain phase images that brings out layer by layer information of the sample*	*Ravibabu Mulaveesala et al* [32]	*2006*
28. Diffraction theory for transverse photothermal deflection spectrometry	*Measurement of thermo physical and mass-diffusion properties of gases*	*J H Rohling et al* [33]	*2008*

3.2 Photothermal effect in solids

Primary source of photothermal signal arises due to the periodic heat flow from solid to its surrounding as the solid is heated using a modulated light. Only a relatively thin layer of medium (0. 2 cm for a chopping rate of 100 Hz) adjacent to the surface of the solid responds thermally to the periodic heat flow from the solid. This is a diffusive process that produces a periodic temperature distribution and the amplitude of the signal thus generated depends on the quantity of the heat emanating from the illuminated sample; there is a close correspondence between the strength of the signal and the amount of light absorbed.

Photothermal signal amplitude also depends on the sample's overall light absorption irrespective of whether it is volume or surface related. On other hand, photothermal phase signal depends also on the localization of the absorption. In fact, in an absorbing sample, the light absorbed in part or in the entire sample volume acts as an effective centre of heating source, whose position depends on the sample optical absorption depth, ($\mu_\beta=1/\beta$) of the sample and thermal diffusion length, ($\mu = 1/a$). Farther the position of this centre from the sample front surface, the greater will be the phase lag (the smaller the phase value) with respect to a reference signal. When the bulk absorption only is involved, the centre of the source will be located somewhere in the sample volume and this will correspond to a definite phase value. If surface states are also present on the sample front or rear surface or even buried within the sample volume, position of the "centre" shifts towards the absorbing layer and the phase value will correspondingly change. From a simultaneous analysis of both the photothermal signal amplitude and phase, it is possible to locate the eventual presence of surface states and to measure their absorption.

3.3 Theoretical approach

Photothermal beam deflection theory shows that the transverse deflection from the original trajectory of the probe beam depends on the thermal gradients in the direction orthogonal to the path only according to the well-known formula, which, in geometric optics, is written as,

$$\Phi = \frac{1}{n_{air}}\left(\frac{dn_{air}}{dT}\right)\int_{path}\Delta_t T_{air}(x,y,z)ds \qquad 3.1$$

Where n_{air}, dn_{air}/dT represent the air refractive index and the optothermal parameter respectively, T_{air} is the temperature rise in air, and Δ_t is the gradient transverse to the probe paths.

A one-dimensional model of heat flow in the cell resulting from the absorbed light energy was put forth by Rosencwaig et al [1] for measuring the signal generated in photoacoustic technique. Later in 1990, U Zammit et al [10] developed a 1-D theoretical model for analysis of photothermal deflection signal amplitude and phase. According to this theory any light absorbed by the solid is converted, in part or whole, into heat by non-radiative deexcitation processes within the solid. The general 1-D expression for deflection signal [S] for a compact photothermal defection spectroscopy assembly with CCl_4 as coupling medium is given by,

$$S = T_r = \left(\frac{1}{n_0}\right)\frac{dn}{dT}\,l\,\frac{dT(z_0)}{dz}e^{i\omega t} \qquad 3.2$$

Where T_r is the transducer factor, $(1/n_0)(dn/dT)$ is the relative index of refraction change with temperature of the deflecting medium, l is the interaction length, z_0 is the distance of the probe beam

from the sample surface, and $T(z)=T_0 e^{-\sigma_m z}$ *is the ac temperature rise above the average temperature in the deflecting medium, where* $\sigma_j=(1+i)\,a_j$, $a_j=(c_j\rho_j\omega/2k_j)$, *j=1, 2, m, b; Subscripts 1, 2, m and b refer, respectively, to sample top layer (the layer close to probe laser beam), the bottom layer, the deflecting medium and backing material.* ρ_j *the densities,* c_j *the specific heats,* k_j *the thermal conductivities,* ω *is the modulation frequency in rad/s.*

3.4 One-dimensional model for calculating temperature distribution in solids (R-G theory)

One dimensional sample geometry for a three layer (fluid-sample-backing) model is shown in figure 3.1, where *f* is the coupling fluid, *s* is the optically absorbing sample layer, and *b* is the backing material. In this model it was assumed that the system extends infinitely in *XY*-direction, and the heat diffusion along *z*-direction is alone considered.

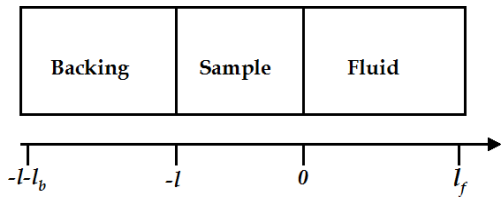

Figure 3.1 Sample geometry of 1-D model

The absorbing sample is uniformly irradiated by a modulated plane wave, whose intensity is,

$$I=\frac{I_o}{2}(1+\cos\omega t) \tag{3.3}$$

Where I_o *is in* W/cm^2

Considering that backing and fluid are supposed to be optically transparent, the heat diffusion equations in the three different regions (fluid, sample and backing) is,

$$\begin{aligned}
&\frac{\partial^2 T_f(z,t)}{\partial z^2}=\frac{1}{\alpha_f}\frac{\partial T_f}{\partial t}, && \text{Re } gion \quad I \quad 0\le z\le l_f\\
&\frac{\partial^2 T_s(z,t)}{\partial z^2}=\frac{1}{\alpha_s}\frac{\partial T_s}{\partial t}-\frac{\beta\eta I_0}{2k_1}e^{\beta z}\left(1+e^{i\omega t}\right) && \text{Re } gion \quad II \quad -l\ \le z\le 0\\
&\frac{\partial^2 T_b(z,t)}{\partial z^2}=\frac{1}{\alpha_b}\frac{\partial T_b}{\partial t}: && \text{Re } gion \quad III \quad -l-l_b\le z\le -l
\end{aligned} \tag{3.4}$$

With the following boundary conditions:

$$\begin{aligned}
&T_f(z=0)=T_s(z=0)\\
&T_s(z=-l)=T_b(z=-l)\\
&T_f(z=l_f)=T_b(z=-(l-l_b))=0
\end{aligned} \tag{3.5}$$

$$k_f \frac{dT_f}{dz}(z=0) = k_s \frac{dT_s}{dz}(z=0)$$
$$k_s \frac{dT_s}{dz}(z=-l) = k_b \frac{dT_b}{dz}(z=-l) \quad 3.6$$

With l_f and l_b being much larger than lengths on which the periodic heat diffuses. *T (z, t)* is the temperature field. The term *A exp (a, z)(1+expjωt)* represents the modulated heat source due to light absorbed by the sample whose optical coefficient is α,

$$A = \frac{\alpha I_0 \eta}{2k_s} \quad 3.7$$

Where η is the light-heat conversion efficiency by non-radiative de-excitation processes

The solution of these equations will lead to temperature field that will contain both static and periodic steady as well as transient solutions. Here importance is given only to determination of steady periodic solution, which is needed for photothermal signal analysis. The thermal waves propagate in the system with a wavelength $2\pi\mu_i$ and a speed $(2\omega D_i)^{1/2}$.

Where μ_i is called the thermal diffusion length and characterizes the length upon which the heat diffuses during a period ($T=2\pi/\omega=1/f$), $\mu_i=(D_i/\pi f)^{1/2}=(2D_i/\omega)^{1/2}=(2k_i/\rho_i c_i \omega)$

The complex amplitude of modulated temperature *T (z)* in three regions is thus given by:

$$T(z) = T_s e^{(-\sigma_f z)}$$
$$T_s(z) = Ue^{(\sigma_s z)} + Ve^{(-\sigma_s z)} - Ee^{\alpha z} \quad 3.8$$
$$T_b(z) = We^{(\sigma_b (z+l))}$$

With

$$T_s = E\frac{(r-1)(1+b)\exp(\sigma_s l) - (r+1)(b-1)\exp(-\sigma_s l)}{D} + \frac{2(b-r)\exp(-\alpha l)}{D}$$
$$W = E\frac{2(r+g) - \exp(-\alpha l)[(r+1)(1+g)\exp(\sigma_s l) + (r-1)(1-g)\exp(-\sigma_s l)}{D}$$
$$U = E\frac{(r+g)(1+b)\exp(\sigma_s l) - (r-b)(1-g)\exp(-\alpha l)}{D} \quad 3.9$$
$$V = E\frac{(r+g)(1-b)\exp(-\sigma_s l) - (r-b)(1+g)\exp(-\alpha l)}{D}$$

$$D = \exp(\sigma_s l)(1+g)(1+b) - \exp(-\sigma_s l)(1-g)(1-b)$$
$$E = +\frac{\alpha I_0}{2k_s\left(\alpha^2 - \sigma_s^2\right)}$$
$$b = \frac{k_b \sigma_b}{k_s \sigma_s} \qquad 3.10$$
$$g = \frac{k_f \sigma_f}{k_s \sigma_s}$$
$$r = \frac{\alpha}{\sigma_s}$$

Usually measurements are achieved by using a probe beam propagating in the transparent fluid in contact with the sample surface. Thus the temperature field along the probe beam path is function of both surface temperature $T_S\ (0)$ and sample surface to probe beam distance ($e^{-\sigma_f z}$).

The complex amplitude of the surface temperature is given by,

$$T_S(0) = \frac{\alpha I_0}{2k_s\left(\alpha^2 - \sigma_s^2\right)} \times \frac{(r-1)(b+1)\exp(\sigma_s l) - (r+1)(b-1)\exp(-\sigma_s l) + 2(b-r)\exp(-\alpha l)}{(\exp(\sigma_s l)(1+g)(1+b) - \exp(-\sigma_s l)(1-g)(1-b))} \qquad 3.11$$

3.5 Photothermal effect in semiconductors

When a semiconductor material is illuminated with photons of sufficient energy, electron-hole pairs are generated which diffuse through the crystal from their place of generation to regions of lower excess pair concentration. Each pair transports energy approximately equal to the band separation, thus contributing to the thermal conductivity. This energy is deposited where the pair undergoes non-radiative recombination increasing the local measurable temperature of the lattice. A non-uniform temperature distribution is therefore established in the sample which depends on the nature of the incident radiation, on the characteristics of optical absorption, on the boundary conditions for temperature and energy flux, and on the ordinary thermal conductivity of the material. Thus establishment of a temperature distribution in a solid by optical excitation, diffusion and recombination of carriers and the attendant modification in thermal conductivity is called "photothermal effect".

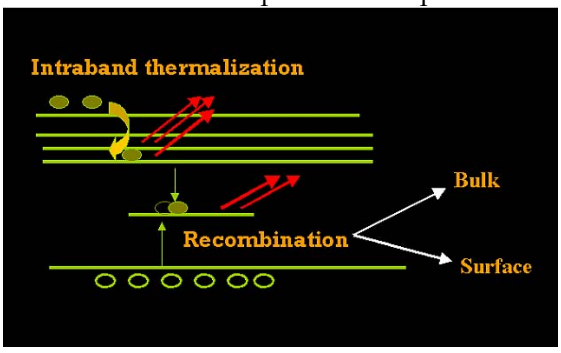

Figure 3. 2 Photothermal effect in semiconductors

3.6 One-dimensional theoretical model for photothermal signal generation from semiconductors

Earlier only thermal diffusivity of semiconductors was measured, using signal amplitude as function of modulation frequency. Fournier et al extended this approach of photothermal deflection technique to probe transport properties of semiconductors, such as the thermal diffusivity, the electronic diffusivity, the excess carrier lifetime, and surface recombination velocity. It is an extension of the photothermal deflection technique mentioned above (Sec 3.4) and has advantages that it yields both thermal and electronic transport parameters within the bulk of a semiconductor and also at the surface or at an interface.

An intensity modulated light beam generates a periodic thermal wave due to the optical heating, and in the case of semiconductors the incident light also generates a photo excited carrier population. The thermal wave will propagate into the solid according to usual diffusion process creating a thermal gradient. The photo excited minority carriers will also diffuse away from the surface layer where they are generated and set up population gradient determined by the electronic diffusion, the recombination kinetics (ie., lifetime), and the surface recombination. The recombining carriers will further influence the thermal gradient. Both the thermal gradient and the free carrier gradient will induce a change in the local index of refraction of the solid, which can be probed in situ by the deflection of a probe beam propagating through the fluid adjacent to surface of the solid. Since the changes in the index of refraction are directly related to various transport properties, (namely the thermal and electronic diffusivities, the minority carrier lifetime, and the surface recombination velocity), these parameters can be determined from the dependence of the deflection on modulation frequency.

A one-dimensional theory, which predicts deflection amplitude and phase, allowing the measurement of the transport parameters is demonstrated. A one-dimensional treatment is sufficient since in this case the pump beam, whose dimensions are much larger than both the thermal diffusion and carrier diffusion lengths, uniformly illuminates the front face. In addition, the probe beam is focussed and centred well away from the adjoining sides. In order to calculate the resulting deflection, it is necessary to determine the temperature distribution and the carrier distribution throughout the solid. Time dependent deflection of narrow probe beam propagating through an inhomogeneous medium at depth x is given by,

$$\Theta(x,t) = \frac{l}{n}\frac{\partial n(x,t)}{\partial x} \qquad 3.12$$

Where Θ is the angular deflection, l is the interaction length (l >x, and also much larger than both thermal and carrier diffusion lengths), n is the local index of refraction, and dn (x,t)/dx is the photoinduced gradient in the index of refraction.

In the case of semiconductors, *dn (x,t)/dx* has two contributions, one is thermal and other is free carrier term. This is given by,

$$\frac{\partial n(x,t)}{\partial x} = \frac{\partial n}{\partial T}\frac{\partial T(x,t)}{\partial x} + \frac{\partial n}{\partial N}\frac{\partial N(x,t)}{\partial x} \qquad 3.13$$

Where T (x,t) and N(x,t) are time dependent temperature and the minority carrier density distribution, respectively.

The thermal term has two components; one is due to thermal wave from the surface heating, which includes the immediate thermalization of carriers to band gap, and the second one is due to the thermal energy released by non-radiative recombination of photo excited carriers which have diffused into the semiconductor. The thermal term is weakly dependent on the probe beam wavelength. The free carrier term, on other hand, depends strongly on the probe beam wavelength. Here the term due to index of refraction variations is associated with light-induced excess carriers.

3.6.1 Thermal contribution

Equation describing the thermal contribution follows from standard heat diffusion equation with a source term due to carrier recombination and a surface source boundary condition**.**

$$D_{th}\frac{d^2T}{dx^2} = \frac{dT}{dt} - \frac{E_G D_{th}}{k}\frac{N(x,t)}{\tau}, \qquad 3.14$$

With the boundary conditions

$$\begin{aligned} &T(x,0) = 0, \\ &-k\frac{dT}{dx}(0,t) = sN(0,t)E_G + \frac{h\nu - E_G}{h\nu}\phi_o e^{i\omega t} \end{aligned} \qquad 3.15$$

Where D_{th} is the thermal diffusivity (cm^2/s), k is the thermal conductivity (W/cm K), E_G is the semiconductor gap energy (J), $h\nu$ is the photon energy (J), ϕ_o is the light flux (W/cm^2), s is the surface recombination velocity (cm/s), and τ is the minority carrier lifetime (s).

3. 6.2. Free carrier contribution

The carrier population distribution is given by the non-homogeneous diffusion equation,

$$D\frac{d^2N}{dx^2} = \frac{dN}{dt} + \frac{N}{\tau} \qquad 3.16$$

Here the boundary conditions are,

$$N(x,0)=0$$
$$D\frac{dN}{dx}(0,t)=-\frac{\phi_o}{h\nu}e^{i\omega t}+sN(0,t) \tag{3.17}$$

Where D is the minority carrier diffusion (cm²/s).

The steady state solution for the temperature distribution is given by,

$$T(x,t)=\mathrm{Re}\left(\begin{array}{l}\dfrac{(\phi_o E_G/\lambda_{el})\left(\dfrac{e^{-x/\lambda_{th}}}{1/\lambda_{th}}-\dfrac{e^{-x/\lambda_{el}}}{1/\lambda_{el}}\right)e^{i\omega t}}{h\nu\tau Dk(s/D+1/\lambda_{el})[1/\tau D+i(\omega/D)-i(\omega/D_{th})]} \\ +\left(\dfrac{\phi_o E_G s}{h\nu Dk(s/D+1/\lambda_{el})}+\dfrac{(h\nu-E_G)\phi_o}{h\nu k}\right)\lambda_{th}e^{-x/\lambda_{th}}e^{-i\omega t}\end{array}\right) \tag{3.18}$$

Where

$$1/\lambda_{th}=\sqrt{i\omega/D_{th}}\quad 1/\lambda_{el}=\sqrt{(1+i\omega\tau)/D\tau} \tag{3.19}$$

Which yields the thermal gradient

$$\frac{dT}{dx}(x,t)=\mathrm{Re}\left[\begin{array}{l}\left(\dfrac{\phi_o E_G/\lambda_{el}}{h\nu Dk(s/D+1/\lambda_{el})[1/\tau D+i(\omega/D-\omega/D_{th})]}\right)Xe^{-x/\lambda_{el}}e^{i\omega t} \\ -\left(\begin{array}{l}\dfrac{\phi_o E_G/\lambda_{el}}{h\nu\tau Dk(s/D+1/\lambda_{el})[1/\tau D+i(\omega/D-\omega/D_{th})]} \\ +\dfrac{\phi_o E_G s}{h\nu Dk(s/D+1/\lambda_{el})}+\dfrac{(h\nu-E_G)}{h\nu}\dfrac{\phi_o}{k}\end{array}\right)e^{-x/\lambda_{th}}e^{i\omega t}\end{array}\right] \tag{3.20}$$

For minority carrier distribution, one obtains

$$N(x,t)=\mathrm{Re}\left(\frac{\phi_o e^{-x/\lambda_{el}}}{h\nu(s/D+1/\lambda_{el})}e^{i\omega t}\right) \tag{3.21}$$

And for the refractive index gradient

$$\frac{dN}{dx}(x,t)=\mathrm{Re}\left(\frac{-\phi_o/\lambda_{el}}{h\nu(s/D+1/\lambda_{el})}e^{-x/\lambda_{el}}e^{i\omega t}\right) \tag{3.22}$$

Then equations (3.20) and (3.22) can be combined to get

$$\frac{dn}{dx} = \left[C_1^{th}\right] e^{-x/\lambda th} + \left[C_2^{th}\right] e^{-x\sqrt{(1+i\omega\tau)/D\tau}} + \left[C_3^{FC}\right] e^{-x/\lambda_{el}} \qquad 3.23$$

Where C_1^{th} and C_2^{th} are coefficients of thermal contribution and C_3^{FC} is the coefficient for the free carrier contributions.

There are several important physical implications: -

i) The deflection has an exponential dependence on the depth away from the illuminated face, and also an exponential dependence on the square root of the modulation frequency of the pump beam illumination. This decay is characterized by the complex thermal and electronic diffusion lengths λ_{th} and λ_{el}, respectively.

ii) There are two contributions to the deflection, one from the thermal effects and one from the photo-excited carriers. The thermal term has 2 components - thermal and electronic. The latter is due to the thermal energy released by minority carrier recombination. The thermal and electronic regimes are clearly seen at low and high modulation frequencies, respectively. At low frequencies, term 1 dominates as ω goes to zero, since $D > D_{th}$; the electronic behaviour dominates at high frequencies through term 2 and term 3. The third domain is for intermediate frequencies, where there is a complex interaction, which is highly sensitive to the carrier lifetime and surface recombination velocity.

We employed this model for determining the mobility of the carriers successfully; but the theory was futile when applied for determination of surface recombination velocity and minority carrier lifetime. Hence a one-dimensional theoretical model was developed taking into consideration our experimental limitations and properties of sample under investigation.

3.6.3 Determination of thermal diffusivity and minority carrier mobility

The mobility was measured as presented by Fournier et al [9] and Paulraj et al [34] from the slope of curve in plot of Log_e (signal amplitude) versus (chopping frequency) $^{1/2}$. From equation 3.23, we can determine thermal diffusivity and electronic diffusivity at different frequency regimes

- ***i)*** Thermal diffusivity from low frequency regime
- ***ii)*** Electronic diffusivity from high frequency regime

i) For low frequencies $\omega\tau < 1$, $\lambda_{el} \rightarrow (D\tau)^{1/2}$ while λ_{th} increases. Hence, the thermal properties dominate. If in addition, $\omega\tau < D_{th}/D$, then equation 3.23 reduces to,

$$|signal| \infty \left|\frac{dn}{dx}\right| = const\ e^{-x\sqrt{\omega/2D_{th}}}$$
$$\log_e \left|\frac{dn}{dx}\right| = const - x\sqrt{\omega}\left(\frac{1}{\sqrt{2D_{th}}}\right) \quad 3.24$$

Thus D_{th} can be determined from the slope of $\log_e$ (signal amplitude) versus (chopping frequency) $^{1/2}$ in the low frequency regime (Figure 3.3).

ii) In the limit of high frequencies, $\omega\tau > 1$, $\lambda_{el} \rightarrow (D/i\omega)^{1/2}$, and the electronic properties dominate and equation 3.23 reduces to,

$$\left|\frac{dn}{dx}\right| = const\ e^{-x\sqrt{\omega/2D}} \quad 3.25$$

Thus D can be determined from the slope of loge (signal amplitude) versus (chopping frequency) $^{1/2}$ in high frequency regime (figure 3.3). Thus mobility can be determined from Einstein's relation using equation 3.26.

$$D = \frac{kT}{e}\mu \quad 3.26$$

Where μ is minority carrier mobility

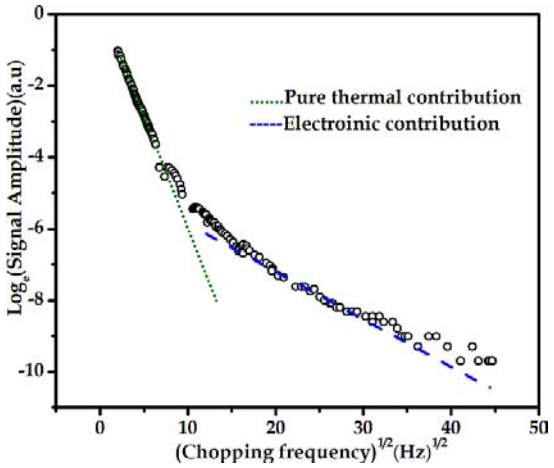

Figure 3.3 Plot to determine thermal diffusivity and mobility

3. 7 One-dimensional theoretical model for photothermal wave generation and propagation in semiconductor thin films

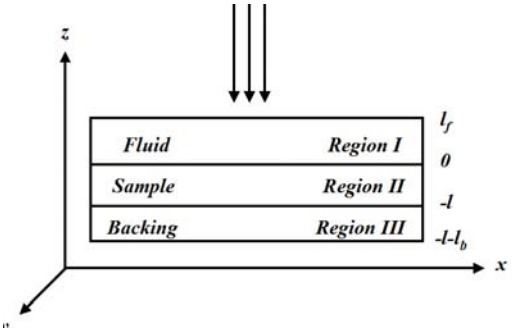

Figure 3. 4 Three-layer sample geometry (backing-sample-fluid)

Theoretical model for photothermal analysis of semiconductor put forth by U Zammit et al [10] does not include non-radiative recombination and surface recombination processes taking place in the semiconductors and the model given by Fournier et al [9] does not suit the three layer sample geometry with fluid, sample and backing layer; hence the present model was extended to suit the transverse photothermal beam deflection technique with three-layer sample geometry, assuming the sample to be a semiconductor thin film. Accuracy of the measurement technique can be improved by further refinement of the theoretical model. We applied this technique for simultaneous measurement of minority carrier lifetime, surface recombination velocity and thermal diffusivity of semiconductor thin films. This technique has further scope for improvement as it can be extended into large area applications as well.

Let us consider the three-layer sample model geometry as shown in figure 3.4. The sample under investigation is irradiated with an intensity modulated laser beam with angular frequency $\omega_{mod} = 2\pi f$, where f is the modulation frequency. Intensity of the laser beam is given by,

$$I = \frac{I_0}{2} e^{-\beta z} \,\mathrm{Re}[1 + e^{i\omega t}] \qquad 3.27$$

Where I_0 is the incident monochromatic light flux (W/m^2), β is the absorption coefficient (m^{-1}) of the illuminated sample and t is the time. It is assumed that the excitation beam energy $E = h\nu$, is greater than the band gap of the material, where 'h' is Planck's constant and 'ν' is the frequency of the beam.

The semiconductor is considered to be isotropic, thermally and electronically, and we assume that fluid and backing do not absorb the incident beam and hence they donot act as thermal sources. This is true in this case as we used light beam from a He-Ne laser for the optical excitation. The sample is assumed to be optically thin ($\mu_\beta > l$) and thermally thin (μ_s

> l), where μ_β and μ_s is optical penetration length and thermal diffusion length of the sample respectively. Hence the optical absorption is taken to be finite i.e., the absorption takes place throughout the sample volume rather than sample surface alone. Excitation beam is assumed to be of finite size with guassian profile, having spot size larger than the electronic diffusion length of the material. Hence a one-dimensional treatment of the heat diffusion equations is sufficient.

3.7.1 Heat diffusion equations

The light absorbed by a sample is converted by part or whole into heat by non-radiative deexcitation processes in the material. Thermal conduction is a diffusive process by which the generated heat is transferred from point of origin to other parts of the sample and its surroundings as a result of temperature gradient. Heat conduction is a diffusive process governed by a parabolic differential equation, which lacks second derivative with respect to time. From Fourier's law for heat conduction, the heat flux is proportional to negative of local temperature gradient.

$$q = -kA\frac{dT(z,t)}{dz} \tag{3.28}$$

The continuity equation is given by,

$$\rho\, c\frac{dT(z,t)}{dt} = -\frac{dq}{dz} \tag{3.29}$$

Where k is the thermal conductivity (W/mK), T (z, t) is the temperature, ρ is the density (kg/m^3) and c is the specific heat (J/kg K), space coordinate z and time t.

The heat diffusion equation in one-dimensional form, when there is no heat source and sink is given by,

$$\frac{\partial T(z,t)}{\partial t} = \frac{1}{D_s}\frac{\partial^2 T(z,t)}{\partial z^2} \tag{3.30}$$

Where T (z, t) is the temperature, D_s is the thermal diffusivity $\frac{k}{\rho c}\left(\frac{cm^2}{s}\right)$

A semiconductor thin film absorbs the photons with energy greater than the band gap [E_g] of the material, resulting in excess carrier distribution within the semiconductor with energy above (below) the conduction (valence) band. In a time scale of few pico seconds, these photo-injected carriers distribute the energy within themselves through coulomb interaction and finally this extra energy is given to lattice by relaxing to the bottom of the conduction band via carrier phonon interaction. As the excess carriers diffuse through the sample the electron hole pairs will eventually recombine producing a second source of

heat. This will also diffuse into the semiconductor. The heat diffusion equation including the heat sources is given by,

$$\frac{\partial T(z,t)}{\partial t} = \frac{1}{D_s}\frac{\partial^2 T(z,t)}{\partial z^2} + Q(z,t) \qquad 3.31$$

The three major heat sources are defined by *Q (z, t),* the net heat power density, are

i. Nonradiative intraband thermalization: When photo generated carriers relax down to the bottom of the conduction band by creating phonons, the heat power density is given by,

$$Q_T(z,t) = \beta\frac{(h\upsilon - E_g)}{h\upsilon} I_0 e^{-\beta z}\left(1 + e^{i\omega t}\right) \qquad 3.32$$

ii. Nonradiative bulk recombination: Non-radiative recombination of excess electron hole pairs after diffusion occurs through a distance ($\sqrt{D_n \tau_r}$) where D_n is the carrier diffusivity (m^2/s) and τ_r (s) is the carrier lifetime.

The heat power density due to non-radiative recombination is given by,

$$Q_{NR} = \frac{E_g}{\tau_r} N(z,t) \qquad 3.33$$

Where N (z, t) is the density of photo carriers, τ_r is the nonradiative recombination time.

Therefore the total power density is given by,

$$Q = Q_T + Q_{NR} \qquad 3.34$$

iii. Nonradiative surface recombination: When nonradiative recombination takes place at surface, a heat power density is,

$$Q_{SR} = E_g V_{sr} N(z,t) \qquad 3.35$$

This thermal contribution has to be included in the boundary condition of heat diffusion equations.

3.7.2 Minority carrier diffusion equation

When a beam of light irradiates the sample of thickness L, it leads to photo carrier generation; the excess carriers generated can be calculated from minority carrier diffusion.

The continuity equation can be written as,

$$\frac{dn}{dt} = \left.\frac{dN}{dt}\right|_{diffusion} + \left.\frac{dN}{dt}\right|_{drift} + \left.\frac{dN}{dt}\right|_{rec-gen} + \left.\frac{dN}{dt}\right|_{other\ process\ like\ light....} \quad 3.36$$

Where 'N' is the minority carrier concentration. Hence the drift term can be omitted as we consider only low-level injection.

$$\frac{dn}{dt} = \left.\frac{dN}{dt}\right|_{diffusion} + \left.\frac{dN}{dt}\right|_{rec-gen} + \left.\frac{dN}{dt}\right|_{other\ \ process\ like\ light....} \quad 3.37$$

For photo-generated carriers the transport equation is given by,

$$\frac{dN(z,t)}{dt} = D_n \frac{d^2N(z,t)}{dz^2} - \frac{\Delta N}{\tau_r} + G(z,t) \quad 3.38$$

Where G (z, t) is the generation rate carriers,

$$G(z,t) = \frac{\beta I_0}{2h\nu} e^{-\beta z} \quad 3.39$$

To evaluate the excess charge carrier distribution, we make the following assumptions:

i) When the material is in steady state $\frac{dN(z,t)}{dt} = 0$

ii) Since absorption takes place throughout the material thickness, excess carriers are created throughout the material and there is no carrier diffusion along the z direction.

Hence the minority carrier diffusion equation can be written as,

$$\frac{\Delta N}{\tau_r} = G(z,t)$$
$$\frac{\Delta N}{\tau_r} = \frac{\beta I_0}{2h\nu} e^{-\beta z} \quad 3.40$$

The heat diffusion equation in the three regions, fluid, sample and backing is,

$$\begin{aligned}
&\frac{\partial^2 T_f(z,t)}{\partial z^2} = \frac{1}{D_f}\frac{\partial T_f}{\partial t} \\
&\frac{\partial^2 T_s(z,t)}{\partial z^2} = \frac{1}{D_s}\frac{\partial T_s}{\partial t} - Q_T - Q_{NR} \\
&\qquad = \frac{1}{D_s}\frac{\partial T_s}{\partial t} - \beta\frac{\left(h\nu - E_g\right)}{h\nu} I_0 e^{-\beta z}\left(1 + e^{i\omega t}\right) - \frac{E_g}{\tau_r} N(z,t) \\
&\frac{\partial^2 T_b(z,t)}{\partial z^2} = \frac{1}{D_b}\frac{\partial T_b}{\partial t}
\end{aligned} \tag{3.41}$$

One of the boundary conditions is the continuity of temperature at the region boundaries

$$\begin{aligned}
&T_f(z,t)\big|_{z=0} = T_s(z,t)\big|_{z=0} \\
&T_s(z,t)\big|_{z=-l} = T_b(z,t)\big|_{z=-l} \\
&T_f(z,t)\big|_{z=+\infty} = T_b(z,t)\big|_{z=-\infty}
\end{aligned} \tag{3.42}$$

The next boundary condition is obtained from the heat continuity equation, which states that the heat flux flowing out of one region must be equal to heat entering into the adjoining region, must be obeyed.

$$\begin{aligned}
-k_s \left.\frac{\partial T_s(z,t)}{\partial z}\right|_{z=0} &= -k_f \left.\frac{\partial T_f(z,t)}{\partial z}\right|_{z=0} + V_{sr}\Delta N E_g \\
-k_b \left.\frac{\partial T_b(z,t)}{\partial z}\right|_{z=-l} &= -k_s \left.\frac{\partial T_s(z,t)}{\partial z}\right|_{z=-l}
\end{aligned} \tag{3.43}$$

Where k_i, D_i with i =f, s, b, represents the thermal conductivity and thermal diffusivity of fluid (f), sample (s) and backing (b) respectively.

On solving the thermal diffusion equation (3.41) with boundary conditions (3.42) and (3.43), we get the following expression for complex amplitude of temperature *T (z, t)* in the three regions.

$$\begin{aligned}
&T_f(z) = T_s e^{-\sigma_f z} \\
&T_s(z) = C_1 e^{-\sigma_s z} + C_2 e^{-\sigma_s z} - (C_3 + C_4) e^{-\sigma_s z} \\
&T_b(z) = W e^{\sigma_b (z+l)}
\end{aligned} \tag{3.44}$$

Where,

$$C_3 = \frac{\beta I_0}{2k_s}\left(\frac{E-E_0}{E}\right)e^{-\beta z}$$
$$C_4 = \frac{E_g}{\tau_r k_s}\frac{\beta I_0}{2h\nu}e^{-\beta z} \qquad 3.45$$
$$\sigma_i = \sqrt{\frac{i\omega}{D_i}}$$

The coefficients C_1, C_2 and W were obtained using the boundary conditions. Using C_1, C_2, C_3, and C_4 in equation 3.44, we finally obtain the surface temperature distribution is given by the equation 3.46.

$$T_s = \left\{\frac{\left[\begin{array}{l}\sqrt{D_f D_s}\left(\begin{array}{l}-R_1 B\sigma_b^2 D_b^{\frac{3}{2}} k_s + R_2 D_s\left\{\begin{array}{l}\beta\sqrt{D_s k_b}\left\langle B\beta + Ck_s\right\rangle - \\ \sigma_s\left\langle B\sigma_b\sqrt{D_b k_b} - C\sqrt{D_b k_s^2}\right\rangle\end{array}\right\}\end{array}\right)+ \\ D_s k_s\left(R_3 C\left\{\sigma_s\sqrt{D_s k_b} + k_s\beta\sqrt{D_b}\right\}+ R_1 B\beta^2\sqrt{D_b}\right)\end{array}\right]}{\left[\sqrt{i\omega}\left(i\omega-\beta^2 D_s\right)\left(\begin{array}{l}R_2\left\{D_s k_b k_f + \sqrt{D_b D_f}\,k_s^2\right\}+ \\ R_1\left\{\sqrt{D_s k_s}\left\langle\sqrt{D_f K_b} + \sqrt{D_b k_f}\right\rangle\right\}\end{array}\right)\right]}\right\}$$

where

$$R_1 \to 1 + e^{2l\sigma_s}$$
$$R_2 \to -1 + e^{2l\sigma_s} \qquad 3.46$$
$$R_3 \to R_1 - 2e^{l(\beta+\sigma_s)}$$
$$B \to V_{sr} N(0) E_g$$
$$C \to C_3 + C_4$$

3.7.3 Photothermal beam deflection signal

Refractive index gradient in the medium, surrounding the sample, due to heat generated from the sample is given by,

$$\frac{dn}{dz} = \frac{dn}{dT}\frac{dT(z,t)}{dz} \qquad 3.47$$

The deflection of probe beam (signal) thus produced is proportional to the refractive index gradient,

$$Signal \quad \alpha \quad \frac{1}{n_0}\frac{dn}{dT}\frac{dT(z,t)}{dz} \qquad 3.48$$

3.7.4 Determination of thermal diffusivity, minority carrier lifetime and surface recombination velocity

The parameters thermal diffusivity (D_s), minority carrier lifetime (τ_r) and surface recombination velocity (V_{sr}) are to be obtained as 'variable multiple fit parameters' by fitting the experimentally and theoretically obtained plot of modulation frequency versus signal amplitude (Figure 3.5). The experiment was performed first on silicon wafer and there was good agreement with the experimental data. Transport parameters D_s, τ_r, V_{sr} thus obtained were matching with earlier reported values.

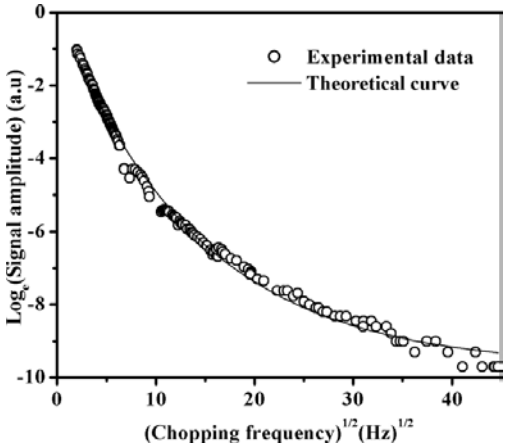

Figure 3.5 Experimental and theoretical fit for semiconductor thinfilm

3.8 Determination of sample-probe distance

In transverse photothermal deflection (mirage effect) technique, accurate knowledge of the distance between a sample and the probe beam axis is usually critical for measuring the sample properties. But it is quite difficult to measure this distance exactly. Distance between the sample surface and probe beam axis is usually referred to as the 'normal offset'. Also the deflection signal amplitude decreases exponentially with increase in 'normal offset'. Hence the signal amplitude reaches its maximum when the probe beam is nearer to sample surface. But if the sample surface and probe are brought closer beyond a limit, sensitivity of the measurement falls [26]. Figure 3.6 shows the variation of signal amplitude as distance between the sample surfaces and probe beam axis (normal offset) increase from 50 μm to 110 μm at modulation frequency of 70 Hz. Sensitivity is the least when probe beam is nearest (50 μm) and reaches a maximum at about 85 μm and starts decreasing with increase in normal offset. The signal amplitude was highest at this normal offset for all chopping frequencies. Thus the signal amplitude is very much sensitive to the 'normal offset' and it is required to keep the distance same for all successive measurements. But that is not always possible; for example, when the sample in the holder is changed, this distance varies and hence measurements get affected. Though the change occurs in order of few micrometers only, the signal and following calculations are affected considerably.

Hence it is necessary to measure the normal offset every time and retain it for all successive measurements. The deflection of probe beam, as it grazes the surface of a sample, is dependent on the refractive index gradient produced in the sample, which is again dependent on the temperature distribution in the fluid in the region around the sample.

The complex amplitude of temperature distribution in the fluid surrounding the sample is given by,

$$T_f(z) = T_s e^{-\sigma_f z} \qquad 3.49$$

Where T_S is the temperature of the sample, which depends on the sample's thermal and electronic properties. And $\sigma_f = \sqrt{i\omega / D_f}$. Where, D_f is the thermal diffusivity of the fluid and z is the distance between sample surface and probe beam axis. We may assume T_S to be a constant for a given sample.

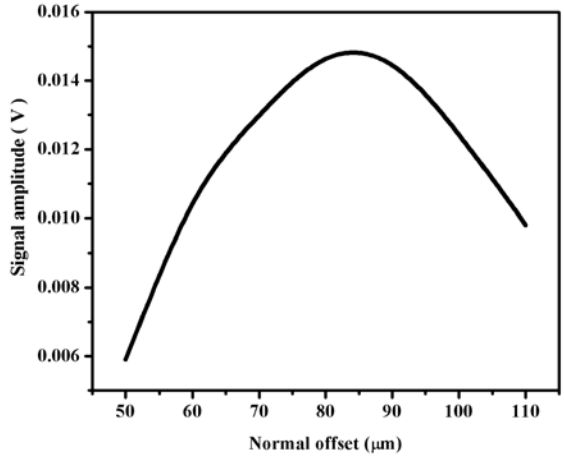

Figure 3.6 Plot of normal offset versus signal amplitude (70 Hz)

In general, for a sample placed inside a medium (fluid) the deflection of the probe beam, which is propagating through the fluid grazing the sample surface, has an exponential dependence on D_f and z. Hence from the plot of (chopping frequency) $^{1/2}$ versus signal amplitude by fitting the data using least square-fitting algorithm we can find the sample probe distance (z).

3.9 Photothermal studies done over silicon wafer

Further for proving the reliability of theory and technique, photothermal beam deflection studies were done on p-type Si wafer (Figure 3.7). Thickness of the wafer was 300-μm and the optical absorption coefficient was 10^3 cm^{-1} for 632 nm. The optical penetration depth is $1/\beta \sim 3$ μm only. Hence the entire incident light is absorbed within the 3-μm distance itself. The deflection signal was higher when the excitation intensity was increased (Figure 3.8).

Figure 3.9 depicts the variation in the signal as the normal offset (distance between samples and probe beam) is varied and we observed that the deflection signal is the maximum when the probe is near the sample surface (since the refractive index gradient is the maximum near surface and decreased as the distance between sample and probe increased).

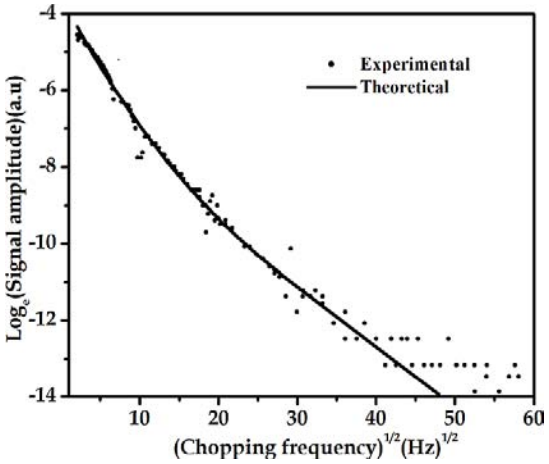

Figure 3.7 Theoretical and experimental plot of photothermal signal for Si wafer

Figure 3.7 shows the theoretical and experimental plot Log_e (signal amplitude) Vs (chopping frequency) $^{1/2}$ for silicon wafer. It is clear that there is good agreement between the experimental and theoretical curves. Keeping the transport properties D_s, τ_r and V_{sr} as 'variable fit parameters', theoretical fitting was done. Further the D_s (0.92×10^{-4} m^2/s), τ_r (30 μs) and V_{sr} (1 m/s) match well with the earlier reports. Table 3.2 shows the parameters used for fitting the experimental plot along with the reported values. Theoretical fitting for different excitation energies and different sample probe distance required the same values for fit parameters. Slight deviation from the theoretical plot for silicon samples could be due to the fact that in theory we assumed that there is no carrier diffusion along the 'z' direction since the absorption of light takes place throughout the thickness. But here the silicon wafer has larger thickness compared to optical absorption length and hence this assumption may not be true. However, for samples of our interest (semiconductor thin films ≤ 1 μm) absorption takes place throughout the film thickness due to which there is no diffusion along 'z' direction. Hence for these samples we obtain very good fit (Figure 3.5). When the thin films are excited using the intensity-modulated beam, there arises a deflection in the probe beam, which is detected using a bi-cell PSD. A Plot of Log_e (Signal amplitude) versus (chopping frequency) $^{1/2}$ clearly shows dependence of signal on frequency. The general trend observed for $CuInS_2$ films, irrespective of the fabrication condition, is their rapid decrease in signal with frequency in the low frequency regime (≤ 100 Hz) and gradual or more "slow" decrease in the high frequency regime (≥ 100Hz). Nature of dependence of signal amplitude on the chopping frequency and the value of frequency at which the change of slope takes place, helped us in finding out the origin of non-radiative processes in the film.

Table 3.2: Fit data and corresponding literature values obtained for silicon wafer

Fit parameter	*Code*	*Unit*	*Fit value*	*Literature values*
Thermal diffusivity of sample	D_s	m^2/s	$0.92x10^{-4}$	$0.90x10^{-4}$ [27]
Thermal diffusivity of fluid	D_f	m^2/s	$7.5x10^{-8}$	
Thermal diffusivity of backing	D_b	m^2/s	$0.92x10^{-4}$	
Thickness	L	m	$300x10^{-6}$	
Thermal conductivity of sample	k_s	W/mK	131	
Thermal conductivity of backing	k_b	W/mK	0.104	
Thermal conductivity fluid	k_f	W/mK	131	
Intensity of beam	I_0	W/m^2	100	
Absorption coefficient	β	m^{-1}	$3x10^3$	
Energy band gap of the material	E_g	eV	1.1	
Wavelength of incident beam	λ	nm	632	
Minority carrier lifetime	τ_r	s	$30x10^{-6}$	$45x10^{-6}$[27]
Surface recombination velocity	V_{sr}	m/s	1	4.5[27]

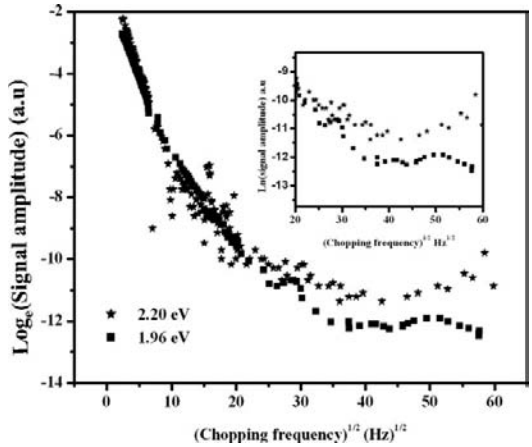

Figure 3.8 Variations in photothermal signal for different excitation intensity

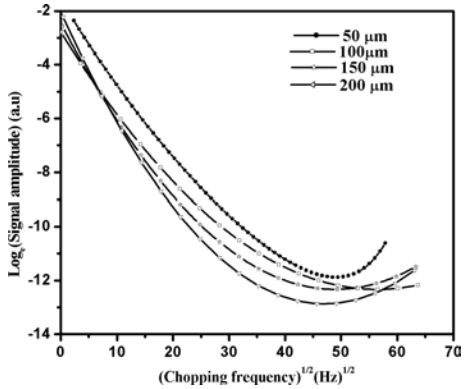

Figure 3.9 Variation in photothermal signal with increase in normal offset

3.10 Conclusion

In this chapter we brief the basic theoretical works that form the foundation of development of photothermal technique and helped it grow into a widely accepted and recognized non-destructive material analysis tool. Along with this the modification done on the theory in the present work, so as to make it suitable for semiconductor thin films, is also presented. Reliability and accuracy of the theoretical model developed in this work is proven with measurements made on Si wafer. Values of thermal diffusivity, carrier lifetime and recombination velocity thus calculated match very well with earlier reports. Theoretical model developed for determining the transport properties of semiconductor thin films is simple and can be extended to suit multilayer films also.

References

[1] A Rosencwaig 1973 *Opt Comm* **7** 305
[2] A C Boccara, D Fournier, W Jackson, N M Amer 1980 *Opt Lett* **5** 377
[3] J A Sell, D M Heffelfinger, P L G Ventzek, R M Gilenbach 1981 *J Appl Phys* **3** 69
[4] M Bertolotti, L Fabbri, C Sibilia, A Ferrari, N Sparvier, G Suber 1988 *J Phys D: Appl Phys* **21** S14
[5] S D George, P Radhakrishnan, V P N Nampoori, C P G Vallabhan 2003 *Phys Rev B* **68** 165319
[6] J C Murphy, L C Amodt, 1980 *J Appl Phys* **51** 4580
[7] H M James 1980 *J Appl Phys* **51** 4666
[8] J Opsal, A Rosencwaig 1982 *J Appl Phys* **53** 4240
[9] D Fournier, C Boccara, A Skumanich, N M Amer 1986 *J Appl Phys* **59** 787
[10] U Zammit, F Gasparrini, M Marinelli, R Pizzoferrato, F Scuderi, S Martellucci 1991 *J Appl Phys* **69** 2577
[11] S Y Zhang, J C Cheng, 1991 *Semicond Sci Technol* **6** 670
[12] J C Cheng, S Y Zhang 1991 *J Appl Phys* **70** 7007
[13] J D Spear, R E Russo 1991 *J Appl Phys* **70** 580
[14] X Quelin, B Perrin, G Louis, P Peretti 1993 *Phys Rev B* **48** 3677
[15] P Grunow, R Schieck 1995 *J Appl Phys* **77** 2773
[16] T T N Lan, H G Walther 1996 *J Appl Phys* **80** 5289
[17] G G de la Cruz, Y G Gurevich 1996 15th International conference on Thermoelectrics, California 217
[18] A Mandelis, A Salnick, J Opsal, A Rosencwaig 1998 *J Appl Phys* **85** 1811
[19] S Galovic, M D Dramicanin 1999 *J Phys D Appl Phys* **32** 1511
[20] C Glorieux, R Li Voti, J Thoen, M Bertolotti, C Sibilia 1999 *Inverse Problems* **15** 1149
[21] R Li Voti, C Melchiorri, C Sibilia, M Bertolotti 2001 *Anal Sci* **17** S410
[22] R Li Voti, G L Liakhou, S Paoloni, C Sibilia M Bertolotti 2001 *Anal Sci* **17** S414
[23] A Salnick, J Opsal 2002 *J of Appl Phys* **91** 2874
[24] Y G Gurevich, G N Logvinov, G G de la Cruz, G E López 2002 *Int J of Therm Sci* **42** 63
[25] E Marin, J M Antuna, P D Arencibia 2002 *Eur J Phys*. **23** 523
[26] J H Zhao, J Shen, C Hu 2002 *Opt Lett* **27** 1755
[27] Y G Gurevich, G N Logvinov, G G de la Cruz, G E Lopez 2003 *Int J of Therm Sci* **42** 63
[28] B Li, A Mandelis, Z Z Kish 2004 *J of Appl Phys* **95** 1042
[29] K Boubaker 2004 *Eur Phys J Appl Phys* **28** 249
[30] M Soltanolkotabi, M H Naderi 2004 *Jpn J Appl Phys* **43** 611

[31] G N Logvinov, M C Irisson, I M Lashkevych, J E Velazquez, Y G Gurevich 2006 *Brazlian J of Physics* **36** 1097
[32] R Mulaveesala, S Tuli 2006 *Appl Phys Lett* **89** 191913
[33] J H Rohling, J Shen, C Wang, J Zhou, C E Gu 2008 *Eur Phys J* **153** 99
[34] M Paulraj 2004 *PhD Thesis*, Cochin University of Science and Technology, India

4

Photothermal analysis of absorber layer materials

Photothermal beam deflection technique is applied for determining the thermal diffusivity, minority carrier lifetime, surface recombination velocity and minority carrier mobility of $CuInS_2$, $CuInSe_2$ and SnS thinfilms, which are used as absorber layer in solar cells. The film fabrication history, composition and post deposition treatments play crucial role in deciding the transport properties and solar cell parameters. From these studies we could optimize the deposition parameters, which are most essential for fabrication of device quality films. Experimental and theoretical photothermal signal data are in good agreement resulting in a good fit; the transport parameters thus determined match well with earlier reports and also correlate with other evaluation studies such as X-Ray diffraction and AFM analysis performed on the material. Through this study, photothermal beam deflection technique as a thermal imaging tool is also established.

4.1 Introduction

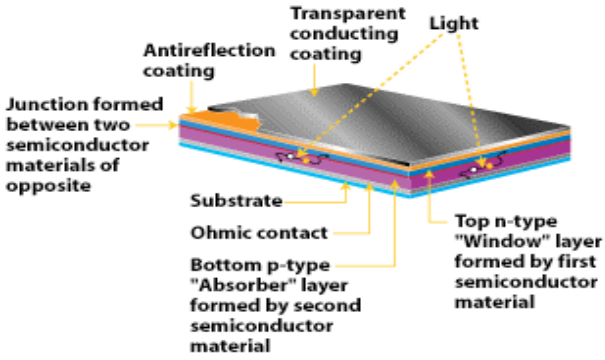

Figure 4. 1 Basic heterojunction structure of photovoltaic cell

Basic heterojunction thinfilm photovoltaic structure (Figure 4.1) consists of transparent conducting oxide, buffer layer and absorber layer deposited over glass substrate. Each of the component layers has different physical and chemical properties and each affects the overall performance of the device in some form or the other. Therefore critical understanding of the behavior of these individual components is essential for designing a device. An ideal absorber layer should be a material with direct band gap of 1 to 1.5 eV, with high absorption coefficient (10^5 cm/s), high quantum efficiency of excited carriers,

long diffusion length and low recombination velocity. They should be capable of forming a good junction (homo/hetero/Schotkky) with compatible materials. These parameters along with the absorber layer's crystallinity and chemical composition have important influence on cell characteristics. And the other conditions that constraint the commercial feasibility of a photovoltaic material is their availability and environmental issues. A wide variety of competent materials have been developed which give thrust to thin film technology for photovoltaic industry over the well-developed crystalline technology. The studies presented here is limited to $CuInS_2$, $CuInSe_2$ and SnS thin films. For serving the purpose of non-destructive analysis of semiconductor thin films that are used in solar cell fabrication we work in developing the transverse PTBD technique.

This work aims at establishing PTBD technique for reliable measurements and proving its capability in determining the transport properties of semiconductor thin films. The non-radiative nature of $CuInS_2$, $CuInSe_2$ and SnS thin films and their thermal and electronic transport properties were determined using PTBD technique. The film deposition parameters play a crucial role in deciding the films optoelectronic properties. Advantage of this technique for insitu measurements was exploited for optimisation of film deposition parameters to obtain device quality absorber layers with high τ_r, μ, low V_{sr} and least non-radiative losses.

4.2 Copper indium disulphide

I–III–VI chalcopyrite materials are reported to have very desirable properties for photovoltaic application. $CuInS_2$ (Figure 4.2) belonging to this group of compound semiconductor is a promising absorber layer material with optimum optoelectronic properties; cells of this material have already reported efficiencies as high as 12.5% [1] in laboratory scale and 10.2% in industry level [2]. $CuInS_2$ meets the requirements for PV technology with a band gap of 1.5 eV, high absorption coefficient and good stability [3] that suits both terrestrial and space applications [4]. A theoretical calculation by Meese et al (1975) predicted solar conversion efficiencies between 27% and 32% for $CuInS_2$ based homojunction having a direct band gap of 1.55 eV [5]. Moreover, $CuInS_2$ based devices show excellent stability and can be produced with low energy consumption. If a material is to attain any large scale and economical device utilization, its production in thin film form is a necessity. Hence for this purpose thin films of $CuInS_2$ have been fabricated by various methods such as thermal evaporation [6], rapid thermal evaporation [7], RF sputtering [8], flash evaporation [9], chemical spray pyrolysis (CSP)[10], etc. Several workers have studied the growth and physical properties of $CuInS_2$ thin films prepared using a variety of methods and modifications [11, 12, 13]. Abo El Soud

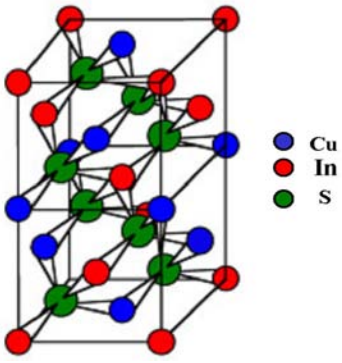

Figure 4.2
Crystal structure of $CuInS_2$

et al (1993) reported the transport properties of $CuInS_2$ thinfilms prepared by thermal vacuum evaporation [14]. The device performance has also improved in the recent years. In present work we report on studies done on $CuInS_2$ thin films deposited using CSP technique. CSP is a relatively cost effective method suitable for large area film deposition with ease of doping [15]. Table 4.1 shows the optoelectronic and transport properties of this $CuInS_2$ thin films as reported by other groups. But there are very few reports on the D_S, τ_r, V_{sr} and μ of $CuInS_2$ thin films due to dearth of techniques that are simple and efficient in measuring the transport properties of thin films. The practical difficulties of making such measurements have affected extensive analysis of these properties, which are most essential for fabrication of devices.

Table 4.1
Optoelectronic and transport properties of $CuInS_2$ absorber film

Band gap	1.3 – 1.55 eV [16]
Absorption coefficient	10^5-10^6/cm [16]
Mobility	1-10 cm^2/Vs [6, 17]
Surface recombination velocity	1.2x10^5 cm/s [18]
Carrier concentration	2x10^{18} cm^{-3} [19]
Carrier life time	1.2 x 10^{-10} s [18]
Resistivity	10^3 to 10^{-1} Ω cm [20, 21]

4.3 Fabrication

$CuInS_2$ thin films were deposited over micro glass slides applying CSP technique by spraying aqueous solutions of $CuCl_2$, $InCl_3$ and thiourea; indigenously developed automated spray unit was used for this purpose. Details of the automated spray unit have been reported earlier [22]. Deposition conditions are the deciding factors for the formation of good quality films. So the optimisation of the film fabrication conditions is very much essential for obtaining films that can be further used for device fabrication. Substrate temperature, concentration, volume of spray solution, rate of spray and speed of X and Y movements of spray head are the parameters, which require utmost care. Even a slight variation from the optimum setting can affect the films quality considerably and may sometimes render them even useless. Extreme care has to be taken while deciding the optimum spray condition. For studying the effect of these deposition parameters, films were deposited at different substrate temperature, spray volume and concentration of the precursors in the spray solution. The sample size was 4 x 2 cm and thickness of the films (measured using stylus depth profiler Dektak 6M) was found to vary (0.6 µm to 0.2 µm) with the deposition condition. We studied the influence of variation in; substrate temperature from 250 ^{0}C to 400 ^{0}C; spray volume from 20 ml to 60 ml and Cu/In ratio from 0.5 to 1.5. To study the effect of post deposition H_2S treatment, samples were prepared with Cu/In ratio 1, with substrate temperature 300 ^{0}C, spray volume 30 ml and spray rate 8 ml/min. These samples were annealed in H_2S atmosphere at 400 ^{0}C for one hour in indigenously fabricated sulphurisation chamber.

4. 4 Photothermal analysis of $CuInS_2$ thin films

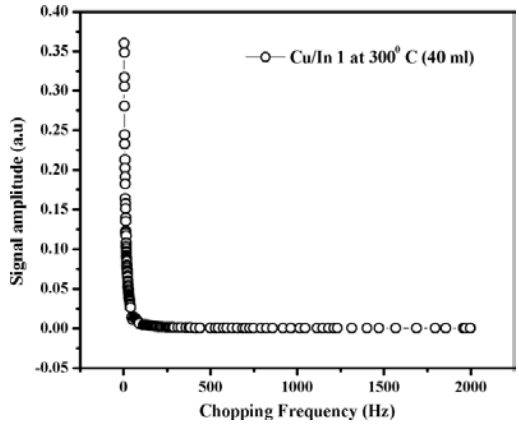

Figure 4.3 Plot of signal amplitude versus chopping frequency for $CuInS_2$ thin films

Thin films of $CuInS_2$ were excited using the intensity-modulated beam of wavelength 632 nm and the deflection of probe beam was detected using a bi-cell PSD. Figure 4.3 shows the plot indicating the variation of the amplitude of the deflection of the signal (i.e. probe beam) with respect to the modulation frequency. A Plot of Log_e (Signal amplitude) versus (chopping frequency) $^{1/2}$ (Figure 4.4) clearly shows dependence of signal on frequency. The general trend observed for $CuInS_2$ films, irrespective of the fabrication condition, is the rapid decrease in signal with frequency in the low frequency regime (≤ 100 Hz) and gradual or more "slow" decrease in the high frequency regime (≥ 100 Hz). Nature of dependence of signal amplitude on the chopping frequency and the frequency from which the change of slope (showing the 'rapid' or 'slow' decrease) alters with changes in the composition and surface morphology of the investigated film assist us in finding out the origin of non-radiative processes in the film. This can be correlated to the fabrication process and hence useful for optimisation of fabrication process. In the present work, we have made a study on the impact of alternations in film fabrication condition on the transport properties of film.

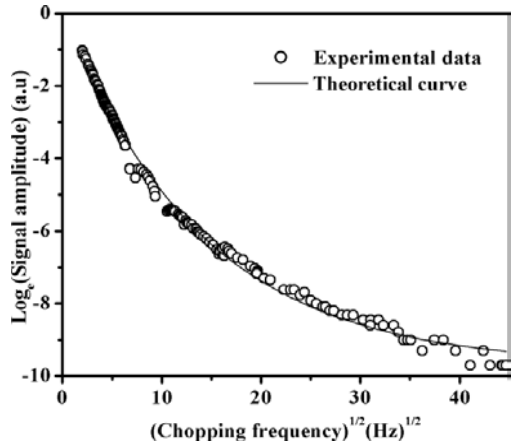

Figure 4.4 Plot of Log_e (signal amplitude) versus (chopping frequency) $^{1/2}$

4. 4.1 Influence of substrate temperature

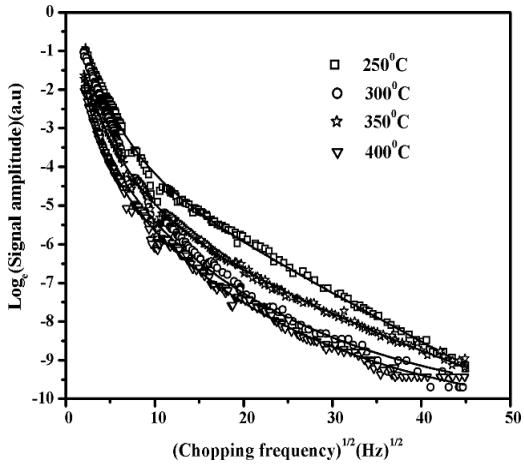

Figure 4.5 Photothermal response of $CuInS_2$ films deposited at 250 ^{0}C, 300 ^{0}C, 350 ^{0}C, 400 ^{0}C

Figure 4.5 shows the dependence of the photothermal signal (plot of Log_e (Signal amplitude) versus (chopping frequency) $^{1/2}$) for $CuInS_2$ thin films prepared at different substrate temperatures 250 ^{0}C, 300 ^{0}C, 350 ^{0}C and 400 ^{0}C. X-ray diffraction studies were done using Rigaku (D Max C) X-Ray diffractometer employing CuK_α line (λ=1.5405 A). From the XRD pattern (Figure 4.6) of this film we could find that, for higher substrate temperature (> 300 ^{0}C), the crystallinity of the films has improved while for lower deposition temperature (< 300 ^{0}C) the films had poor crystallinity. We observe that there is no significant variation in the nature of photothermal signal plot except for a slight increase in the deflection signal amplitude for lower substrate temperature (250 ^{0}C). This suggests that for films prepared at this temperature the non-radiative emission is higher. One of the reasons for having increased non-radiative emission is the presence of surface states and defects in the material, which act as traps with continuum energy states. Electron-hole recombination takes place through this continuum of states with release of phonons that result in photothermal signal generation. D_s, V_{sr}, τ_r determined from the fitting of theoretical and experimental data curve is shown in Table 4.3. τ_r is highest (350 ns) for the films prepared at 300 ^{0}C, which is ~ 10 times higher than films fabricated at other substrate temperatures. The V_{sr} is least at this temperature, which implies that the surface states are reduced considerably. But μ (Table 4.3) was found to be highest for samples prepared at 400 ^{0}C, which could be attributed to the good crystallinity of these films compared to those, fabricated < 400 ^{0}C. V_{sr} describes directly the recombination rate of the excess carriers via the surface electronic states and is determined mainly by the surface imperfection and contamination. Higher V_{sr} at the front surface of a semiconductor solar cell will lead to higher surface losses of excess photo carriers and inversely affects the photo response. Recombination activity increases proportionally to defect density and hence lifetime measurements give an estimate of the defect concentration as well. Unintentional lattice defects in semiconductors affect the τ_r.

Table 4.3
Fit data obtained for $CuInS_2$ thin films prepared at different substrate temperature.

Sample ^0C	Thickness (μm)	D_s (x $10^{-3}cm^2/s$)	τ_r (ns)	V_{sr} (x 10^8 cm/s)	μ (cm^2/Vs)
250	0.51	0.85	20	5	0.40
300	0.46	0.85	350	2	0.50
350	0.35	0.88	50	8	0.30
400	0.27	0.88	40	10	1.59

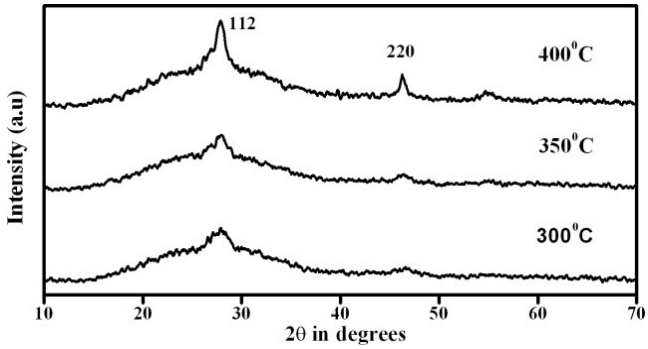

Figure 4.6 XRD patterns of samples deposited at substrate temperature 300 ^0C, 350 ^0C and 400 ^0C

This also suggests that 300 ^0C is comparatively the best temperature suited for preparation of $CuInS_2$ films using CSP technique, as it offers very high τ_r. Also the non-radiative emission at this temperature is the least; this indicates better films with low recombination losses. So the substrate temperature plays a critical role in deciding the transport properties of the fabricated film. The formation of defects and deformities can be reduced to certain extend by choosing the optimum deposition temperature.

4.4.2 Influence of film composition

Concentration of copper and indium in the spray solution has to be controlled. The excess or deficiency of the "metal" (Cu & In) in the film would alter the film's properties. So it is essential to choose the concentration of constituents in the film in accordance with device requirements. For the present study, films were prepared by varying the ratio Cu/In as 0.5, 1 and 1.5, and figure 4.7 shows variations in the photothermal signal plot for different Cu/In in the film. We observed that for Cu deficient samples (Cu/In~0.5) the decrease in signal amplitude with modulation frequency is almost linear in the low frequency regime while in high frequency region, the signal decrease is very slow (Figure 4.7). In other samples, the contribution from defects in the bulk is high in the low frequency region. As a result, we could not observe a sudden or linear decrease in signal amplitude. Instead, there is a slow variation in which the thermal contribution is due to immediate thermalization of carriers to the bottom of conduction band and bulk recombination with release of phonons. Transport properties determined from the theoretical best-fit show that V_{sr} is very high for Cu deficient samples, while for Cu rich (Cu/In ~1.5) samples, V_{sr} reduced by 10^4 times. These values were in good agreement with reported values [18, 23]. Also the crystallinity is

better for Cu rich films (Figure 4.8). Surface morphology is much better when there is Cu excess in the film. The AFM images of Cu rich (Figure 4.9 a) and Cu-deficient films (Figure 4.9 b) also support the conclusions from photothermal analysis. Surface quality of Cu-rich films has improved due to better crystallinity mainly induced by the $Cu_{2-x}S$ phase. Cu deficiency in a sample surface can cause formation of complex defects in the surface. Hence for Cu deficient film, the grain formation is rather incomplete and has an irregular pattern while for Cu rich samples; the grains are triangular and have regular arrangement. For stoichiometric films (Cu/In ~ 1), carrier lifetime was the highest and mobility was also higher compared to Cu rich and Cu poor films (Table 4.4). Hence the stoichiometric films are best suited for device fabrication.

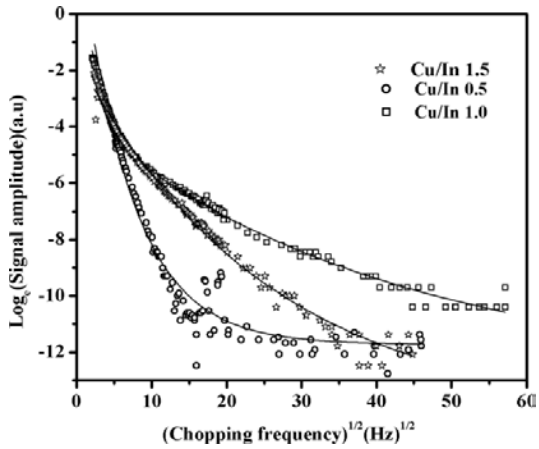

Figure 4.7 Photothermal response of $CuInS_2$ films with Cu/In 0.5, 1, 1.5

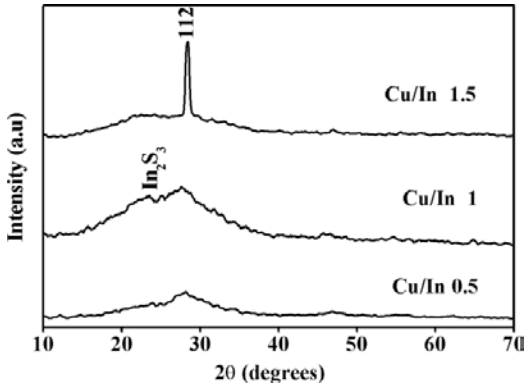

Figure 4.8 XRD patterns of $CuInS_2$ samples with Cu/In 0.5, 1, 1.5

Table 4.4
Fit data obtained for $CuInS_2$ thin films prepared by varying Cu/In ratio

Sample (Cu/In)	Thickness (μm)	D_s (x 10^{-3}cm^2/s)	τ_r (ns)	V_{sr} (x 10^5cm/s)	μ (cm^2/Vs)
0.5	0.58	0.79	10	13x10^4	0.23
1.0	0.46	0.85	350	2x10^3	0.80
1.5	0.25	1.90	1	5	0.21

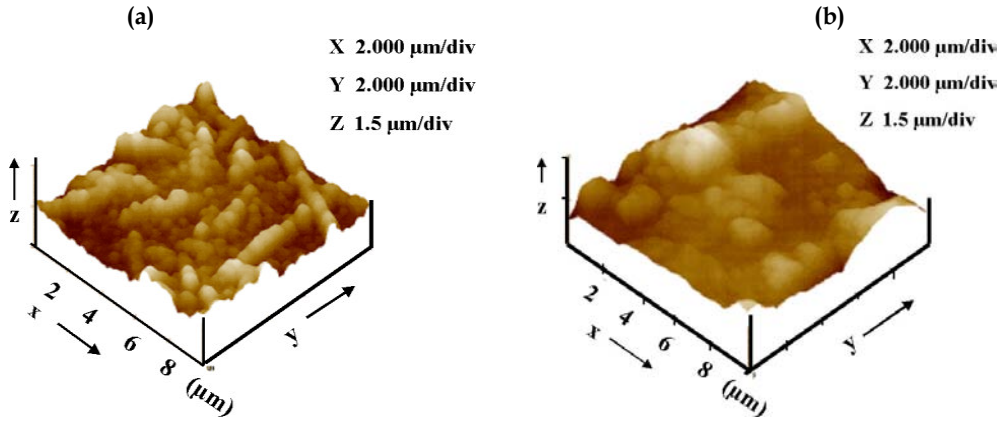

Figure 4.9 2-D AFM image (a) Cu rich (b) Cu deficient

4.4.3 Influence of spray volume

Figure 4.10 show that variation in spray volume slightly altered the non-radiative nature of the films. But the crystallinity improved with increase in volume of spray solution (Figure 4.11). Value of V_{sr} was highest for 20 ml spray volume since the film formation is rather incomplete when spray volume in less than 30 ml; hence the formation of surface states is higher, resulting in high non-radiative loss, in this case. While for spray volume 30 ml and 40 ml, V_{sr} is the least and lifetime is slightly better for films with 30 ml spray volume. Films fabricated with 40 ml spray solution exhibited good crystallinity (Figure 4.11).

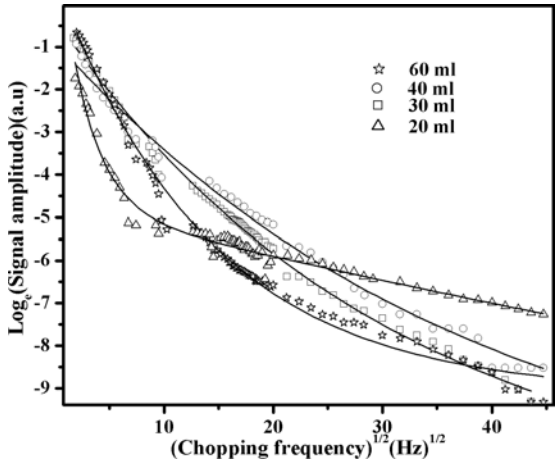

Figure 4.10 Photothermal response of $CuInS_2$ films with spray volume 20, 30, 40 and 60 ml

However D_s was higher for 30 ml sample (Table 4.5). High D_s implies that the scattering of thermal waves is low in these samples. Scattering of thermal waves occurs mostly due to the presence of impurities or grain boundary effects, which could affect the carrier mobility and hence the conductivity. Thus high D_s also indicate lower impurity and grain boundaries. Hence from these results, one can conclude that it is better to choose spray

volume at 30 ml as optimum spray volume for fabrication of good quality solar cell absorber layer, since at this spray volume, the film has high D_s ($4.8x10^{-3}$ cm^2/s), high τ_r (4 ns), low V_{sr} ($5 x10^5$ cm/s) and high μ (0.30 cm^2/Vs).

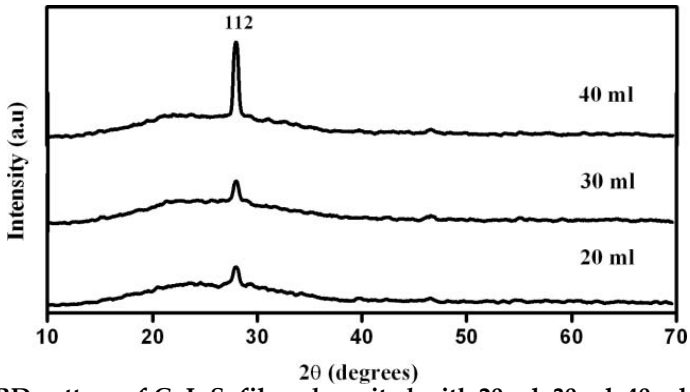

Figure 4.11 XRD pattern of $CuInS_2$ films deposited with 20 ml, 30 ml, 40 ml spray volume

Table 4.5
Fit data obtained for $CuInS_2$ thin film prepared by varying the spray volume

Sample	Thickness (μm)	D_s (x $10^{-3}cm^2/s$)	τ_r (ns)	V_{sr} (x 10^5cm/s)	μ (cm^2/Vs)
20 ml	0.13	0.73	0.7	50	0.025
30 ml	0.17	4.8	4.0	5	0.30
40 ml	0.25	1.9	1.0	5	0.16
60 ml	0.33	1.7	0.3	10	0.056

4.4.4 Influence of H_2S treatment on $CuInS_2$ thin films

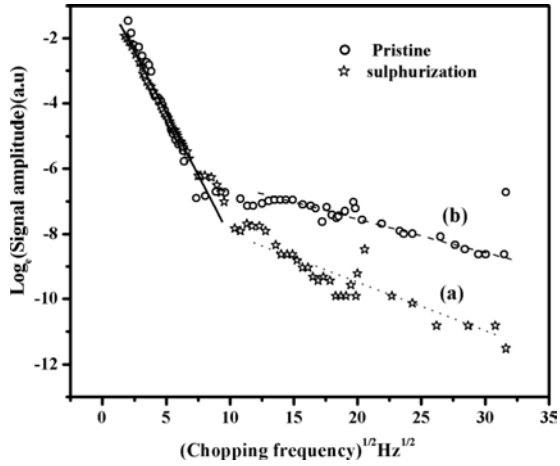

Figure 4.12 Photothermal response of $CuInS_2$ films with and without post deposition H_2S treatment

Non-radiative response of 'sulphurized' and 'unsulphurized' sample is shown in figure 4.12. The 'as deposited films' grown at temperatures below 400 ^{0}C in air contain residues originating from both the precursors and the ambient. Post deposition treatments in sulphur atmosphere were found to be effective to remove undesired residues and improve the structural properties without affecting the carrier transport properties [24]. We observed that the non-radiative recombination loss is lower for sulphurized samples. These samples (sulphurized) have better transport properties too. V_{sr} reduced by one order ($7x10^4$ cm/s); τ_r has also increased considerably (2 μs)(Table 4.6). Figures 4.13 and 4.14 show the J-V plot of $Ag/In_2S_3/CuInS_2/ITO$ cells CIS (Without H_2S treatment) and CIS-S (with H_2S treatment). It is known that μ plays a major role in determining the cell's open circuit voltage through its effect on saturation current. As a result, the 'sulphurized' sample shows no shift on illumination inspite of better V_{sr} and τ_r. This is because the sulphurized samples have comparatively low mobility (0.37 cm^2/Vs) while for untreated samples μ is higher by one order (1.2 cm^2/Vs).

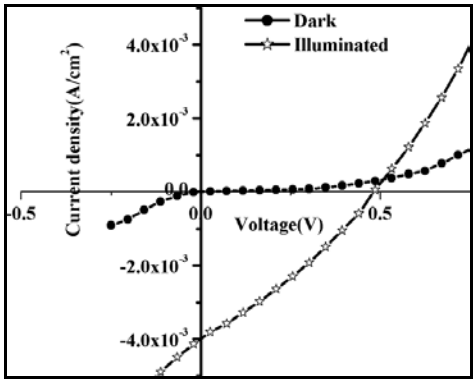

Figure 4.13 J-V Plot of $CuInS_2/In_2S_3$ cell without H_2S treatment

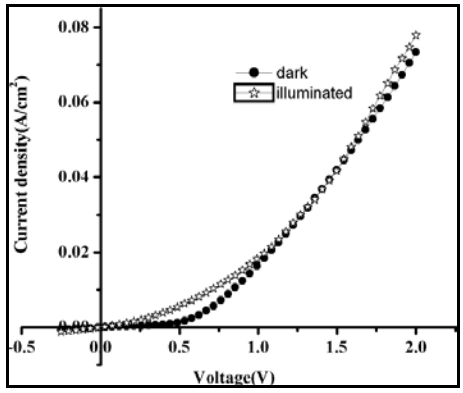

Figure 4.14 J-V Plot of $CuInS_2/In_2S_3$ cell with H_2S treatment

Table 4.6
Transport properties of $CuInS_2$ films with and without H_2S treatment

H_2S Treatment	D_s (cm^2/s)	τ_r (s)	V_{sr} (cm/s)	μ (cm^2/Vs)
Without	$0.8x10^{-7}$	$0.8x10^{-6}$	$1x10^5$	1.2
With	$1.6x10^{-7}$	$2x10^{-6}$	$0.7x10^5$	0.37

Earlier reports also advocate that for sprayed $CuInS_2$ films H_2S treatment results in significant improvement of structural and optical properties while conductivity and concentration of carriers decreased [20]. This may be due to the 'scavenging' of Cu atoms in $CuInS_2$ films through sulphur annealing [25] and heavy compensation of the intrinsic defects in the material. As a result, the number of holes (majority carriers) reduces considerably. Hence the probability of electron–hole recombination falls resulting in an increase in lifetime of minority carriers. Thus we observe that an increase in lifetime with increase in number of minority carriers which cause decrease in μ.

Stoichiometric conditions and substrate temperature during the formation of the absorber layer directly influence the physico-chemical properties of the resultant material, which in turn, determine its optoelectronic behavior. For films fabricated at 300^0C, τ_r improved greatly while non-radiative recombination loss is the least. Stoichiometric $CuInS_2$ films have less surface states and hence low V_{sr}. Further, volume of the spray solution is an important factor in controlling surface properties of the films; low spray volume is insufficient for film formation and very large spray volume can result in increased porosity due to increased thickness. H_2S treatment meant for improving the cells efficiency affected it adversely by reducing the carrier mobility inspite of the decrease in surface recombination velocity. Thus the control of substrate temperature, stoichiometry and spray volume of the solution are very important for obtaining the desired transport properties.

4.5 Copper indium diselenide

$CuInSe_2$ is a ternary compound semiconductor that crystallizes in the chalcopyrite crystal structure (Figure 4.15). It has a direct energy gap at 1 eV and an absorption coefficient of $>10^5$ cm^{-1}, as well as good outdoor stability making it an excellent solar cell absorber. The National Renewable Energy Laboratory (NREL) USA [26] reported that $CuInSe_2$-based solar cells achieved a conversion efficiency of 19.9% $CuInSe_2$ thin films are as good an electronic material as its single-crystal counterpart. This makes $CuInSe_2$ based solar cells less sensitive to impurities, grain size and crystalline defects [27]. Alloying with Ga[64], Al[65] or S[66] increases the bandgap of $CuInSe_2$ so as to make it more suitable for high-efficiency single-junction and multijunction devices [27]. Increase in the bandgap and improved process conditions resulted in the fabrication of high-performance solar cells with efficiencies of 19.2% for small-area and 13.1% for a large area (90x 60 cm^2) [28]. Even though the efficiency and stability of the device are very promising, there are several factors that are less favourable for large-scale production of such devices.

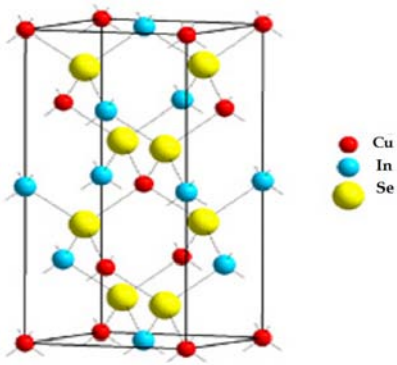

Figure 4.15
Crystal structure of $CuInSe_2$

Table 4.7
Optoelectronic and transport properties of $CuInSe_2$ films

Band gap	1.04 eV [37]
Absorption coefficient	10^5 cm^{-1} [38]
Resistivity	10^1-10^4 Ω cm [39]
Hole Mobility	3 - 6 cm^2/Vs [40, 41,42]
Electron mobility	6, 50, 900 cm^2/Vs [41, 42]
Surface recombination velocity	4.2 x10^6 cm/s [43]
Carrier concentration	10^{17} cm^{-3} [44]
Minority carrier lifetime	1-2 ns [45]

One of the major concerns is fabrication film with desirable electrical and optical properties that are reproducible [29, 30]. Many deposition techniques have been attempted in the last few years, such as flash evaporation, co evaporation [31], spray pyrolysis [32], molecular beam epitaxy [33], RF sputtering [34], selenization [35] and MOCVD [36]. Table 4.7 shows the optoelectronic and transport properties of $CuInSe_2$ thinfilms as reported from earlier works.

4.6 Fabrication

In the present work, $CuInSe_2$ thin films were deposited through sequential evaporation of selenium, indium and copper, at moderately low substrate temperature, as an alternative to high temperature deposition of the elements or compound evaporation. Structure of the film was Glass/In/Se/Cu [46]. This technique has the advantage of accurate composition and low cost. Material to be evaporated is placed in a molybdenum boat and vaporized by resistive heating method. Indium was evaporated at 100 ^oC; Selenium at 50 ^oC and Copper at room temperature and this multilayer was annealed for one hour at 400 ^oC. All these processes were carried out at a pressure of $2x10^{-5}$ mbar. The samples were coded according to the Cu/In ratio 0.2, 0.25 and 0.3 as CISE1, CISE2 and CISE3. The films had band gap value 1.2 eV and thickness 0.5 μm.

4.7 Photothermal analysis of $CuInSe_2$ films

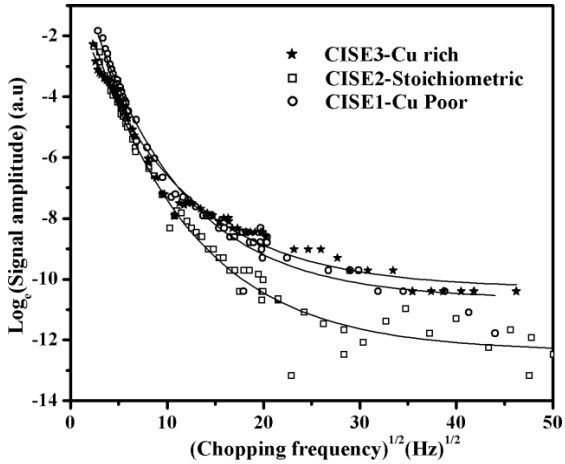

Figure 4.16 Photothermal response of CISE1, CISE2, CISE3

$CuInSe_2$ thinfilms were excited using intensity-modulated beam of wavelength 632 nm (He -Ne laser, 10 mW). The plot of Log_e (Signal amplitude) versus (chopper frequency) $^{1/2}$ for $CuInS_2$ and $CuInSe_2$ thin films (Figure 4.16) prepared by varying the Cu/In ratio show the variation of amplitude of signal with modulation frequency. For $CuInSe_2$ films the non-radiative contribution is the least for stoichiometric samples (Figure 4.16). For Cu poor films the shallow acceptor level due to Cu vacancy (V_{Cu}) is assumed to be the main dopant (For Cu rich films Cu in In antisites (Cu_{In}) form similar kind of defect) and Se vacancies

(V_{se}) act as compensating donors as well as defects due to double donor (like Indium in Cu (In_{Cu})) vacancies are created.

Table 4.8
Transport properties of CISE samples

Code	$D_S x10^{-3}$ (cm^2/s)	μ (cm^2/Vs)	τ_r (μs)	V_{sr} (cm/s)
CISE1	0.83	1.25	2	3000
CISE2	0.96	32	12	1500
CISE3	0.8	2.12	4	1000

Surface states due to V_{Se} cause band bending in the film, which leads to liberation of Cu from its lattice sites and cause Cu migration towards the neutral part of the film. The remaining Cu vacancies (V_{Cu}) close to the surface result in high density of acceptor states or formation of p^+ defect layer at the film surface. This defect layer could be responsible for the high recombination velocity observed in Cu poor films. Density of defects is generally reported to be lower for $CuInSe_2$ films with stoichiometric composition. This can be correlated to the improvement in μ and τ_r for stoichiometric films. Table 4.8 shows the μ, τ_r and V_{sr} obtained for $CuInSe_2$ films. Similar to $CuInS_2$ films, for Cu rich $CuInSe_2$ films, the V_{sr} decreased and was three times lesser (1000 cm^2/s) than the Cu poor $CuInSe_2$ films (3000 cm^2/s). From AFM images (Figure 4.17 a and 4.17 b), the surface is triangular and regular for Cu rich films, while for Cu poor films the surface is rather irregular, obtained from EDAX is shown in Table 4.9. In Cu rich samples there are reported presence of $Cu_{2-y}Se$ phases, which was found to enhance the conductivity of the material. But in device form, films with excess Cu may not be useful due to the presence of secondary phases ($Cu_{2-y}Se$) preferentially at the surface of the film, since the metallic nature of this phase does not allow the formation of efficient junctions. We also observed that the μ and τ_r were suppressed due to excess Cu in the film. XRD pattern (Figure 4.18) indicates that the crystallinity of the stoichiometric film was better. Concentration of copper plays a profound role in deciding surface quality of the film and stoichiometric films are required for obtaining films with high μ and τ_r.

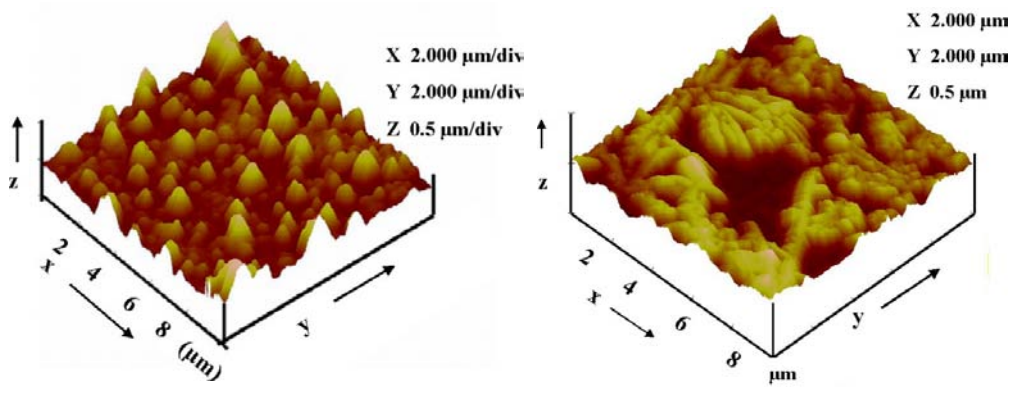

(a) **(b)**

4.17 2-D AFM image of (a) Cu-rich and (b) Cu-poor $CuInSe_2$ samples

Table 4.9
EDAX report of CISE samples

Code	Cu%	In%	S%
CISE1	19.75	20.21	60.04
CISE2	24.92	24.98	50.10
CISE3	22.84	20.19	56.97

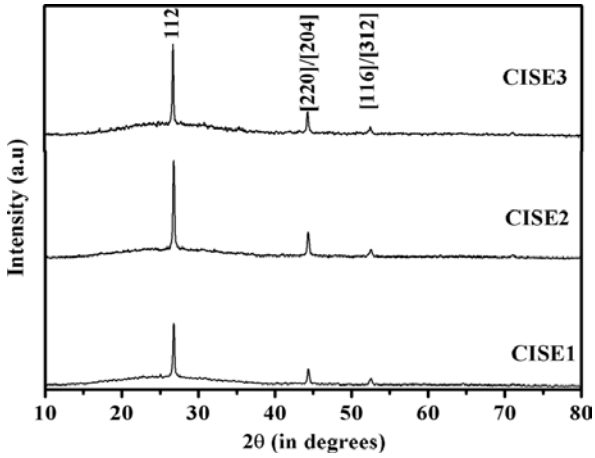

Figure 4.18 XRD pattern of samples CISE1, CISE2 and CISE3

4.8 Tin mono sulphide

Tin mono sulphide (SnS), which is one of IV-VI compound semiconductors, has been attracting considerable interest in recent years [47]. This material is highly useful for photovoltaic application as an alternative to the presently existing materials due to its favourable physical properties like, direct band gap of 1.3 -1.5 eV, high light absorption coefficient (>10^4 cm^{-1}) [48], hole mobility of 90 cm^2/Vs [49] and photoconductivity for wavelengths less than 1.2 μm [50]. Apart from these properties, its non-toxicity and abundance in nature have further enhanced its prospects in the field of compound semiconductor thin film solar cells [51]. It has orthorhombic crystal structure (Figure 4.19) and contains layers of tightly bound Sn and S atoms, while the bonding between the layers is through weak Vanderwaals force which provides an intrinsically chemically inert surface with no dangling bonds, no surface states and hence without Fermi level pinning at the surface [52]. Such layered semiconductors are of great importance in solar energy conversion due to the ingenious arrangement of cations and anions with better chemical stability in avoiding

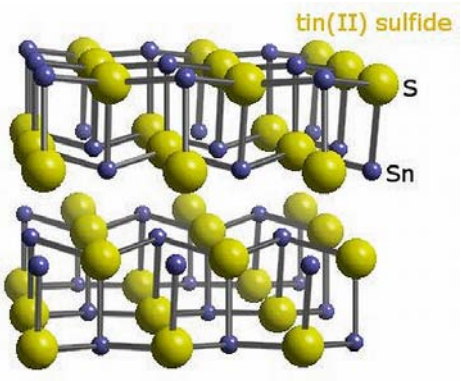

Figure 4.19
Crystal structure of SnS

corrosion in photoelectrochemical cells. Such materials are useful for the fabrication of highly mismatched solid-state junction without interface states [53]. In addition, it has high theoretical solar conversion efficiency [53]. Thin films of SnS have been prepared using several techniques such as vacuum evaporation [54], RF sputtering [55], cathodic electro deposition [56], CSP [57], electrochemical deposition [58], and atmospheric pressure CVD [59].

4.9 Fabrication

In the present work thin films of SnS were deposited on glass substrates using CSP. Details of the CSP technique for fabrication of SnS thin films were reported earlier by Sajeesh et al [60]. Four sets of uniform films were fabricated by taking equal volumes of doubly hydrated stannous chloride ($SnCl_2.2H_2O$) and thiourea ($CS(NH_2)_2$) as precursor solution. In set I while maintaining the substrate temperature at 250 ^{0}C, Sn/S ratio at 1 and concentration at 0.2 M, the spray rate was varied as 1 ml/min, 2 ml/min, 4 ml/min and 6 ml/min deposited films. These samples were named as SR1, SR2, SR4 and SR6 where 1, 2, 4 and 6 represent the values of 'spray rate'. In set II, films were prepared at fixed spray rate of 2ml/min, substrate temperature 250 ^{0}C, and Sn/S ratio of 1, while the molarity of the spray solution was varied as 0.075 M, 0.1 M, 0.15 M and 0.2 M. These samples were coded as SM1, SM2, SM3 and SM4 respectively. In set III, films were deposited with fixed substrate temperature (250 ^{0}C); solution molarity (0.1 M) and spray rate (2 ml/min) while the Sn/S ratio was varied as 1/1, 1/2, 1/3 and ¼. These films were coded as S11, S12, S13 and S14 respectively. Finally in set IV, films were deposited with fixed spray rate of 2 ml/min, fixed Sn/S ratio at 1, molarity was kept 0.1 M while the substrate temperature was varied as 250^{0}C, 300^{0}C, 350^{0}C and 400^{0}C. The films were coded accordingly as S250, S300, S350 and S400, where 250, 300, 350, 400 represent the deposition temperature (^{0}C). The volume of spray solution was 30 ml for all depositions.

4.10 Photothermal analysis of SnS thin films

4.10.1 Influence of spray rate

Figure 4.20 depicts the photothermal beam deflection signal plot of Log_e (signal amplitude) versus (chopping frequency) $^{1/2}$ for the SnS samples SR1, SR2 and SR6. Films deposited at low rates tend to produce films with good surface. Table 4.10 depicts values of D_s, μ, V_{sr}, τ_r of SR1, SR2, SR4 and SR6. As expected, films deposited at a rate of 1 ml/minute have the lowest V_{sr} value, representing a surface with least surface states, as the film formation at this spray rate is complete and has a surface with minimum number of dangling bonds. But as the spray rate increases V_{sr} also increases, which indicates the creation of more recombination centres at film surface. However at low deposition rate (1 ml/minute) even though V_{sr} is very low ($4x10^2$ cm/s), which are nearly two orders less than other samples, it is observed that τ_r is also very low (0.9 μs). Such a decrease in τ_r is probably due to the

incorporation of oxygen in the bulk of the film when deposition is happening at very slow rate.

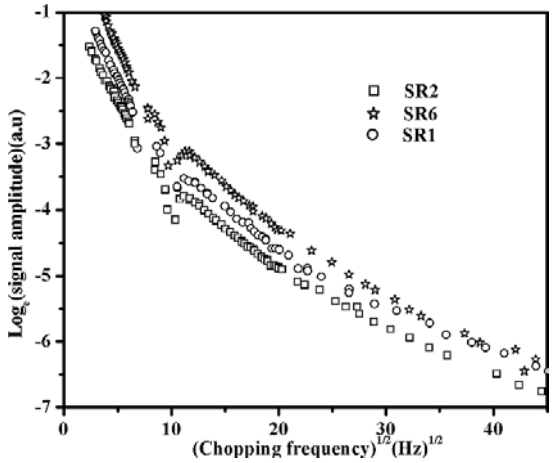

Figure 4.20 Photothermal response of SnS samples coded SR1, SR2, and SR6

Table 4.10
Transport properties of SnS thin films coded SR1, SR2, SR4 and SR6

Sample code	D_s (x10^{-4} cm^2/s)	μ (cm^2/Vs)	V_{sr} (cm/s)	τ_r (μs)
SR1	7	0.93	4x10^2	0.9
SR2	9	1.10	1x10^4	3.5
SR4	9	0.75	1.8 x10^4	3.3
SR6	9	0.36	3x104	3.0

When spray rate is 2 ml/minute values of V_{sr} (1x10^4 cm/s) and τ_r (3.5 μs) are comparatively high. In addition to this, figure 4.20 also makes it clear that the non-radiative loss is least in this sample. Hence in sample SR2, despite having V_{sr} values higher than SR1 samples, the formation of non-radiative recombination centres is the least. Mobility (1.1 cm^2/Vs) is the highest for sample SR2. Hence the spray rate of 2 ml/minute was chosen for further studies, as it yielded films with least non-radiative states, high lifetime and high mobility. Figure 4.21 shows the photothermal image of sample prepared at rate of 1 ml/min. The surface uniformity of this film is also better compared to films prepared at higher spray rates.

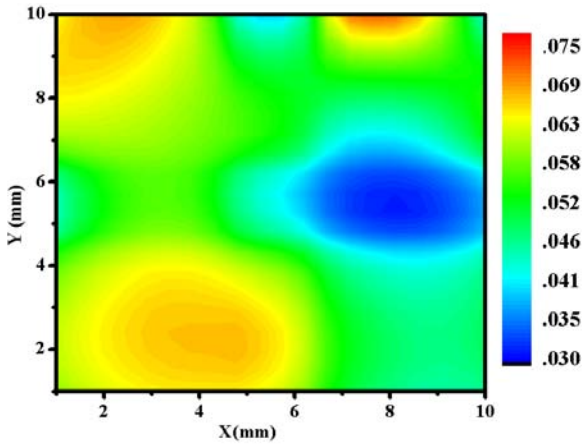

Figure 4.21
2-D Photothermal image of SnS thin film (SR1)

4.10.2 Influence of molarity of spray solution

Figure 4.22 depicts the plot of Log_e (signal amplitude) versus (chopping frequency) $^{1/2}$ of films deposited with different spray solution concentrations. Here one can note that the non-radiative thermal emission is the least for sample SM4 and falls off rapidly with increase in chopping frequency. Table 4.11 gives the transport properties of SM1, SM2, SM3 and SM4. We find that in terms of transport properties, SM4 is slightly better in quality, with least V_{sr} ($1.2x10^4$ cm/s), higher τ_r (0.5 **μ**s) and μ (1.11 cm/Vs). This is because, as concentration of spray solution increases, the film gets thicker. Hence the surface defects, which could have led to high non-radiative recombinations, are not much effective in this case. But at this high concentration, formation of other phases (like Sn_2S_3 and SnS_2) occurs due to the presence of excess sulphur (Figure 4.22). XRD pattern in figure 4.23 shows that films SM2 with molarity 0.1 M are single phase and have better crystallinity. Hence, despite the better transport properties, the sample SM4, which has mixed phases of Sn_2S_3, is not preferred in fabrication of solar cells. Instead we choose SM2 with spray solution concentration 0.1 M for further studies.

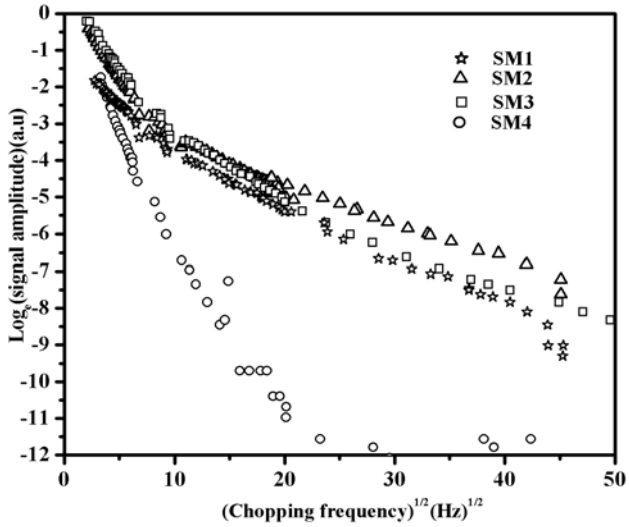

Figure 4.22 Photothermal response of SnS samples SM1, SM2, SM3, SM4

Table 4.11
Transport properties of SnS films coded SM1, SM2, SM3, SM4

Sample Code	D_s (10^{-4} cm^2/s)	μ (cm^2/Vs)	V_{sr} (cm/s)	τ_r (μs)
SM1	10	0.17	$7x10^6$	.2
SM2	10	0.90	$5x10^6$	.2
SM3	10	0.82	$1.2x10^6$	.2
SM4	20	1.11	$1.2x10^6$	.5

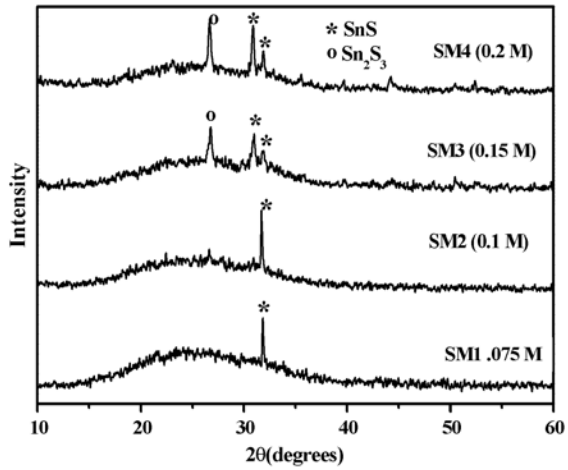

Figure 4.23 XRD pattern of SM1, SM2, SM3 and SM4 samples

4.10.3 Influence of Sn/S ratio in precursor solution

Chemical composition of the constituents in the sample is another important parameter in controlling the optoelectronic properties. So films of different stoichiometry were prepared using precursors of different ratios. Figure 4.24 shows the plot of Log_e (signal amplitude) versus (chopping frequency) $^{1/2}$ of SnS samples S11, S12, S13 prepared at different Sn/S ratio. When the ratio of Sn and S in the precursor solution is varied, the non-radiative thermal emission and transport properties are affected considerably. Excess/deficiency of Sn/S leads to formation of defects and mixed phase compounds, which lead to non-radiative losses and can affect the transport properties of the films. Films prepared at ½ ratio are stoichiometric as observed from EDAX report (Table 4.12) and for this set of films, V_{sr} was the least and τ_r the highest (Table 4.13). μ of S12 was also found to be the highest. This correlates well with our other results. Hence this particular ratio of Sn/S (1/2) was chosen for further studies. Also these films had the least non-radiative loss.

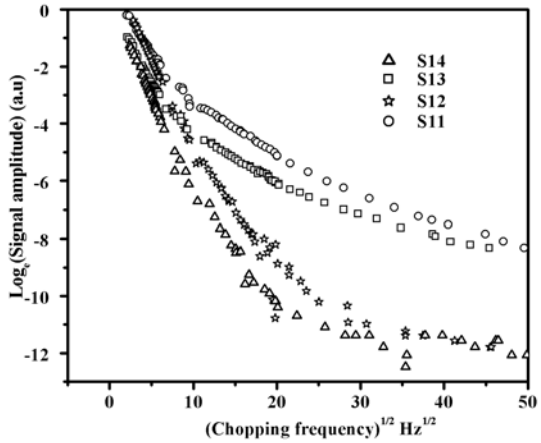

Figure 4.24 Photothermal response of SnS samples S11, S12, S13 and S14

Figure 4.25 (a, b, c, d) shows the photothermal image of samples S11, S12, S13 and S14. Thus composition of film also plays a critical role in deciding the thermal uniformity of the film. The image of S12 sample (Figure 4.24 b), which was found to have low non-radiative loss throughout the film and higher uniformity, exhibited better electronic and thermal transport properties.

Table 4.12
EDAX report of S11, S12, S13 samples

Ratio	Sn	S	Cl	Sn/S
1/1	58.52	33.94	8.34	1.72
1/2	48.78	46.42	4.79	1.05
1/3	49.01	48.55	2.44	1.009

Table 4.13
Transport properties of SnS film S11, S12, S13, S14

Sample code	D_s (x 10^{-4} cm^2/s)	μ (cm^2/Vs)	V_{sr} (cm/s)	τ_r (μs)
S11	10	1.33	$5x10^4$	0.2
S12	20	4.75	$2x10^4$	0.6
S13	9.5	0.90	$7x10^4$	0.1
S14	15	1.21	$3x10^4$	0.4

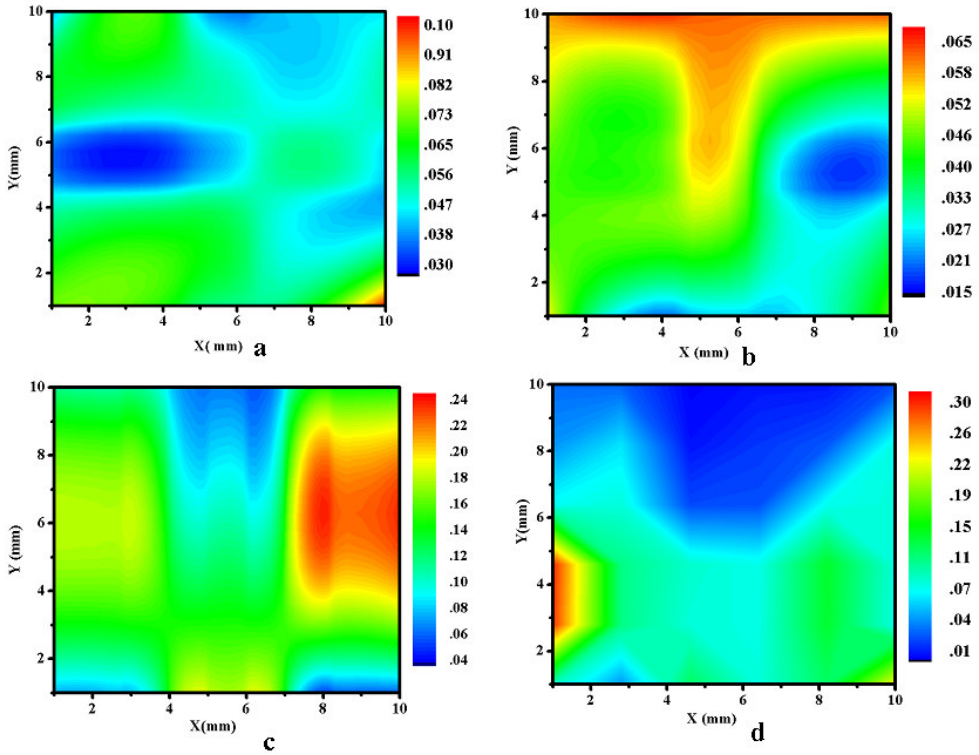

Figure 4.25 2-D Photothermal image of (a) S11 (b) S12 (c) S13 (d) S14

4.10.4 Influence of substrate temperature

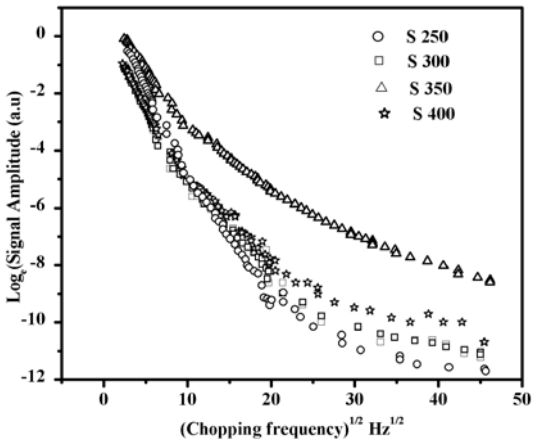

Figure 4.26 Photothermal response of SnS samples S250, S300, S350, S400

Figure 4.26 shows the plot of Log_e (signal amplitude) versus (chopping frequency) $^{1/2}$ for samples S250, S300, S350 and S400. Here photo thermal signal amplitude increases with increase in deposition temperature and is highest for the sample S350. Table 4.14 exhibits the values of μ, τ_r, V_{sr} and D_s obtained for this set of films. With increase in deposition temperature V_{sr} tends to have low value for the samples prepared at temperature lower than 300^0C. But for $T_S > 300\ ^0$C, V_{sr} increases with temperature. It has been reported earlier that films grown at temperatures between 150 ^{0}C and 300 ^{0}C showed presence of Sn_2S_3 and SnS_2 phases; but at higher temperatures ($300\ ^0C < T_S < 360\ ^0C$) films exhibited only SnS phase and for $T_S > 360\ ^0$C, SnO_2 phase was formed [61]. This explains why the value of V_{sr} is the least for films prepared at substrate temperature 300 ^{0}C and 350 ^{0}C.

Table 4.14
Variation of transport properties with deposition temperature

Sample code	D_s (x10^{-4} cm^2/s)	μ (cm^2/Vs)	V_{sr} (cm/s)	τ_r (μs)
S250	20	4.75	$2x10^4$	0.6
S300	12	2.3	$9x10^3$	0.13
S350	11	4.3	$2x10^4$	0.8
S400	14	0.69	$8x10^4$	0.3

Presence of mixed phase compounds can lead to formation of incomplete bonds in the film surface. Depositions at high temperature can also cause oxidation of film component, more predominantly at film surface, because higher evaporation of sulphur from film can lead to reaction of excess Sn with oxygen to form SnO_2. There are reports stating that at high temperature formation of SnO_2 as well as the conversion of SnS to SnO_2 may take place on the surface of the film; this surface layer of oxide film inhibits further oxidation of the film towards the interior [62]. Thus at high temperatures surface quality of the film is affected

by oxidation making V_{sr} high for temperatures greater than 350 ^{0}C. Hence the temperature 350 ^{0}C, which offers high mobility and τ_r was chosen as the optimum substrate temperature for deposition of SnS films that would act as absorber layer in a heterojunctions solar cell.

Photothermal signal dependence on V_{sr}, τ_r, μ and D_s is exploited to evaluate these parameters and thus study their dependence on deposition parameters. Photothermal imaging results also assist in identifying the films with good thermal uniformity. Hence the optimum spray parameters required for obtaining good quality SnS films, which can be used as absorbers in thin film solar cells, were identified.

4.11 Conclusion

PTBD technique was successfully used to measure D_S, μ, τ_r and V_{sr} of $CuInS_2$, $CuInSe_2$ and SnS thin films, which find application as absorber layer in thin photovoltaic devices. The non-radiative nature of films is also analyzed and the results are correlated with other optical, structural and composition analysis tools, to optimize the deposition parameters that yield device quality thin films. Thus, through this work, we could establish the application of PTBD as an efficient and simple tool for real time thin film analysis for controlling the device fabrication process.

References

[1] J Klaer, I Luck, A Boden, R Klenk, I G Perez, R Scheer 2003 *Thin Solid Films* **431/432** 534
[2] J Klaer, J Bruns, R Henninger, K Siemer, R Klenk, K Ellmer, D Bräunig 1998 *Semicond Sci Technol* **13** 1456
[3] J D Harris, K K Banger, D A Scheiman, M A Smith, M H C Jin, A F Hepp 2003 *Mat Sci Eng* **B98** 150
[4] S L Castro, S G Bailey, R P Raffaelle, K K Banger, A F Hepp 2003 *Chem Mater* **15** 3142
[5] J M Meese, J C Manthurathil, D R Locker 1975 *Bull Am Phys. Soc.* **20** 696
[6] L L Kazmerskii, M S Ayagari, G A Sanborn 1975 *J Appl Phys* **46** 4865
[7] C Guillén 2006 *Semicond Sci Technol* **21** 709
[8] Y B He, W Kriegseis, B K Meyer, A Polity, M Serafin 2003 *Appl Phys Lett* **83** 1743
[9] M K Agarwal, P D Patel, S H Chaki, D Lakshminarayana 1998 *Bull Mater Sci* **21** 291
[10] A N Tiwari, D K Pandya K L Chopra 1985 *Thin Solid Films* **130** 217
[11] G Hodes, D Cahen, J Manassen M David 1980 *J Electrochem Soc* **127** 2252
[12] H L Hwang, B H Tseng, C Y Stin, J J Loferski 1980 *Solar Energy Mater* **4** 67
[13] A N Y Saman, S M Wasim, A E Hill, D G Armour, R D Tamlinson 1986 *Phys Stat Sol (a)* **93** 317
[14] A M Abo El Soud, H A Zayed, L A Soliman 1993 *Thin Solid Films* **229** 232
[15] B Pamplin, R S Feigalson 1979 *Thin Solid Films* **60** 141
[16] T T John 2004 *PhD Thesis*, Cochin University of Science and Technology, India
[17] K T Yamaguchi, H Nakamura, T Nabetani, Y Matsumoto 2006 *Phys Stat Sol (c)* **3** 2606
[18] Y Akaki, K Nomoto, S Nakamura, T Yoshitake, K Yoshino 2008 *J Phys: Conf Ser* **100** 082022
[19] S Mora, N Romeo, L Tarricone 1979 *Solid State Commun* **29** 155
[20] H Bihri, M Abd-Lefdil 1999 *Thin Solid Films* **354** 5
[21] L Hwang, C Y Sun, C Y Leu, C L Cheng, C C Tu 1978 *Revue de Physique Appliquée* **13** 745

[22] T Sebastian, M Gopinath, C S Kartha, K P Vijayakumar, T Abe, Y Kashiwaba 2009 *Solar Energy* **83** 1683
[23] K Dejessas, G Masse, Ibannaim 2000 *J of Electrochem Soc* **147** 1235
[24] M Krunks, A Mere, A Katerski, V Mikli, J Krustok 2006 *Thin Solid Films* **434** 511
[25] R Scheer, M Alt, I Luck, and H J Lewerenz 1997 *Sol Energy Mater Sol Cells* **49** 423
[26] I Repins et al 2008 *33rd IEEE Photovoltaic Specialists Conference,* San Diego
[27] K L Chopra, P D Paulson V Dutta 2004 *Prog Photovolt Res Appl* **12** 69
[28] K Ramanathan et al 2003 *Prog Photovolt Res Appl* **11** 225
[29] M Varela, E Bertran, M Manchon, J Esteve, J L Morenza, 1986 *J Phys D Appl Phys* **19** 127
[30] A H Moharram, M M Hafiz, A Salem 2001 *Appl Surf Sci* **172** 61
[31] N Romeo, V Canevari, G Sberveglieri, A Bosio L Zanotti 1986 *Solar Cells* **16** 155
[32] M Gorska, R Beaulieu, J J Loferski, B Roessler J Beall 1980 *Solar Energy Materials* **2** 343
[33] S Niki, P J Fons, Y Lacroix, K Iwata, A Yamada, H Oyanagi, M Uchino, Y Suzuki, R Suzuki, S Ishibashi, T Ohdaira, N Sakai, H Yokokawa 1999 *J Cryst Growth* **201/202** 1061
[34] J Piekoszewski, J J Loferski, R Beaulieu, J Beall, B Roessler, J Shewchun 1980 *Solar Energy Mater* **2** 363
[35] M E Calixto, P J Sebastian 1998 *J Mater Sci* **33** 339
[36] M C Artaud, F Ouchen, L Martin, S Duchemin 1998 *Thin Solid Films* **324** 115
[37] A Ashour, A A Ramadana, K Abd EL-Hady, A A S Akl 2005 *J of Optoelectron Adv Mater* **7** 1493
[38] J C Garg, R P Sharma, K C Sharma 1988 *Thin Solid Films* **164** 269
[39] A Ashour, A A Akl, A A Ramadan, K A E Hady 2005 *J Mater Sci* **16** 599
[40] M R A Magomedov, S M Ismailov, D K Magomedova, P P Khokhlachev 2000 *Semiconductors* **34** 662
[41] M Tabib Azar, H J Moller, N Shoemaker 1993 *IEEE Trans Ultrason Ferroelectr Freq control* **40** 149
[42] C H Champness 1999 *J Mater Sci* **10** 605
[43] J Piekoszewski, L Castaner, J J Loferski, J Beall, W Giriat 1980 *J Appl Phys* **51** 5375
[44] H F Myers, C H Champness, I Shih 2010 *Nanotechnology* **21** 134004
[45] K Puech, S Zott, K Leo, M Ruckh, H W Schock 1985 *Appl Phys Lett* **69** 3375
[46] K G Deepa, P M Ratheesh Kumar, C S Kartha, K P Vijayakumar 2006 *Sol Energy Maters Sol cells* **90** 3481
[47] M Ristov, G J Sinadianovski, I. Grozdanov, M Mttoeski 1989 *Thin Solid Films* **173** 53
[48] H Noguchi, A Setiyadi, H Tanamura, T Nagatomo, O Omoto 1994 *Sol Energy Mater Sol cells* **30** 325
[49] W Albers, C Haas, H J Vink J D Wasscher 1961 *J Appl Phys* **32** 2220
[50] A M Elkorashy 1991 *Physica B* **168** 257.
[51] M Gunasekharan, M Ichimura 2007 *Sol Energy Mater Sol cells* **91** 774
[52] R H Bube 1960 *Photoconductivity of Solids*, Wiley, New York
[53] J J Loferski 1956 *J Appl Phys* **27** 777
[54] L Price, I P Parkin, A M E Hardy, R J H Clark 1999 *Chem Matter* **11** 1792
[55] W G Pu, Z Z Lin, Z W Ming, G X Hong, C W Quin 1994 *Proc First World conf Photovoltaic Energy Conversion*, Hawaii, 365
[56] Z Zainal, M Zobir Hussein, A Ghazali 1996 *Sol Energy Mater Sol Cells* **40** 347
[57] H B H Salah, H Bouzouita, B Rezig 2005 *Thin Solid Films* **480/481** 439
[58] S Cheng, Y Chen, C Huang, G Chen 2006 *Thin Solid Films* **500** 96
[59] A S Juarez, A Ortiz 2002 *Semi Cond Sci Technol* **17** 931
[60] T H Sajeesh, A R Warrier, C S Kartha, K P Vijayakumar 2010 *Thin Solid Films* **518** 4370
[61] N Koteeswara Reddy, K T Ramakrishna Reddy 2005 *Physica B* **368** 25.
[62] P K Nair, M T S Nair, R Z Zingaro, E A Meyers 1994 *Thin Solid Films* **239** 85

5

Photothermal analysis of buffer layer material

PTBD technique is used for investigation of indium sulphide thin films, which are used as buffer layer material in compound semiconductor thin film solar cells. β-In_2S_3 thin films with different atomic ratios (i.e., In: S ratio), deposited using CSP method, is excited using energy 2.81 eV for determining the transport properties of this material. Variation of photothermal response due to 'above band gap' (2.81 eV) and 'sub band gap' (2.33 eV and 1.96 eV) excitations are analysed to study the non-radiative defect nature of the film. Study also revealed that the inherent dopant chlorine plays a substantial role in influencing the transport properties of the film. Photothermal signal amplitude and phase information obtained from this technique is used for studying the effect of diffusion of Ag, which is used as electrode material, into In_2S_3 films.

5.1 Introduction

Optimisation of junction layers of a solar cell is essential for achieving its high performance. In thin film solar cells, buffer layers are used to enhance empirical V_{OC} and this effectively improves the junction efficiency [1]. Buffer layer, when used near the top of a cell, is beneficial for optical enhancement because of reduced absorption and reflection losses. This layer in a solar cell is also responsible for a number of effects that significantly influence the efficiency of solar cells [2]. For example, it assists in improving the cells efficiency by separating the contact, which has high minority-carrier recombination loss from the absorber or base layer. An effective injection of carriers (between the face electrode and the absorbing layer) and a maximum transmission of light can be attained by using optimum material as the buffer layer. This layer is usually made from high-optical-quality, *n*-type films based on a wide band gap semiconductor compound. A wide band gap material is well suited for efficiently transmitting the blue spectrum of sunlight to the PN junction, thus enhancing the solar cell efficiency. One of the most promising buffer materials suitable for this purpose is In_2S_3. It is a wide band gap material (2.6 eV) [3] and cells, fabricated using In_2S_3 as the buffer layer, have shown efficiency as high as 16.4%[4]. This material has been widely used to replace the use of toxic CdS layer [5]. Materials such as ZnO, ZnSe, $ZnIn_xSe_y$ and In_xSe_y are also promising candidates to be used as buffer materials in CIS based solar cells.

Motivation for the present work on photothermal analysis of In_2S_3 films is the earlier studies done on spray pyrolysed In_2S_3 films by our group. These works have revealed several interesting aspects of the material and could also produce cells with high efficiency [6]. We studied how the film composition and dopant affect the non-radiative transitions and transport properties of the material; these results were applied for improving the fabrication process to achieve better transport properties and to produce more effective solar cell junction.

5.2 Indium sulphide

In_2S_3 belonging to III-VI group is a wide band gap semiconductor with high absorption coefficient and intense luminescence [7] and is a promising buffer layer material for compound semiconductor heterojunction thin film solar cell. Figure 5.1 illustrates the crystal structure of In_2S_3. It crystallizes in spinel structure and exists in four crystallographic modifications. Room temperature phase of β-In_2S_3 crystallizes in defect spinel structure with high degree of vacancies in tetrahedral sites [8]. Ordering of the vacant tetrahedral sites is a parameter having major influence on the electrical conductivity of thin films of this material [9]. With such a defect structure, its properties can be tailored easily to meet the device requirements either by changing the stoichiometry or by doping [10, 11]. Several key aspects of device performance like photoresponse, electrical conductivity depend on the presence of defects such as vacancies and interstitials. These defects play an important role in improving the photosensitivity of the materials to white light, as they enable carrier generation through sub band gap photon absorption [12, 13]. Manipulation of atomic concentration in the film or doping can control such defects. There are several works reporting the electrical and optical characterization and tuning of the properties of β-In_2S_3 films [14, 15, 16]. The optimal electrical and optical properties, together with its ability to generate free carriers under sub band gap excitation boost the demand of this material in photovoltaic market as a viable candidate for fabrication of high efficiency solar cells [17]. Substantial advancements have been done in this area, proving it to be a successful binary base material for growth of $CuInS_2$ based thin film heterojunction solar cells [18]. In_2S_3 buffer layers deposited using the 'Spray-Ion Layer Gas Reaction (Spray-ILGAR)' technique have recently been used with Cu (In, Ga)(S, Se) $_2$ as absorber, resulting in cells with an efficiency of 13.1% which is equal to that obtained from CdS based cells [19]. It is thus viewed as a potential eco-friendly material replacing toxic cadmium in CIGS based solar cells [20]. Spiering et al deposited In_2S_3 buffer layer employing MOVCD with Cu (In, Ga) Se_2 as absorber and reported an efficiency of 12.3% [21]. Teny et al fabricated $CuInS_2/In_2S_3$ solar cells with 9.5 % efficiency using CSP technique [6].

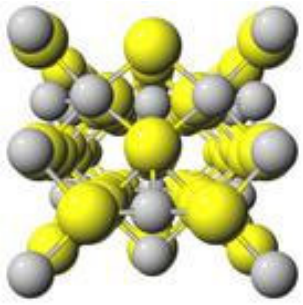

Figure 5.1 Crystal structure of In_2S_3

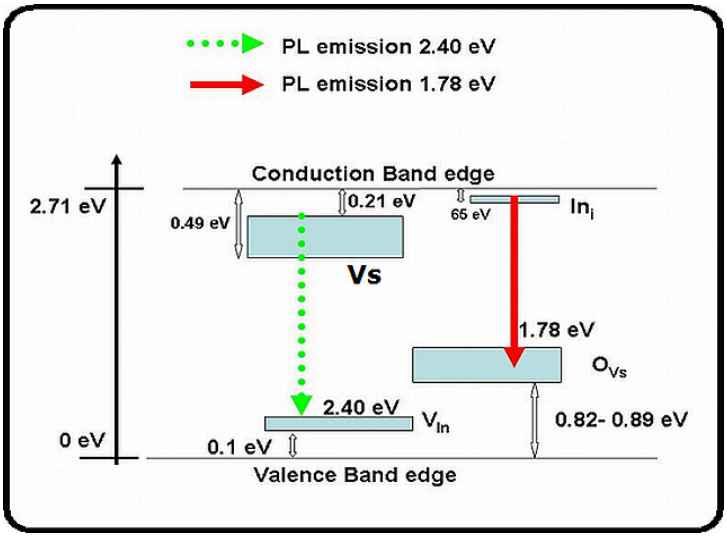

Figure 5.2: Energy band diagram of β-In_2S_3 films as determined by PL studies

The interesting optical and electrical properties exhibited by this material motivated the present work on photothermal analysis of In_2S_3 films. β-In_2S_3 films are inherently n-type and the grains showed preferential orientation along 220 plane. Depending on the film composition, band gap was reported to vary from 2.64 eV to 2.71 eV and these films had high absorption coefficient of order 10^5 cm^{-1} in blue region. Our group itself reported earlier that β-In_2S_3 films prepared using CSP with indium chloride and thiourea as precursors contained traces of chlorine. XPS analysis of these samples showed that chlorine in elemental form was present throughout the sample thickness [13]. Studies also showed that incorporation of chlorine in prescribed quantity could enhance crystallinity and photosensitivity of the film [22]. Thermally stimulated current (TSC) measurements helped us in understanding how the defects rule electrical properties and non-radiative transitions occurring in this material [23]. Using photoluminescence (PL) studies, Jayakrishnan et al [24] had put forth an energy level scheme (Figure 5.2) for this material, which provides insight on various radiative recombination processes taking place in the film. Role of stoichiometry in deciding the probability of recombination process was also clearly depicted in this report [24]. Defect analysis from TSC measurements and PL studies had revealed the presence of four types of defects (viz., indium vacancy (V_{In}), sulphur vacancy (V_S), oxygen in sulphur vacancy (O_{VS}) and chlorine impurity) and identification of their activation energies and trapping crossection. Photoresponse of these films was studied to analyse the role of grain boundaries and persistent photoconductivity in this material [25]. In semiconductors, metallic impurities are known to introduce deep levels at which non-radiative recombination occurs [26]. The defects, which assist sub band gap photon absorption and free carrier generation, depend on the film stoichiometry and impurities present in it. We aim to study how the defects contribute to non-radiative nature and transport properties of the film.

5.2.1 Fabrication of Indium sulphide thin films

β-In_2S_3 thin films were deposited over glass slides (37 x 12 x 1.4 mm^3) using CSP technique [13]. The films were fabricated with indium chloride and thiourea as precursor solution, keeping the spray volume at 400 ml, spray rate at 20 ml/min and substrate temperature at 300^0C. Stoichiometry of the films was varied by adjusting the molarity of the precursor solutions. Films chosen for the photothermal analysis had different compositions with In/S as 0.64, 0.68 and 0.79 (coded as, P_1, P_2, and P_3 respectively). All these films (P-series), which had indium chloride as a precursor, contained traces of chlorine existing as an inherent dopant [13]. To obtain films with no chlorine, another set of films (coded D-series), were fabricated under similar deposition conditions using indium nitrate and thiourea as precursors. Chlorine was subsequently introduced in to the samples, in calculated amount, by adding ammonium chloride in the spray solution. The amount of chlorine incorporated in the film was controlled by varying the quantity of ammonium chloride (3.5 ml, 5.5 ml, 7.5 ml). These samples, in which chlorine was deliberately incorporated, were coded as D_1, D_2 and D_3 respectively and the film with no chlorine was coded as D_0.

5.2.2 Photothermal analysis of β-Indium sulphide thin films

Samples of size 1x1 cm^2 were irradiated using CW laser beams of 'above band gap' energy (2.81 eV) and 'sub band gap' (2.33 eV and 1.96 eV) with power 10 mW to analyse their photothermal response. The power of all three incident beams was maintained at 10 mW using ND filters. In β-In_2S_3 films, irradiated with beam of energy 2.81 eV, carriers are excited from valence band to highest possible level of conduction band. Later they de-excite by thermal emission to the minimum of conduction band (intra band transitions) and some diffuse before they recombine; other carriers recombine radiatively or non-radiatively and relax back to valence band. Thermal waves thus generated produce photothermal signals whose signal amplitude varies with chopping frequency.

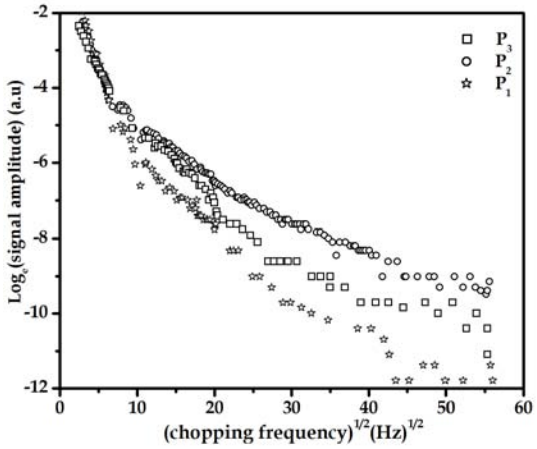

Figure 5.3 PTBD response of samples P_1, P_2 and P_3 upon 2.81 eV excitation

Variation of slope of the photothermal signal with chopper frequency in the lower frequency is an indication of the intraband transitions occurring in the material and response in higher frequency region implies the presence of non-radiative recombination centres in the bulk and surface of the material. Photothermal responses of samples P_1, P_2 and P_3 are depicted in figure 5.3.

The signals due to intraband transitions are almost the same in all the three samples and as the frequency reaches 100 Hz, the response is lowest for P_1 having least In/S (0.64) and highest for sample P_2 (In/S 0.68). But for sample P_3 with highest In/S (.79) the non-radiative emission is lower than P_2. Hence the defect density is higher for sample P_2. Table 5.1 shows the EDAX measurements of samples P_1, P_2 and P_3.

Table 5.1

EDAX report of the β-In_2S_3 films with 'inherent' chlorine (P series)

Sample code	In/S	Cl	Cl/In+S
P_1	0.64	8.6	0.094
P_2	0.68	10.77	0.12
P_3	0.79	15.38	0.18

Table 5.2
Transport properties of P-series sample

Sample code	D_s (10^{-4} cm^2/s)	μ (cm^2/Vs)	$V_{sr}x10^3$ (cm/s)	τ_r (μs)
P_1	9	0.46	5	100
P_2	8.4	2.0	10	100
P_3	10	2.68	5	100

Table 5.2 shows the transport properties obtained using PTBD technique. V_{sr} was highest ($1x10^4$cm/s) for P_2, while it was almost same for other samples. High V_{sr} indicates the presence of more surface defects in film P_2, which contribute to the high non-radiative losses. However τ_r remained same (100 μs) for all samples. μ was high for P_2 and P_3 with values 2.68 and 2.0 cm^2/V_s respectively. Higher non-radiative loss is an indication of high defect density and there is a tendency to affect the transport properties by shortening the carrier diffusion length due to scattering and / or recombination of carriers at defects. But in this case, we find mobility is high for samples (P_1 and P_2), which showed high PTBD signal. Variation in V_{sr} alone with no change in lifetime in the sample suggests that bulk defects are not very much affected with change in composition. For P_2 the non-radiative loss is high mainly due to surface defects which donot affect diffusion of carriers in the bulk of the material. Also in samples P_2 and P_3, interestingly chlorine incorporation is highest. Chlorine has been reported to be beneficial in improving the grain size and hence the crystallinity [22]. Hence for films with high chlorine incorporation, scattering of carriers at grain boundaries is reduced considerably and this increased the carrier mobility. Thermal diffusivity is slightly high for P_3, which also proves that the increase in chlorine content, which improved the grain size reducing the scattering effect of thermal waves at

grain boundaries. It has been reported that in chlorine doped CdS films (thermally evaporated), mobility increased and resistivity decreased with increase in chlorine doping [27]. Further, carrier diffusion in solids is influenced by presence of vacancies or grain boundaries as they provide additional path for carriers [28]. Such conducting boundaries in Cl doped In_2S_3 films have been observed reported earlier [25].

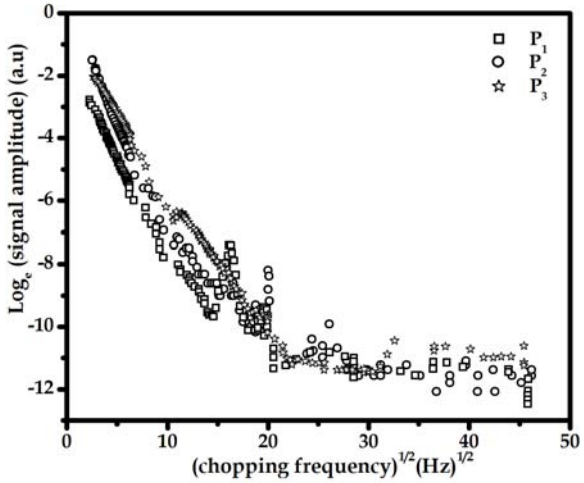

Figure 5.4a PTBD signal response on excitation using 2.33 eV

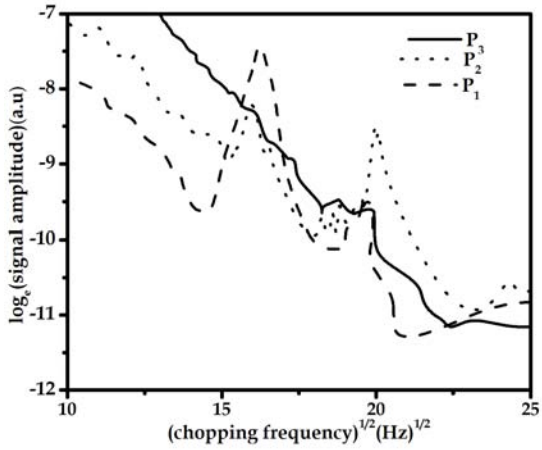

Figure 5.4b PTBD signal response in 100 Hz to 500 Hz for P_1, P_2, P_3 upon 2.33 eV excitation

All the facts suggest that incorporation of chlorine has major role in altering the transport properties of the In_2S_3 films. To study the role of chlorine in creation of defect levels that can cause non-radiative losses, the films were excited using 2.33 eV and 1.96 eV. Upon excitation using 2.33 eV, the carriers were possibly excited from the valence band to a defect level formed due to vacancy of sulphur (V_S) (Figure 5.2). Hence the photothermal response we observe here is due to the relaxation of carriers from this defect level. Figure 5.4a and 5.4b show the photothermal signal plot of samples P_1, P_2 and P_3 when excited using 2.33 eV. The photothermal response due to 2.33 eV is highest for P_3 and decreases for P_2 and P_1 with the decrease in In/S ratio. The samples P_1 and P_2 show a peak at high

frequency (> 200 Hz), with the peak intensity being higher for sample P_1 while for sample P_3 this peak is not seen (figure 5.4b). Such peaks are due to the non-radiative emission occurring at the non-radiative recombination centres. The incorporation of chlorine can passivate these recombination centres and hence we find that these peaks are curbed in sample P_3 with high chlorine incorporation. Peak intensity is highest for P_1 with low chlorine incorporation. The increase in photosensitivity [22] and minority carrier mobility in films with high Cl incorporation is possibly due to purging of non-radiative recombination centres that affect the photosensitivity of the films. The photothermal response obtained on excitation using 1.96 eV carriers were due to deexcitation from conduction band because the absorption of 1.96 eV can excite the carriers from defect level O_{VS} to conduction band (Figure 5.2). Figure 5.5 illustrates the photothermal signal variation of P_1, P_2 and P_3 with 1.96 eV, where we find the non-radiative emission varies only slightly with signal; this is the highest for P_2, similar to the result due to excitation using 2.81 eV. For understanding the photothermal response of each sample at different excitation wavelength and hence realise the role of defects in affecting the signal response due to sub band gap energy absorption, we plotted the photothermal response for 2.81 eV, 2.33 eV and 1.96 eV (Figure 5.6 a, 5.6 b and 5.6 c for samples P_1, P_2 and P_3 respectively).

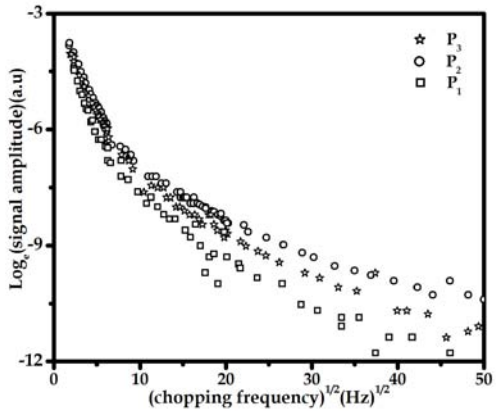

Figure 5.5 PTBD signal response of P_1, P_2 and P_3 due to 1.96 eV excitation

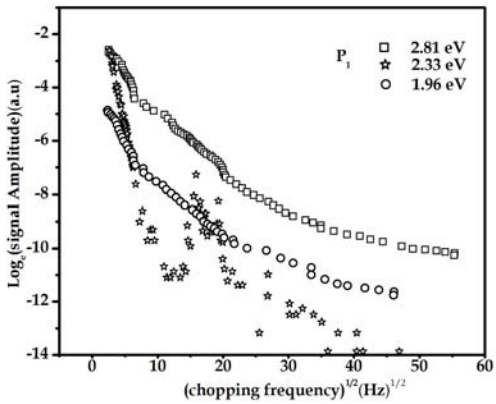

Figure 5.6a Photothermal responses of P_1 on excitation with 2.81, 2.33, 1.96 eV

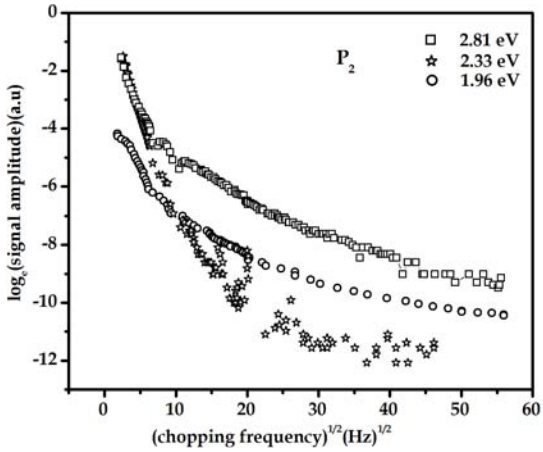

Figure 5.6b Photothermal response of P_2 on excitation with 2.81, 2.33, 1.96 eV

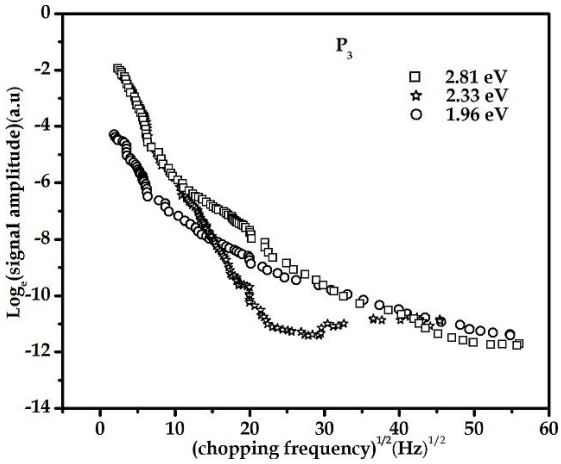

Figure 5.6c Photothermal response of samples 2.33 eV

For sample P_1 (Figure 5.6a), the slope of photothermal signal variation for 2.33 eV excitation shows a rapid decline (in frequency regime < 200 Hz), whereas the slope of the signal for both 2.81 eV and 1.96 eV excitation varies slowly. The signal variation for chopping frequency < 200 Hz is due to intraband transitions. For the 'above-band gap' excitations, (i.e., using 2.81 eV), the photothermal signal is due to transitions occurring within the conduction band and hence these signals are strong and their decrease with chopping frequency is rather slow. But for 2.33 eV excitation, the carriers can reach only the defect level due to V_S and interestingly this defect level is appearing to be a 'defect band' [24]. The photothermal signal due to transition of carriers from V_S is naturally weak as there is low number of carriers in the defect band and hence decreases rapidly i.e., the level V_S is localized and less dense in sample P_1. But for sample P_2 (Figure 5.6 b) the photothermal signal due to 2.33 eV excitation is stronger (higher amplitude) in low frequency regime and signal variation is more gradual than sample P_1. This indicates that the 'defect band' V_S is denser and hence the probability of non-radiative (intraband) transitions occurring in this level is also higher in this sample. For sample P_3 (Figure 5.6 c), the photothermal response

due to 2.33 eV excitation (frequency region < 200 Hz) is same as the signal variations due to 2.81 eV. This implies that the defect Vs is much denser and appears as a wider 'defect band'. So for sample P_3, the signal due to non-radiative transitions occurring in the defect band is similar to that due to transitions occurring in the conduction band. We may conclude that for sample P_3 for which In: S is least and Cl content is high, the defect V_S exist as a band and for sample P_1 for which the In: S is high and Cl content is low the defect V_S is localized.

The amplitude of photothermal signal due to irradiation with 1.96 eV is lower while nature of the signal variation is similar to that due to 2.81 eV excitation for all the samples (Figure 5.6 a, b and c). This indicates that the signal due to 1.96 eV excitation is resulting from transitions occurring within the conduction band. But as the carriers are excited from defect O_{VS} to conduction band, the number of carrier available for non-radiative decay process is lower and hence the signal is weaker. Thus from photothermal analysis we can also understand the nature of the defect in which the non-radiative transitions take place.

The transport parameters μ and V_{sr} calculated from the photothermal signal due to absorption of 1.96 eV are almost of same order as that for 2.81 eV. But for 1.96 eV excitation τ_r is slightly higher (150 μs); this could be due to the lower number of carrier available in conduction band. As a result, the carrier scattering is reduced when excitation is from a defect level to conduction band rather than from valence band and hence the carriers can propagate farther before they recombine. However the transport properties measured from the signal obtained for 2.33 eV (Table 5.3) are higher than that obtained for 2.81 eV (Table 5.2). The mobility in the defect level is highest for P_3 where the defect level exists as a band. The mobility in extended states is higher than that for localized defect states as the motion of carriers occur by hopping conduction, which is a thermally activated tunnelling between states.

Table 5.3

Transport properties of P_1, P_2, and P_3 (excitation using 2.33 eV)

Sample	D_s (10^{-4} cm^2/s)	μ (cm^2/Vs)	V_{sr} (cm/s)	τ_r (μs)
P_1	7.4	1.6	$5x10^5$	0.1
P_2	8.7	9.63	$2x10^5$	0.1
P_3	9.3	7.4	$2x10^5$	0.1

Table 5.4

EDAX report of the β-In_2S_3 films with 'doped' chlorine (D series)

Sample code	In/S	Cl	Cl/In+S
D_0	0.65	0	0
D_1	0.70	3	0.03
D_2	0.74	10.58	0.12
D_3	0.75	12.5	0.14

Mobility was highest for sample P_3, which had high In/S and high chlorine incorporation. To deduce the role of chlorine in improving the transport properties and deciding the defect nature of the film, we performed PTBD analysis on films with no chlorine D_0 and those containing chlorine in increasing amount ie. Samples D_1, D_2 and D_3 respectively. The atomic concentration of In: S and Cl incorporated in the film is shown in table 5.4. Figure 5.7 shows the plot of (modulation frequency) $^{1/2}$ versus Log_e (signal amplitude) for samples D_0, D_1, D_2, D_3 when excited using 2.81 eV. The photothermal signal is slightly higher for sample D_0 than the other chlorine incorporated films. The density of defects, leading to non-radiative heat losses, is higher in chlorine free films and decreases with increase in chlorine incorporation. The transport parameters D_s, V_{sr}, μ and τ_r obtained for D series samples are shown in Table 5.5. We find that μ is highest for D_3 films in which chlorine incorporation is higher. The V_{sr} is lowest (7 x10^3 cm/s) and τ_r is highest (130 μs) for D_2 which has considerably high Cl content compared to D_1. Mobility and lifetime are the least for D_0 films, which contains no trace of chlorine. Therefore incorporation of chlorine certainly plays an active role in improving the transport properties by controlling the density of V_S and V_{In} in the film.

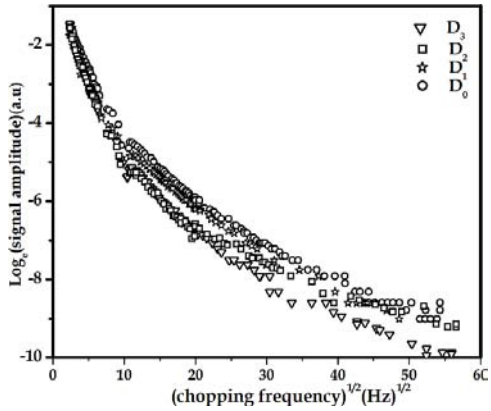

Figure 5.7 Photothermal signal responses of samples D_0, D_1, D_2, D_3 on 2. 81 eV excitation

Table 5.5
Transport properties of D-series sample

Sample	D_s (10^{-4} cm^2/s)	μ (cm^2/Vs)	V_{sr} (cm/s)	τ_r (μs)
D_0	9.2	0.23	11	30
D_1	9	0.38	11	90
D_2	9.2	0.48	7	130
D_3	8	0.60	11	50

Upon excitation with 2.33 eV, the photothermal response, which occurs due to transitions in defect band V_S, was highest for samples with high chlorine incorporation D_3, thus indicating that chlorine incorporation assist in creation of V_S and thus enhancing the absorption of 2.33 eV (Figure 5.8). In EDAX report (Table 5.4) also we find that sulphur content decreases with increase in chlorine, leading to high V_S density.

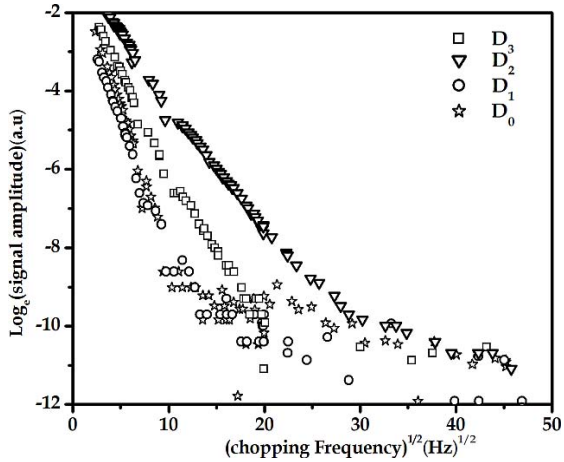

Figure 5.8 Photothermal signal response of samples D_0, D_1, D_2, D_3 on 2.33 eV excitation

In figure 5.9a, showing the PT response for D_0, we find that PTBD signal variation for 2.33 eV is unlike the signal obtained for 2.81 eV. In this sample, the thermal contribution due to intraband transition within defect band V_S is very low and the small peak that is seen at frequency > 300 Hz is due to non-radiative recombinations alone, where as in D_3 and D_2, the defect band due to V_S is well formed and thermal emission from intraband transition and non-radiative recombination equally contribute to the PTBD signal generation. For these samples at lower frequency < 300 Hz, the signal amplitude is similar to that on excitation with 2.81 eV. In figure 5.9b for sample D_2, we observe that PT signal variation due to 2.33 eV excitation is almost similar to that for 2.81 eV. These results are similar to those obtained for P-series sample where we were quite uncertain about the role of chlorine due to the variation in In/S during fabrication. These results confirm that chlorine is responsible for non-radiative transitions occurring in the defect level that causes absorption of 2.33 eV, as the In/S constituents were kept constant during fabrication and only the chlorine content was varied. But on excitation with 1.96 eV, only sample D_3 showed PT response (Figure 5.10). The absorption of 1.96 eV is considered to be due to excitation of carriers from OV_S to conduction band. So in the D-series samples, OV_S defects are lower and oxygen incorporation in sulphur vacancy is reduced.

But for D_3 the chlorine incorporation is highest, and hence chlorine also plays a role in creation of OV_S in the sample, assisting the red absorption. Thus chlorine not only improves the transport properties but also trigger the creation and annihilation of defects present in In_2S_3. Hence by suitably doping with chlorine, one can tune the material properties. Photothermal analysis of β-In_2S_3 films upon excitation using 2.81 eV, 2.33 eV and 1.96 eV impart better understanding of the non-radiative nature of the film, its dependence on films composition and the influence of chlorine. Sample with highest chlorine showed high mobility. From the analysis of samples, which contain accidental incorporation of chlorine (P series) and calculated quantity of chlorine (D series), we could prove that incorporation of chlorine improves the absorption of 2.33 eV due to creation of defect band V_S. Also the studies reveal the creation of defect OV_S, which leads to

absorption of 1.96 eV; interestingly here also chlorine plays an important role. Mobility, surface recombination velocity and minority carrier lifetime were determined using PTBD technique. Chlorine incorporation assists in improving the transport properties of the film as the films with highest chlorine incorporation had high mobility also. PTBD technique is thus demonstrated as an efficient tool for defect analysis of semiconductors.

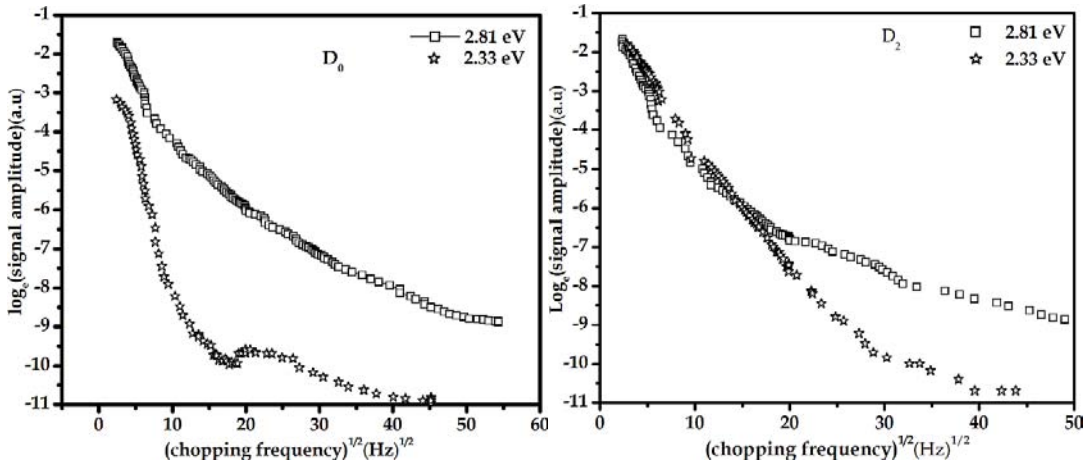

(a) (b)

Figure 5.9 Photothermal response for 2.81 eV and 2. 33 eV excitation of samples (a) D_0 and (b) D_2

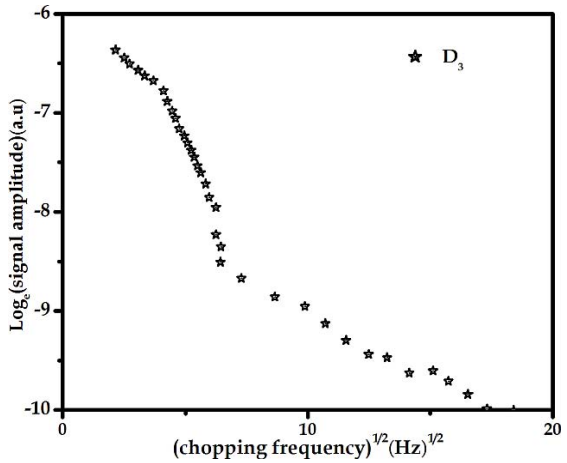

Figure 5.10 Photothermal response of samples D_3 on 1.96 eV excitation

These studies have enabled us to determine the thermal diffusivity, mobility, surface recombination velocity and lifetime of In_2S_3 films and identify the best-suited composition (In/S ~ 0.79) for fabrication of solar cells. Non-radiative transitions occurring due to absorption of above band gap (2.81 eV) and sub band gap (2. 33 eV and 1.96 eV) excitation vary with different chlorine doping level. It can be concluded from this studies that irrespective of the composition of In/S used in spray solution for deposition of In_2S_3 films, chlorine incorporation controls the creation of defect Vs. It was also deduced that the incorporation of chlorine assists in improving the transport properties of the film by the

passivation of unwanted recombination centres and formation of defects that facilitate carrier generation.

5.3 In_2S_3 films fabricated by automated CSP unit

The uncertainties concerning the reproducibility and repeatability of fabrication process for deposition of uniform films using manually controlled chemical spray pyrolysis unit can be overcome to a great extent by automating the spray unit. Production of films using automated units is major requirement for industrial purposes. So buffer layer films for solar cells were fabricated using automated spray unit. Altering slightly the spray parameters, the slight differences arising in the film properties due deposition using different units can be overcome. This work is motivated by the need to determine the transport properties of the films that were later used in fabrication of solar cells.

5.3.1 Fabrication

Films were deposited with $InCl_3$ and thiourea as precursor solution and the composition (In/S) of the film was varied from 1.2/8, 2/8, 2.2/8, 2.5/8, 2.8/8 and 3/8. The spray parameters were the volume of spray solution (200 ml), spray rate (6 ml/min) and substrate temperature (300 ^{0}C). The other essential details of film fabrication the automated spray unit have described in previous chapter.

5.3.2 Photothermal analysis

The films were irradiated with beams of energy 2.81 eV, 2.33 eV and 1.96 eV. Photothermal signal is least for the sample 2/8 for "above band gap" excitation (Figure 5.11a), thereby making the non-radiative losses the least for particular composition. But for sub band gap excitations, these films show high photothermal signal (Figure 5.11b and 5.11c), which is also an indication of the absorption-taking place at a defect band in the forbidden gap region. These defect bands can trigger absorption of energies lower than the band gap energy and films with such defects have the ability to generate more carriers by absorbing all the three wavelengths. Hence on illumination with white light, losses are reduced considerably. Hence it is beneficial to have high density of the defects that assist in sub band gap energy absorption.

The transport properties measured are shown in table 5.6. We obtained a high mobility of 30 cm^2/Vs for films prepared at 2/8. But lifetime was highest for 2.5/8 in which the non-radiatve loss is lower. Again lifetime was highest for 2.5/8 (1 ms). On correlating this results with V_{oc} and J_{sc} of $CuInS_2$ based cells fabricated using In_2S_3 as buffer layer, we find that In_2S_3 layer with In/S ratio 2/8 (which offered high mobility and least V_{sr}) showed highest J_{sc} (3.48 mA/cm^2) and cells fabricated with 2.5/8 having high life time gave maximum V_{oc} (306 mV). Figure 5.12 shows the dependence of cells V_{oc} on the lifetime of the buffer layer.

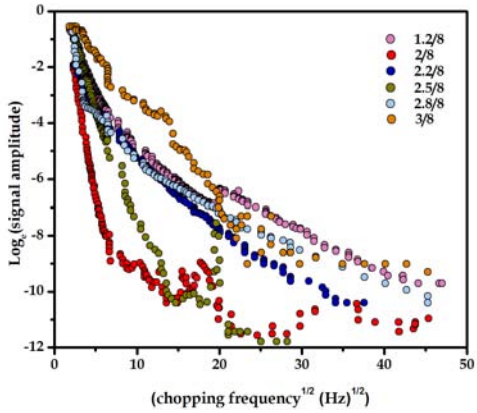

Figure 5.11a Photothermal signal responses for automated spray samples on 2.81 eV

Table 5.6
Transport properties of buffer layer

Sample	D_s (x10^{-3} cm^2/s)	V_{sr} cm^2/s	τ_r (μs)	μ (cm^2/Vs)
1.2:8	1.2	2x10^8	200	1.46
2:8	0.8	1x10^7	300	30
2.2:8	0.8	1x10^8	40	0.27
2.5:8	0.8	2 x10^7	1000	0.5
2.8:8	0.8	6 x10^8	60	3.6
3:8	1.1	1x10^8	500	1.9

The In/S ratio of In_2S_3 buffer layer that gives high mobility, low recombination velocity and high lifetime has been deduced. Film 2/8 has high mobility; but the high defect density in this material reduced the lifetime of the carriers. Film with ratio, 2.5/8 with least non-radiative losses in both above band gap and sub band gap absorption, has high lifetime too. The correlation between the buffer layer transport properties and final cell parameter has been brought out from the studies, where we find that the films with high mobility and lower surface recombination velocity gave high J_{sc} while V_{oc} increase with increase in carrier lifetime of buffer layer.

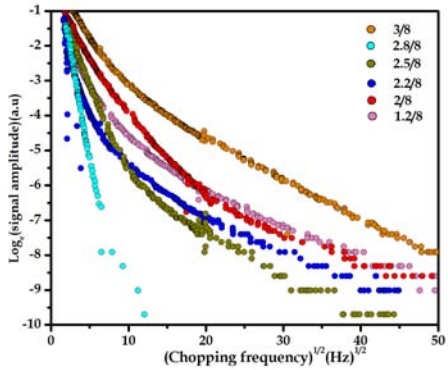

Figure 5.11 b Photothermal signal responses for automated spray samples 2.33 eV

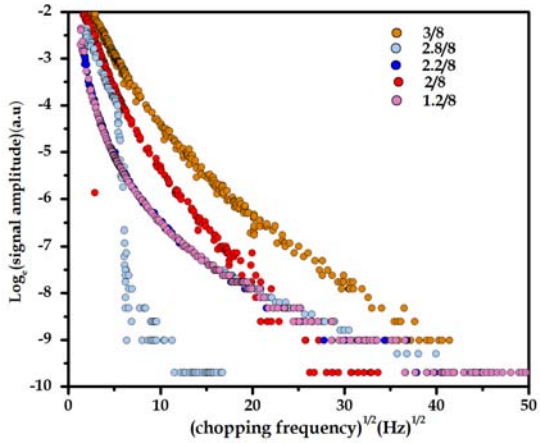

Figure 5.11 c Photothermal signal responses for automated spray samples 1.96 eV

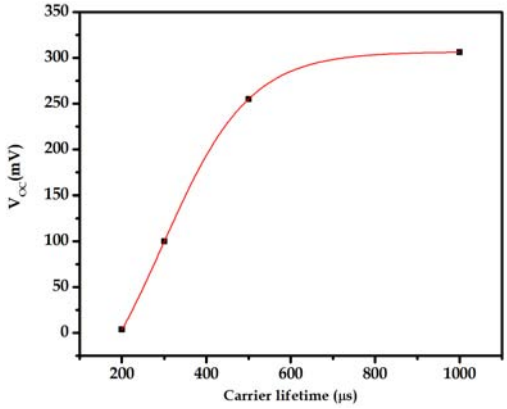

Figure 5.12 Dependence of Voc on carrier lifetime

5.4 Ag doped In_2S_3 thin films

Several materials (like Copper, Indium, Aluminium and Silver) are suitable for doping in In_2S_3. But it was silver that offered considerably high J_{sc} and V_{oc}. So to analyse the role of Ag in optical, electrical, structural properties, studies were carried out on this material that were doped with Ag. Photosensitivity of the films increased from 450 to 538 on Ag doping. Apart from that, resistivity of the films also reduced from $1.2x10^3$ Ω cm to 0.06 Ω cm. The crystallinity of the films improved very much; the grain size increased from 16 nm to 36 nm [29]. Probably because of all these factors, films with Ag electrode produced high efficiency [30].

5.4.1 Fabrication

In_2S_3 films of thickness 0.75 μm were deposited on glass slides using automated chemical spray pyrolysis, with spray rate 8 ml/min, spray volume 200 ml and substrate temperature 300 ^{0}C and In/S ratio 2/8. On the surface of this film, 13 mg of silver was deposited using

vacuum evaporation at 10^{-6} mbar. We fabricated 3 films; 1) the pure In_2S_3 film were coded as "InS"; 2) In_2S_3 film doped with Ag coded "InS: Ag" and 3) In_2S_3 film doped with Ag and vacuum annealed at 100 ^{0}C for one hour under pressure of 10^{-6} m bar was coded In_2S_3: Ag (100^{0}C).

5.4.2 Photothermal analysis of Ag doped In_2S_3 thin films

Photothermal analysis was done on the films InS, InS: Ag and InS: Ag (100 ^{0}C) to understand the influence of Ag "doping" and "diffusion" on the materials transport properties. Results of Transport properties obtained using this technique is shown in table 5.7. It is clear that Ag doping has improved the transport properties considerably. For example, the mobility has shot up by ~ 3 times and lifetime increased from 500 μs to 900 μs. Doping of silver has not however helped in reducing the surface defects. In fact the surface recombination increased slightly with doping of Ag. Annealing of Ag enhances the diffusion of Ag into the bulk of the material. Figure 5.13, shows the plot of 'phase' versus 'chopping frequency' for the three films. Photothermal signal phase shows a sudden (step-like) increase when there are 2 layers of different materials due to the difference in thermal diffusivity of the two materials. Such a step change is clear for In_2S_3: Ag. But on annealing this material at 100^{0}C for one hour the dopant diffused into the material and the step change in photothermal signal phase disappeared (Figure 5.13). But the diffusion of Ag did not improve the transport properties, except that there is a slight decrease in mobility to 0.63 cm^2/Vs.

Another interesting result of the study is that the Ag deposited on the material surface diffuses into the bulk of the material with time. Figure 5.14 depicts this result; the In_2S_3: Ag existed as 2 different layers till the third day after fabrication. But later Ag diffused slowly into the bulk to form a single layer. Also the transport properties were degraded after the second day of deposition. This analysis also explores the versatility of the technique, which can be used to study various layers present in the given thin film. Further analysis and studies are required for finding the depth of diffusion and extracting the information on material properties from different layers.

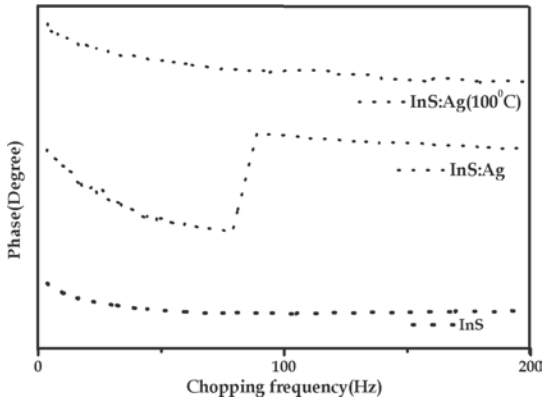

Figure 5.13 Photothermal signal plot versus chopping frequency of Ins, InS: Ag, InS: Ag (100^{0}C)

Table 5.7
Transport properties of In_2S_3 with and without Ag doping

Sample	D_s(x10^{-3} cm^2/s)	V_{sr} cm^2/s	τ_r (μs)	μ (cm^2/Vs)
InS	0.91	0.27	500	1
InS: Ag	1.1	0.76	900	2
InS: Ag (100^0C)	1.4	0.63	900	2.1

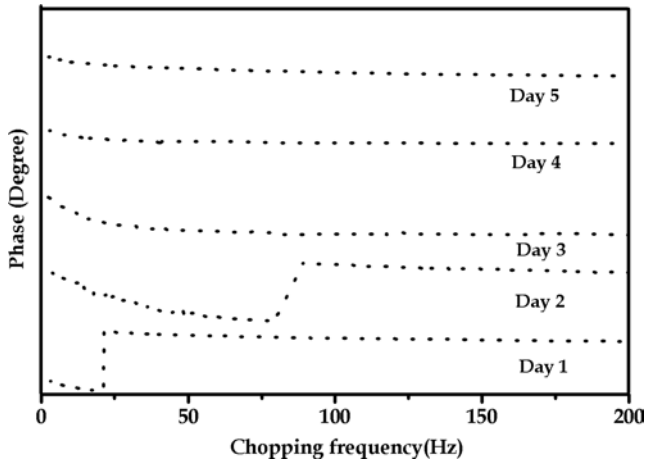

Figure 5.14 Photothermal signal plot versus chopping of InS: Ag with time (in days)

We explored another interesting application of photothermal deflection technique apart from determining the transport properties of Ag doped In_2S_3 films. Here we have shown that the technique can be used for depth profiling of a film to differentiate the formation of different layers. Ag doping has definitely improved the transport properties of In_2S_3 thin films by increasing the mobility and carrier lifetime. However it has no role in affecting the surface quality of the film as surface recombination velocity is altered only slightly with Ag doping.

5.5 Conclusion

The non-radiative transitions occurring in the conduction band and defect band of In_2S_3 films were analysed using PTBD technique and the study strongly proved the role of chlorine in improving the transport properties by annihilation of non radiative recombination centres and creation of defect bands that assist in carrier generation. The study also allowed us to find out the composition best suited for device fabrication by correlating the measured transport properties of buffer layer with the final cell parameters. Ag, which is used as electrode, when deposited over the buffer layer, improved the transport properties widely. Depth profiling, which is another important application of PTBD technique, is exploited here to study the diffusion of Ag into bulk of the material on annealing. More over the study also gave information on the period for which the Ag layer

deposited on In_2S_3 remained as a separate layer. After this period, it diffused into the bulk forming a single layer.

References

[1] M Taguchi, H Sakata, Y Yoshimine, E Maruyama, A Terakawa, M Tanaka 2005 *Proc of the 31st IEEE PVSC Orlando, FL*, 866

[2] K R Kumar, M Zeman 2008 *Bull Mater Sci* **31** 737

[3] J George, K S Joseph, T I Palson 1988 *Phys Stat Sol* **23** 1061

[4] N Nagavi, S Speiring, M Powalla, C Cavana, D Lincot 2003 *Prog Photovolt Res Appl* **11** 437

[5] N Naghavi, R Henriquez, V Laptev, D Lincot 2004 *Appl Surf Sci* **222** 65

[6] T T John, M Mathew, C S Kartha, K P Vijayakumar, T Abe, Y Kashiwaba 2005 *Sol Energy Mater Sol Cells* **89** 27

[7] W Rehwald, G Harbeke 1965 *J Phys Chem Solids* **26** 1309

[8] C J M Rooymann 1959 *J Inorg Nucl Chem* **11** 78

[9] V G Bessergenev, E N Ivanova, Y A Kovalevskaya, S A Gromilov, V N Krinchenko, S V Larionov 1996 *Inorg Mater* **32** 592

[10] M Mathew, M Gopinath, C S Kartha, K P Vijayakumar, Y Kashiwaba, T Abe 2010 *Solar Energy* **84** 888

[11] R S Becker, T Zheng, J Elton, M Saeki 1986 *Sol Energy Mater* **13** 7

[12] L Cuadra, A Martí, A Luque 2004 *Thin Solid Films* **451/452** 593

[13] T T John, S Bini, Y Kashiwaba, T Abe, Y Yashuhiro, C S Kartha, K P Vijayakumar 2003 *Semicond Sci Technol* **18** 491

[14] W T Kim, W S Lee, C S Chung, C D Kim 1988 *J Appl Phys* **63** 5472

[15] L Bhira, H Essaidi, S Belgacem, G Couturier 2000 *Phys Stat Sol (a),* **181** 427

[16] A A El Shazly, D A Elhady, H S Metwally, M A M Seyam 1998 J *Phys Condens Matter* 10 5943

[17] K Benchouk, J Ouerfelli, M Saadoun, A Siyoucef 2009 *Phys Procedia* **2** 971

[18] T Yukawa , K Kuwabara, Koumoto 1996 *Thin Solid Films* **286** 151

[19] [19] N A Allsop, A Schönmann, H J Muffler, M Bär, M C Lux-Steiner, C H Fischer 2005 *Prog Photovoltaics: Res & Appl* **13** 607

[20] V Yu Rud, Yu V Rud, V F Gremenok, V B Zalesski 2009 *Phys stat Sol* **6** 1269.

[21] S Spiering, L Bürkert, D Hariskos, M Powalla, B Dimmler, C Giesen, M Heuken 2009 *Thin Solid Films* **517** 2328

[22] A S Cherian, M Mathew, C S Kartha, K P Vijayakumar 2010 *Thin Solid Films* **518** 1779

[23] R R Pai, T T John, Y Kashiwaba, T Abe, K P Vijayakumar, C S Kartha 2004 *J Mat Sci* **39** 1

[24] R Jayakrishnan, T T John, C S Kartha, K P Vijayakumar, T Abe , Y Kashiwaba, 2006 *Semicond Sci Technol* **20** 1162

[25] R Jayakrishnan, T T John, C S Kartha, K P Vijayakumar, D Jain, L S S Chandra V Ganesan 2008 *J Appl Phys* **103** 053106

[26] V N F1eurov, K A Kikoin 1976 *J Phys C: Solid Stat Phys* **9** 1673

[27] H H Abu-Safe, M Hossain, H Naseem, W Brown, A A Dhafiri 2004 *J Electron Mater* **33** 128

[28] W K Metzger, M Gloeckler 2005 *J of Appl Phys* **98** 063701

[29] M Mathew, R Jayakrishnan, P M Ratheesh, C S Kartha, K P Vijayakumar, T Abe, Y Kashiwaba 2006 *J Appl Phys* **100** 033504

[30] M Mathew, C S Kartha, K P Vijayakumar 2009 *J Mater Sci: Mater Electron* **20** S294

6

Photothermal analysis of thin film solar cells

In this chapter we demonstrate the versatility and utility of PTBD technique for analysis of compound semiconductor thin film solar cells. A trial for measuring the series resistance, optimum load resistance and efficiency of $CuInS_2/In_2S_3/Ag$ solar cells using PTBD was performed. Series resistance and efficiency thus determined agree with electrical measurements.

6.1 Prospect of PT techniques for solar cell analysis

Basic principle of PT and PA techniques is the detection of heat produced in a sample due to non-radiative deexcitation process, resulting from the absorption of modulated light. Consequently, their signals are proportional to the conversion efficiency of light into heat and, therefore, complementary to the other photoinduced energy conversion processes [1]. This aspect was explored by several research groups for investigating the photoinduced conversion processes ranging from study of photosynthetic processes in leaves [2, 3] to monitoring of photovoltaic conversion efficiency of solar cells [4, 5] and for the study of non-radiative recombination processes in semiconductors [6]. In case of photothermal characterization of solar cells, first work was reported in the field using photoacoustic spectroscopy [4]. Though a variety of photothermal spectroscopy techniques were successfully developed, only few of these techniques were found to be useful for photovoltaic cell characterization. These include photothermal radiometry [7], photopyroelectric detection [8] and photothermal beam deflection schemes [9].

The basic phenomenon of direct solar energy conversion into electrical energy involves absorption, and emission of radiation, which are irreversible processes. Consequently, a part of the incoming solar radiation flux is always dissipated as heat within the absorber. In case of solar cells that use unconcentrated radiation, the quantity of dissipated heat can exceed 70% of the incoming energy flux. Usually this heat is lost to the ambient. But this mechanism of heat rejection is rarely considered in the literature i.e., the heat lost through this process is normally neglected, leading to an over estimation of solar cell efficiencies. Efficiency losses in surface barrier solar cells can be separated into two parts: recombination during collection process, usually described in terms of quantum efficiency and on the other hand, the leakage currents limiting the reachable photo voltage in the

loaded cell. In solar cells, quantum efficiency of unity is often realized. At the same time, its photovoltaic efficiency often limits the dark current over an insufficient interface or a poor space charge region. The contactless nature of the method presented allows an investigation of the interface quality separate from other problems in the solar cell, such as back or front contact problems, which play a role in IV measurements.

Photothermal techniques also lead to non-destructive means of locating and identifying power losses in a semiconductor device and evaluating semiconductor material parameters, such as minority carrier lifetime and surface recombination velocity. For a pn junction device, the larger the photothermal signal, the more power is the loss. These analyses provide the possibility of choosing the optimum parameters, by which energy losses in p-n junction devices will be minimised. This technique is used for identifying the major energy losses in the pn junction devices and for measuring parameters such as the minority carrier lifetime and surface recombination velocity, thus providing guidelines for cell optimisations.

6.2 Compound semiconductor thin film solar cells

Compound semiconductor thin film solar cells are attractive option for efficient photovoltaic energy conversion. Thin film solar cells are sub-micron thick semiconductor layers, whose active material absorb sunlight and allow electrons to flow through the material to generate electricity. This process of conversion of light into electricity is called "photovoltaic effect". The most widely used commercial solar cells are made from single crystalline Si with efficiencies reported up to 26.5% (Amonix, Inc) for commercial products [10]. However, such single crystalline solar cells are relatively expensive with the silicon itself making up 20–40% of the final cost. Amorphous silicon solar cells can be produced at lower temperature on low-cost flexible substrates such as plastics or metal foils [11]. Ultimately, the amorphous cells tend to degrade when exposed to sunlight and their efficiency decreases by 10–20%. In the search for low-cost alternatives to crystalline silicon, thin film compound semiconductor materials are commonly used which offer advantages over silicon. It is more efficient to create an electric field at an interface between two different semiconductor materials, known as a heterojunction. A typical polycrystalline thin film has a thin (0.1 mm) layer on top known as a ''window'' material, which lets most of the light through the interface (heterojunction) to the absorbing layer. The absorbing layer (1–2 mm thick) has to have a high absorption to be effective in the generation of current and a suitable band gap to provide good voltage. Considering these facts $CuInS_2/In_2S_3$ based thin film solar cell is most feasible choice of cell structure. $CuInS_2/ In_2S_3$ thin film solar cells can be fabricated by several techniques such as CSP and co evaporation. For this particular study, $CuInS_2/In_2S_3$/Ag cells were fabricated by CSP technique.

6.3 Fabrication of $CuInS_2/In_2S_3$/ITO cell

For junction fabrication ITO coated glass was used as substrate. Earlier optimised spray conditions were used for fabrication of $CuInS_2$ and In_2S_3 thin film solar cells. Near stoichiometric $CuInS_2$ prepared at 300 ^{0}C, 30 ml, and spray rate 1ml/min with thickness 0.30 μm. In_2S_3 layer with In/S ratio 2/8, substrate temperature 300 ^{0}C, 8 ml/min was deposited over $CuInS_2$ layer. In_2S_3 layer was made thick enough so that despite the diffusion of Cu from $CuInS_2$, a layer of pure In_2S_3 remained on the top surface [12]. Silver electrodes of area 0.25 mm^2 were deposited by vacuum evaporation over In_2S_3 layer. This cell had Jsc of 4 mA/cm^2 and V_{OC} ~ 490 mV.

6.4 Photothermal analysis of $CuInS_2/In_2S_3$ junction

6.4.1 Theory

When a photon of energy larger than the band gap impinges upon a photovoltaic device, it is reflected, absorbed and converted into useful electricity, or absorbed and converted into heat; this can be measured using low frequency photoacoustics. Useful electrical output of the device can be characterized in several ways, using, current and voltage analysis and photocurrent spectroscopy. The third pathway for incident photons, i.e., their photothermal signal is proportional to light into heat conversion efficiency and complementary to other photoinduced energy-conversion processes. This aspect has been explored by several authors for investigating photoinduced conversion processes ranging from the study of photosynthetic process in leaves to the monitoring of photovoltaic conversion efficiency of solar cells, and the study of non-radiative recombination processes in semiconductors. Apart from this, an additional heating due to internal thermal loss in the cell also contribute to photothermal signal. This was identified as due to the current dissipation at solar cell internal resistance [1]. In early PA experiments these internal losses contributions were not observed since the experiment was performed at higher modulation frequencies (> 540 Hz).

In general form, photothermal signal may be written as,

$$Signal \propto \alpha\left[1-\sum\left(\phi_i \Delta E_{p,i} / Nh\nu\right)-\left(\Phi_l \nu_l / \nu\right)-\gamma\right] \qquad 6.1$$

Where α is the fraction of light absorbed by the illuminated sample, Φi is the quantum yield for photochemical reaction i, $\Delta E_{p,i}$ is the molar internal change of product information in this reaction, ν_l and ν are frequencies of emitted and incoming radiation, N is the Avagadro number, h is the Planck's constant, γ is the energy-conversion efficiency for photovoltaic process.

In a solar cell under photothermal analysis, if only a photovoltaic process takes place the signal can be written as,

$$Signal \propto \alpha[1-\gamma(L)] \qquad 6.2$$

Where L is the specific resistance load L
Here, [*1- γ (L)*] can be termed as "photovoltaic loss" as it represents the decrease in the photothermal signal with respect to normal absorption signal, because of photovoltaic process. From equation 6.2, the photothermal conversion efficiency is given by,

$$\gamma(L)=[\alpha - Signal(L)]/\alpha \qquad 6.3$$

By minimizing the photothermal signal (i.e., maximizing $[\alpha - signal(L)]$), we can find the optimum load *L* and conversion efficiency γ at this load. As a photovoltaic device will have zero-energy-conversion efficiency at open circuit (*OC*) condition, photothermal signal under these conditions will equal to' α ', and therefore,

$$\gamma(L)=[signal(OC)-signal(R_L)]/signal(OC) \qquad 6.4$$

Thus from Eq. 6.4, we can calculate the conversion efficiency of the PV device at a given R_L from ratio of the PT signal amplitude under optimal load and open circuit conditions. The importance is that we need not know the iiradiance of the illuminating light and the geometry of the solar cell. According to maximum power transfer theorem, if the R_L is made larger than the R_S, then efficiency is higher, since a higher percentage of the source power is transferred to the load, but the *magnitude* of the load power is lower since the total circuit resistance goes up. If R_L is smaller than the R_S, then most of the power ends up being dissipated in the source, and although the total power dissipated is higher, due to a lower total resistance, it turns out that the amount dissipated in the load is reduced and γ becomes negative for $R_L << R_S$. Furthermore at matching resistance condition $R_L=R_S$ predicts γ=0. Therefore from the plot γ (R_L) of versus R_L (Figure 6.3) (as measured by Eq 6.4), we can determine R_S (using the condition when $R_L=R_S$, γ=0) and optimum R_L as the R_L where the γ is maximum.

6.4.2 Experimental details

The experimental set up is shown in figure 6.1. Photovoltaic device (1x1 cm^2) to be analysed is placed in the sample cell provided. In open circuit mode, the constant bias illumination is supplied by 250 W halogen lamp filtered with an IR filter. The load resistance (R_L) is connected to the solar cell device using external wires that are attached to the electrodes of the device. The material is excited with the intensity modulated pump beam (2.81 eV) using the chopper frequency of 15 Hz.

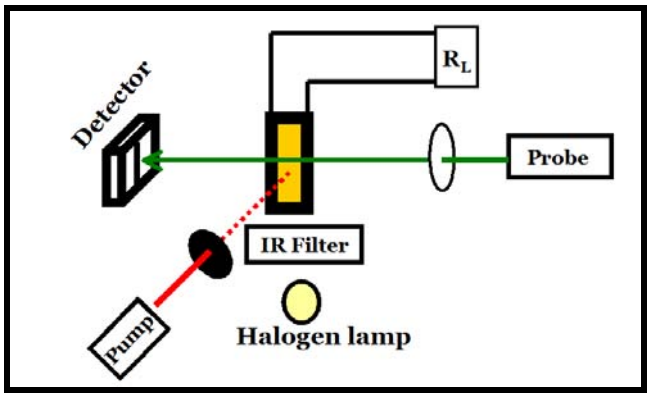

Figure 6.1 Experimental design for photothermal analysis of solar cells

6.4.3 Transport properties

$CuInS_2/In_2S_3$ cells were irradiated with beam of energy 1.96 eV. The beam is thus absorbed entirely at the absorber layer $CuInS_2$; In_2S_3 with low absorption coefficient transmits the light to the bottom absorber layer. Figure 6.2 shows the photothermal signal variation of 'all sprayed' $CuInS_2/In_2S_3$/ITO structure. Similar to the behaviour of single layer absorber/ buffer layer the photothermal signal decline was rather linear in the low frequency region and at higher frequencies the slope of the decline is more gradual. Transport properties measured from this plot gives information only on the absorber layer of the cell. The mobility was 60 mV/cm², lifetime (300 μs) and lowest V_{sr} (x 10^6 cm²/s). We find that the mobility has considerably gone up from that of the single absorber layer and also there is decrease in the V_{sr}. Hence the deposition of In_2S_3 in the optimised composition has definitely assisted in improving the absorber layer properties. The V_{sr} of $CuInS_2$ film has decreased from 10^8 cm²/s to 10^6 cm²/s, by passivation of certain recombination centres that could have formed at $CuInS_2/In_2S_3$ interface due to lattice mismatch and certain deformities in the surfaces.

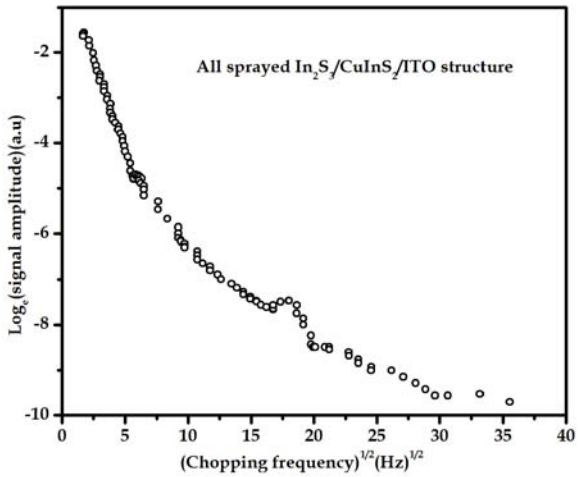

Figure 6.2 Photothermal response of $CuInS_2/In_2S_3$ solar cell

6.4.3 Measurement of series resistance, optimal load resistance and efficiency

Figure 6.3 shows variation in photovoltaic conversion efficiency as a function of load resistance. The data shown in figure 6.3 was recorded at 15 Hz and the main features may be summarized as follows; it shows an optimum load resistance at around 9 Ω, this is the value of R_L at which γ is maximum. For load resistance less than 7 Ω, γ becomes negative. It is to be noted here that R_L at 7 Ω for which γ=0 is the R_S of the cell. This is in agreement with the maximum power transfer theorem. These values were checked by fitting the data of dark current characteristics of the cell [12]. γ becomes negative for resistances lower than series resistance and this means that the deflection is sensitive to some additional thermal loss mechanism [8]. Conversion efficiency as calculated using this technique is ~1% which is almost same as that measured by electrical measurements (Table 6.1). Thus through photothermal technique we can determine the series resistance, optimum load resistance and conversion efficiency of compound semiconductor thin film solar cells.

Table 6.1
Cell parameters determined by electrical and photothermal measurements

Analysis	R_s (Ω)	Optimum load (Ω)	Efficiency (%)
Electrical	9	-	1.15
Photothermal	7	10	1

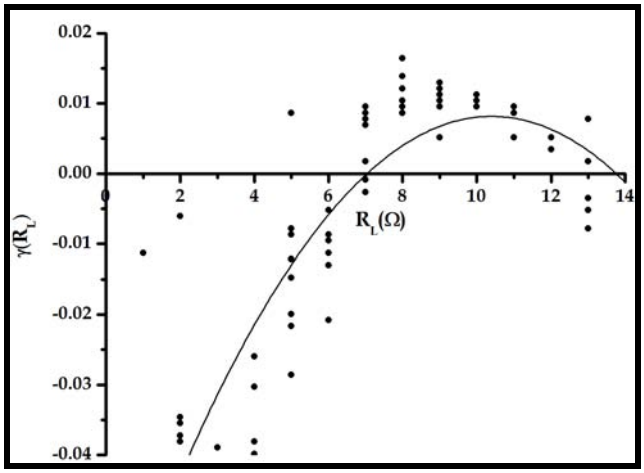

Figure 6.3 Photovoltaic conversion efficiency as function of load resistance

This application can be used for quality control of solar cell in different stages of their deposition process. In the first step the transport parameters, thermal diffusivity, μ, V_{sr} and τ_r can be determined to check quality and finally junction parameters can be determined using this technique.

6.5 Conclusion

PTBD is found to be simple and reliable tool for characterization of PV devices. This technique was applied for measuring the energy conversion efficiency, optimum load resistance and series resistance of $CuInS_2/In_2S_3/Ag$ thin film solar cells. PTBD technique being a non-destructive tool and measurements are made in open circuit conditions, it can be applied to analyse partially completed solar cells, yielding information about every process in fabrication sequence. Thus PTBD is a potential tool of industrial process monitoring.

Reference

[1] H L Riette, L C M Miranda, H Vargas 1987 *Appl Phys A* **44** 219
[2] D Cahen, S Malkin, E I Lerner 1978 *FEBS Letter* **91** 339
[3] C A S Lima, J C V Mattos, A F S Penna, J F W von Bulov, L C M Miranda, C C Ghizoni 1982 *J Photoacoustics* **1** 61.
[4] D Cahen 1978 *Appl Phys Lett* **33** 810
[5] D Cahen, S D Halle 1985 *Appl Phys Lett* **46** 446
[6] C C Ghizoni, L C M Miranda 1982 *Proc IEEE Ultrason Symp*, New York **2** 601
[7] G Bults, P E Nordal, S O Kanstad 1982 *Biochim Biophys Acta* **682** 234
[8] I F Faria, Jr C C Ghizoni, L C M Miranda 1986 *J Appl Phys* **59** 3294
[9] P Grunow, R Schieck 1995 *J Appl Phys* **77** 2773
[10] *www.amonix.com*
[11] P Alpuim, A Samantilleke, E Marins, F Oliveira, M F Cerqueira, L Rebouta, S Stefanov, S Chiussi, C Serra, J E Bourée 2010 *Phys Stat Sol (c)* **7** 1061
[12] T Sebastian 2009 *PhD Thesis*, Cochin University of Science and Technology, India

7

Outlook

This chapter summarizes the applications of photothermal beam deflection technique for studying semiconductor materials while exploring briefly our present status and accomplishments in the field of photothermal science. PTBD technique is used for a wide range of application like measurement of thickness, transport properties, depth profiling, thermal imaging, and characterization of solar cells. Experimental and theoretical data are in good agreement and the correlation with measurements done using other competent tools have established PTBD as a reliable and efficient tool for NDT in industries.

Non-destructive testing and evaluation is identified as an essential tool to enhance the quality and productivity of a project from creation to completion. Non-destructive testing plays a vital role in providing an excellent balance between quality control and cost effectiveness. It provides a more reliable assessment of the state of any project. PT techniques are used by several industries for process monitoring and control. The versatility and non-invasive method of evaluation prompt industries to adopt PTBD technique for material analysis. Therma probe tool by Therma wave Inc was introduced for inline dosage measurements, for monitoring the wafer manufacture process in semiconductor industries [1]. Several other companies have also commercialised thermal wave probing method for material analysis [2].

7.1 State of art

Photothermal beam deflection technique was designed and set up in Applied Optics division, Department of Physics, Cochin University of Science and Technology as a part of PhD work by Dr Ramkumar [3]. This set up was used for analysing semiconductor and polymer materials. The PhD work by Dr M Paulraj proved the efficiency of the tool for measuring film thickness, mobility and thermal diffusivity of semiconductor thin films [4]. In the present work photothermal deflection unit was automated and a theoretical model was developed for measuring the thermal diffusivity, minority carrier lifetime and surface recombination velocity of semiconductor thin films. The measurements were done with an objective to optimize deposition conditions for obtaining device quality thin films. The technique was also useful for measuring the series resistance, optimum load resistance and efficiency of solar cells.

7.2 Achievements

One of our major accomplishments in the field of photothermal science is fabrication a compact photothermal deflection unit that can measure photothermal signal with low signal to noise ratio and good accuracy. This unit was successfully employed for analysis of semiconductor materials. The application was also extended to analysis thermal properties of polymer materials. The possibility of developing PTBD technique as real time process analysis tool for device fabrication is also investigated.

Compact PTBD unit

A compact PTBD unit was set up, which integrates sample displacement stage; probe laser, source and detection technique. The unit is mounted on an in-house developed vibration isolation table. The vibration isolation table is designed with spring, shock absorber combination and air filled tube. The technique is automated using RS232 interface and Lab view programme and can be operated in both manual and automated mode. CW/pulsed laser or a tungsten arc lamp can be used as excitation source. And a low power laser usually serves as probe beam.

Determination of thickness

PTBD technique was employed for measuring the thickness of semiconductor thin films. Thickness of $CuInS_2$ and In_2S_3 thin films fabricated using chemical spray pyrolysis with different spray solution volumes were measured using PTBD technique [3, 4]. Due to its sensitivity, feeble optical absorption could be detected that help in studying transparent samples. Thickness of transparent conducting oxides such as ZnO [5] were measured and verified from the thickness obtained using stylus depth profiler.

Depth profiling

Distribution depth profile of the implanted ion in the sample was studied from the one-dimensional line scanning, performed over the implanted region of sample. The results were comparable with SRIM calculations [6]. Diffusion of Ag into In_2S_3 thin films was studied from photothermal phase analysis. This technique was also used to determine the depth of Cu diffusion in CdS in the case of doped samples. The thickness of the damaged layer due to implantation was also measured. Thus this technique was demonstrated to be useful for studying ion distribution in the sample due to ion implantation.

Imaging

Two dimensional image mapping was done to study the depth wise damage caused due to ion implantation [7]. This also helps identify the region of sample that has low non-radiative loss. Thermal imaging of the sample surface also helps understand the uniformity of thin films.

Measurement of transport properties

The technique was found to be useful for obtaining transport properties like thermal diffusivity, minority carrier mobility, surface recombination velocity and minority carrier lifetime of semiconductor thin films [8]. This method was applied on various ternary and binary compound semiconductor thin films like CdS, In_2S_3, ZnO, $CuInS_2$, $CuInSe_2$, SnS, In_2Se_3, that find application in fabrication of solar cells. The effect of ion implantation, irradiation, doping on the mobility have been analysed.

Solar cell analysis

Photothermal analysis was done in open circuit condition and it was applied to analyse partially completed solar cells, yielding information about every process in fabrication sequence. This technique was applied for measuring energy conversion efficiency, optimum load resistance and series resistance of $CuInS_2/In_2S_3$/Ag thin film solar cells.

Industrial application

The quality of welded joint was studied using this technique. The entrapped air pocket or defect caused during the process of welding could be non-destructively detected [4]. The surface texture of a layer of paint coated over glass substrate was studied. Thickness and thermal diffusivity of a layer of acrylic black paint coated over glass using spin coating method was also determined using this technique [9]. The technique was proved to be efficient for measuring the thermal diffusivity of polyurethane, before and after adding filter components such as Mica, Boron nitrate, ZnO, aluminium oxide [4] and thus identify best candidate.

7.3 Future prospects

PTBD is well-established NDT technique for analysing various aspects of semiconductor thin films. It is also proven to be efficient for solar cell analysis. The technique at present has to be modified and improved for making further advancements in the area of solar cell characterization. The theoretical model presented in this work has to be adapted to include the thermal sources in a device. The heat diffusion equation and minority carrier diffusion equations has to has to be solved by including space charge recombination and diode parameters describing the dark current. Thus can be fitted with the experimentally obtained photothermal signal amplitude in closed circuit and open circuit conditions to obtained the cell parameters such as injection current, recombination current and identify major power loss mechanisms in solar cells as variable fit parameters. The photothermal phase and amplitude signal can be used for depth profiling and determination of transport properties of different layers in multilayer thin films. This technique has to be modified suitably for determining the transport properties of different layers and junction interfaces in a solar cell. Improving the material excitation and probing mechanisms would enable this tool for obtaining information on film grain boundaries and surface defects. The application of photothermal technique for analysis of binary and ternary compound semiconductor thin films is a relatively new area with very few studies being reported.

Semiconductor and photovoltaic industries can be benefited by from these studies for achieving better device performance.

References

[1] A Rosencwaig 1990 *Review of progress in quantitative non-destructive evaluation*, **9** Plenium press, New York

[2] *www.phototherm.de*

[3] S Ramkumar 2006 *PhD Thesis*, Cochin University of Science and Technology, India

[4] M Paulraj 2004 *PhD Thesis*, Cochin University of Science and Technology, India

[5] M Paulraj, S Ramkumar, P R Amjith, T T John, P M Ratheeshkumar, C S Kartha, K P Vijayakumar, K G M Nair 2005 *J Phys IV* **125** 469

[6] M Paulraj, S Ramkumar, K P Varkey, K P Vijayakumar, C S Kartha, K G M Nair 2005 *Phys Stat Sol (a)* **202** 425

[7] M Paulraj, S Ramkumar, C S Kartha, K P Vijayakumar 2005 *J Phys IV* **125** 97

[8] A R Warrier, T Sebastian, C S Kartha, K P Vijayakumar 2010 *J of Appl Phys* **107** 073701

[9] C A V Kartha 2008 *Project report*, Cochin University of Science and Technology, India

Abbreviations

Atomic force microscopy	**AFM**
Cathode ray oscilloscope	**CRO**
Chemical spray pyrolysis	**CSP**
Copper indium sulphide	**CIS**
Indium tin oxide	**ITO**
Laboratory Virtual Instrument Engineering Workbench	**LabVIEW**
Non destructive testing	**NDT**
Optical beam deflection	**OBD**
Photoacoustic	**PA**
Photoacoustic spectroscopy	**PAS**
Photoluminescence	**PL**
Photothermal	**PT**
Photothermal beam deflection	**PTBD**
Photothermal radiometry	**PTR**
Photovoltaic	**PV**
Position sensing detector	**PSD**
Probe beam refraction	**PBR**
Thermally stimulated current	**TSC**
Virtual instrument software architecture	**VISA**